

357040

PB 261 323

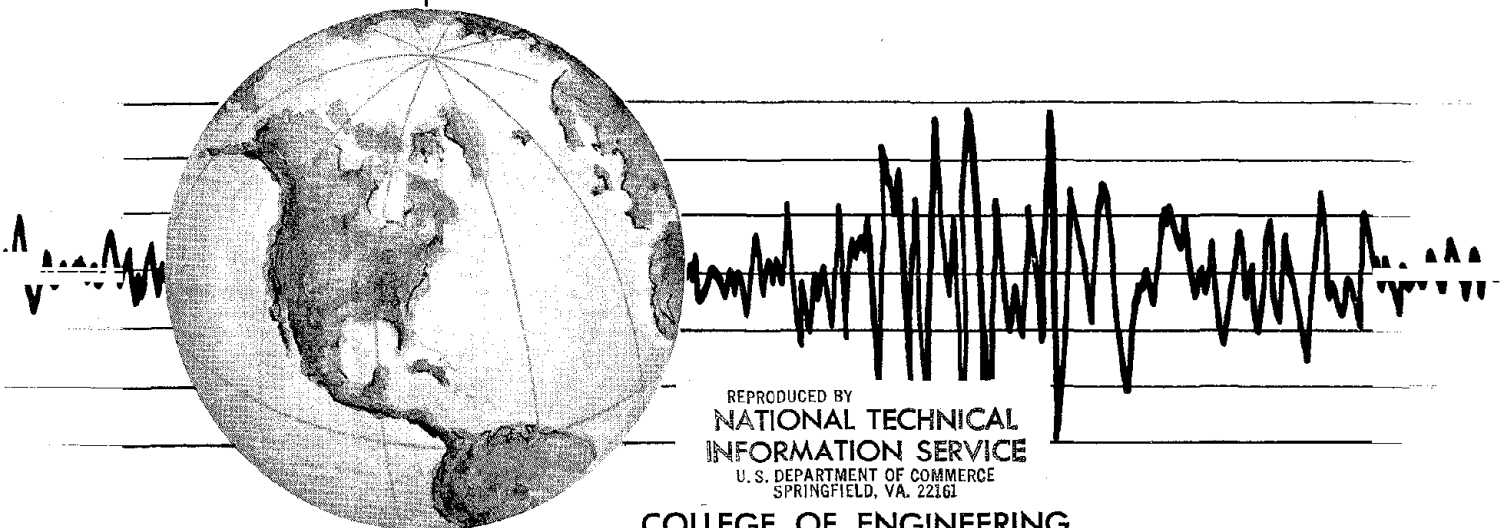
REPORT NO.  
EERC 76-15  
JUNE 1976

EARTHQUAKE ENGINEERING RESEARCH CENTER

# REINFORCED CONCRETE FRAME 2: SEISMIC TESTING AND ANALYTICAL CORRELATION

by  
RAY W. CLOUGH  
and  
JAWAHAR GIDWANI

Report to the National Science Foundation



REPRODUCED BY  
NATIONAL TECHNICAL  
INFORMATION SERVICE  
U. S. DEPARTMENT OF COMMERCE  
SPRINGFIELD, VA. 22161

COLLEGE OF ENGINEERING

UNIVERSITY OF CALIFORNIA • Berkeley, California

For sale by the National Technical Information Service, U. S. Department of Commerce, Springfield, Virginia 22161.

See back of report for up to date listing of EERC reports.

<b>BIBLIOGRAPHIC DATA SHEET</b>		1. Report No. EERC 76-15	2.	3. Recipient's Accession No.
4. Title and Subtitle Reinforced Concrete Frame 2: Seismic Testing and Analytical Correlation		5. Report Date June 1976		6.
7. Author(s) Ray W. Clough and Jawahar Gidwani		8. Performing Organization Rept. No. 76-15		
9. Performing Organization Name and Address Earthquake Engineering Research Center University of California, Berkeley 1301 S. 46th Street Richmond, California 94804		10. Project/Task/Work Unit No.		11. Contract/Grant No. AEN73-07732 A02
12. Sponsoring Organization Name and Address National Science Foundation 1800 G Street Washington, D.C. 20550		13. Type of Report & Period Covered		14.
15. Supplementary Notes				
16. Abstracts The earthquake simulator testing and analytical correlation of the second reinforced concrete frame studied as part of the NSF project "Energy Absorption Characteristics of Structural Systems Subjected to Earthquake Excitation" is described. This frame differed from the first only in avoiding a significant construction error, and in the sequence of earthquake tests to which it was subjected. Except for local damage attributed to the construction error of the first frame, the behavior of this frame was similar to that of the first. Damage apparently is a cumulative result of the total cyclic strain history to which the structure is subjected, and is not sensitive to the testing sequence. Adequate analytical correlation with the observed results was obtained using the same mathematical modeling concepts as were employed with Frame 1, based on a bilinear frame analysis program with a superposed first mode stiffness degradation and determination mechanism.				
17. Key Words and Document Analysis. 17a. Descriptors				
17b. Identifiers/Open-Ended Terms				
17c. COSATI Field/Group				
18. Availability Statement Release Unlimited		19. Security Class (This Report) UNCLASSIFIED		21. No. of Pages 174
		20. Security Class (This Page) UNCLASSIFIED		22. Price 6.75-3.00

**INSTRUCTIONS FOR COMPLETING FORM NTIS-35 (10-70)** (Bibliographic Data Sheet based on COSATI Guidelines to Format Standards for Scientific and Technical Reports Prepared by or for the Federal Government, PB-180 600).

1. **Report Number.** Each individually bound report shall carry a unique alphanumeric designation selected by the performing organization or provided by the sponsoring organization. Use uppercase letters and Arabic numerals only. Examples FASEB-NS-87 and FAA-RD-68-09.
2. Leave blank.
3. **Recipient's Accession Number.** Reserved for use by each report recipient.
4. **Title and Subtitle.** Title should indicate clearly and briefly the subject coverage of the report, and be displayed prominently. Set subtitle, if used, in smaller type or otherwise subordinate it to main title. When a report is prepared in more than one volume, repeat the primary title, add volume number and include subtitle for the specific volume.
5. **Report Date.** Each report shall carry a date indicating at least month and year. Indicate the basis on which it was selected (e.g., date of issue, date of approval, date of preparation).
6. **Performing Organization Code.** Leave blank.
7. **Author(s).** Give name(s) in conventional order (e.g., John R. Doe, or J. Robert Doe). List author's affiliation if it differs from the performing organization.
8. **Performing Organization Report Number.** Insert if performing organization wishes to assign this number.
9. **Performing Organization Name and Address.** Give name, street, city, state, and zip code. List no more than two levels of an organizational hierarchy. Display the name of the organization exactly as it should appear in Government indexes such as USGRDR-I.
10. **Project/Task/Work Unit Number.** Use the project, task and work unit numbers under which the report was prepared.
11. **Contract/Grant Number.** Insert contract or grant number under which report was prepared.
12. **Sponsoring Agency Name and Address.** Include zip code.
13. **Type of Report and Period Covered.** Indicate interim, final, etc., and, if applicable, dates covered.
14. **Sponsoring Agency Code.** Leave blank.
15. **Supplementary Notes.** Enter information not included elsewhere but useful, such as: Prepared in cooperation with . . . Translation of . . . Presented at conference of . . . To be published in . . . Supersedes . . . Supplements . . .
16. **Abstract.** Include a brief (200 words or less) factual summary of the most significant information contained in the report. If the report contains a significant bibliography or literature survey, mention it here.
17. **Key Words and Document Analysis.** (a). **Descriptors.** Select from the Thesaurus of Engineering and Scientific Terms the proper authorized terms that identify the major concept of the research and are sufficiently specific and precise to be used as index entries for cataloging.  
(b). **Identifiers and Open-Ended Terms.** Use identifiers for project names, code names, equipment designators, etc. Use open-ended terms written in descriptor form for those subjects for which no descriptor exists.  
(c). **COSATI Field/Group.** Field and Group assignments are to be taken from the 1965 COSATI Subject Category List. Since the majority of documents are multidisciplinary in nature, the primary Field/Group assignment(s) will be the specific discipline, area of human endeavor, or type of physical object. The application(s) will be cross-referenced with secondary Field/Group assignments that will follow the primary posting(s).
18. **Distribution Statement.** Denote releasability to the public or limitation for reasons other than security for example "Release unlimited". Cite any availability to the public, with address and price.
- 19 & 20. **Security Classification.** Do not submit classified reports to the National Technical
21. **Number of Pages.** Insert the total number of pages, including this one and unnumbered pages, but excluding distribution list, if any.
22. **Price.** Insert the price set by the National Technical Information Service or the Government Printing Office, if known.

REINFORCED CONCRETE FRAME 2:  
SEISMIC TESTING AND ANALYTICAL CORRELATION

by

RAY W. CLOUGH

and

JAWAHAR GIDWANI

Report to  
National Science Foundation

Report No. EERC 76-15  
Earthquake Engineering Research Center  
College of Engineering  
University of California  
Berkeley, California

June 1976



## SUMMARY

The earthquake simulator testing and analytical correlation of the second reinforced concrete frame studied as part of the NSF project "Energy Absorption Characteristics of Structural Systems Subjected to Earthquake Excitation" is described. This frame differed from the first only in avoiding a significant construction error, and in the sequence of earthquake tests to which it was subjected. Except for local damage attributed to the construction error of the first frame, the behavior of this frame was similar to that of the first. Damage apparently is a cumulative result of the total cyclic strain history to which the structure is subjected, and is not sensitive to the testing sequence. Adequate analytical correlation with the observed results was obtained using the same mathematical modeling concepts as were employed with Frame 1, based on a bilinear frame analysis program with a superposed first mode stiffness degradation and determination mechanism.



## ACKNOWLEDGMENT

The research described in this report was performed with the financial support of the National Science Foundation, by research grant AEN73-07732 A02. The continuing support by the National Science Foundation of research making use of the earthquake simulator facility is leading to greatly improved understanding of the behavior of structures subjected to earthquakes, and is gratefully acknowledged.



TABLE OF CONTENTS

	Page
SUMMARY . . . . .	i
ACKNOWLEDGMENT . . . . .	ii
TABLE OF CONTENTS . . . . .	iii
LIST OF TABLES . . . . .	v
LIST OF FIGURES . . . . .	vi
1. INTRODUCTION . . . . .	1
1.1 Background . . . . .	1
1.2 Review of Other Research . . . . .	2
1.2.1 Dynamic Tests . . . . .	3
1.2.2 Dynamic Analysis . . . . .	3
2. THE TEST STRUCTURE . . . . .	5
2.1 Selection and Design of Test Structure . . . . .	5
2.2 Material Properties . . . . .	6
2.3 Section Properties . . . . .	7
2.4 Structural Properties . . . . .	8
2.5 Construction and Repair of Test Structure . . . . .	10
3. TEST PROCEDURES AND INSTRUMENTATION . . . . .	27
3.1 Earthquake Excitation . . . . .	27
3.2 Instrumentation . . . . .	28
3.2.1 Accelerometers . . . . .	28
3.2.2 Potentiometers . . . . .	29
3.2.3 Linear Variable Differential Transformers (LVDT) . . . . .	29
3.2.4 Force Transducers . . . . .	30
3.2.5 Strain Gages in Reinforcing Bars . . . . .	30
3.2.6 LVDTs for Static Displacements . . . . .	31
3.3 Free Vibration Properties . . . . .	31



	Page
3.3.1 Snap Tests . . . . .	31
3.3.2 Flexibility Matrix Measurements . . . . .	32
3.4 Static Test . . . . .	32
4. TEST RESULTS . . . . .	45
4.1 Damage Observations . . . . .	45
4.2 Variation of Free Vibration Frequency and Damping . . . . .	48
4.3 Lateral Flexibility Matrix . . . . .	50
4.4 Global Response Behavior . . . . .	51
4.5 Measured Column Shear Forces . . . . .	53
4.6 Static Test Results . . . . .	53
5. ANALYTICAL PREDICTION OF STRUCTURAL RESPONSE . . . . .	103
5.1 General Comments . . . . .	103
5.2 Evaluation of Linear Stiffness Properties . . . . .	104
5.3 "Linear" Response Correlation - Model B . . . . .	106
5.4 Degrading Stiffness Analysis - Model D . . . . .	108
5.5 Degrading and Deteriorating Stiffness - Models E & F . . . . .	109
6. CONCLUDING REMARKS . . . . .	139
6.1 Structural Performance . . . . .	139
6.2 Analytical Correlations . . . . .	140
6.3 Earthquake Simulator Testing . . . . .	141
REFERENCES . . . . .	143
APPENDIX A . . . . .	145



LIST OF TABLES

<u>Table</u>	<u>Page</u>
2.1 Results for 6"x 12" Concrete Cylinder Tests . . . . .	12
2.2 Column Section Properties . . . . .	13
2.3 Girder Section Properties . . . . .	14
2.4 Vibration Properties of the Test Structure under Different Stiffness Formulations . . . . .	15
2.5 Values for Load-Deformation Curves for a Single Frame Using Elasto-Plastic Analysis . . . . .	16
3.1 Earthquake Simulator Test Program . . . . .	34
3.2 Calibration Values for Force Transducers . . . . .	35
4.1 Variation of Frequency and Damping Values throughout Test History . . . . .	56
4.2 Values of Lateral Flexibility Matrix throughout Test History . . . . .	57
4.3 Peak Values of Story Displacements, Story Shears, Base Overturning Moment through Test History . . . . .	58
5.1 Comparison of Natural Frequencies as given by Analyses and Tests . . . . .	116



## LIST OF FIGURES

<u>Figure</u>	<u>Page</u>
2.1	Test Structure and Test Arrangement on the Shaking Table . . . . . 17
2.2	Test Structure . Details of Reinforcement . . . . . 18
2.3	Test Structure on Shaking Table . . . . . 19
2.4	Typical Stress-Strain Curve of a Reinforcing Steel Bar - Average Values Obtained from Tests . . . . . 20
2.5	Stress-Strain Relationship of Wire Mesh Reinforcement - Average Values Obtained from Tests . . . . . 21
2.6	Stress-Strain Curves for Concrete . . . . . 22
2.7	Actual Reinforcement Layout of Various Sections . . . . . 23
2.8	Idealized Yield Surfaces for Column and Girder Sections . 24
2.9	Actual Dimensions, Mass Distribution and Gravity Loads of the Test Structure . . . . . 25
2.10	Elasto-Plastic Analysis Results . . . . . 26
3.1(a)	Taft 1952 N69W Accelerogram . . . . . 36
(b)	Taft Simulated Table Acceleration - Run W2 . . . . . 37
3.2	Pseudo-Velocity Response Spectra for Taft N69W, July 21, 1952 . . . . . 38
3.3	Pseudo-Velocity Response Spectra for Taft N69W, July 1952, and Table Acceleration for Runs W1, W2, and R3 . . . . . 39
3.4	Column LVDTs to Measure End Rotation, Mounting and Target Frame Details . . . . . 40
3.5	Girder LVDTs Mounting and Target Frame Details to Measure Girder End Rotation at Beam-Column Joint . . . . . 41
3.6	LVDTs, Mounted on Frame, to Measure Column End Rotation . . . . . 42
3.7	LVDTs, Mounted on Frames, to Measure Rotations at the Girder - Column Joint . . . . . 43



LIST OF FIGURES (Continued)

<u>Figure</u>	<u>Page</u>
4.1 Shear Cracks Developed in the Column after Test Run W3 . . .	59
4.2 Cracking and Spalling of Concrete at the Column-Footing Juncture . . . . .	60
4.3 Cracking and Spalling at the Bottom Story Column-Girder Juncture . . . . .	61
4.4 Crack Pattern at Junction of Top Story Column with Bottom Story Slab . . . . .	62
4.5 Vertical Table Acceleration. Run R3 . . . . .	63
4.6 Frequency Variation Throughout Test History . . . . .	64
4.7 Variation of Damping Throughout Test History as evaluated from the Measured Free Vibration Tests . . . . .	65
4.8(a) Bottom Story Relative Displacement. Runs W2 and W3 of Second Structure . . . . .	66
(b) Top Story Relative Displacement. Runs W2 and W3 of Second Structure . . . . .	67
4.9(a) Bottom Story Relative Displacement. Run W1 of Second Structure and Run W2 of First Structure. . . . .	68
(b) Top Story Relative Displacement. Run W1 of Second Structure and Run W2 of First Structure . . . . .	69
4.10(a) Bottom Story Relative Displacement. Run W3 of Second Structure and Run W6 of First Structure . . . . .	70
(b) Top Story Relative Displacement. Run W3 of Second Structure and Run W6 of First Structure . . . . .	71
4.11(a) Bottom Story Relative Displacement. Runs R1 of Second and First Structures . . . . .	72
(b) Top Story Relative Displacement. Runs R1 of Second and First Structures . . . . .	73
4.12(a) Bottom Story Relative Displacement. Runs R2 of Second and First Structures . . . . .	74
(b) Top Story Relative Displacement. Runs R2 of Second and First Structures . . . . .	75



LIST OF FIGURES (Continued)

<u>Figure</u>	<u>Page</u>
4.13(a) Bottom Story Relative Displacement. Runs R3 of Second and First Structure . . . . .	76
(b) Top Story Relative Displacement. Runs R3 of Second and First Structure . . . . .	77
4.14(a) Bottom Story Relative Displacement. Runs W2 and R2 of Second Structure . . . . .	78
(b) Top Story Relative Displacement, Runs W2 and R2 of Second Structure . . . . .	79
4.15(a) Bottom Story Relative Displacement. Runs W3 and R3 of Second Structure . . . . .	80
(b) Top Story Relative Displacement. Runs W3 and R3 of Second Structure . . . . .	81
4.16(a) Bottom Story Relative Displacement. Runs R2 and R3 of Second Structure . . . . .	82
(b) Top Story Relative Displacement. Runs R2 and R3 of Second Structure . . . . .	83
4.17 Peak Values of Relative Story Displacements Attained Throughout Test History. Yield and Collapse Values Obtained by Elasto-Plastic Analysis . . . . .	84
4.18 Peak Story Shears Attained Throughout Test History. Yield & Collapse Values Obtained using Elasto-Plastic Analysis . . . . .	85
4.19 Peak Base Overturning Moments Attained Throughout Test History. Yield and Collapse Levels Obtained by an Elasto-Plastic Analysis . . . . .	86
4.20 Average Bottom Story Shear per Column. Run W1. Acceleration Records vs Force Transducers . . . . .	87
4.21(a) Average Bottom Story Shear per Column. Run W2. Acceleration Records vs Force Transducers, Northside Columns . . . . .	88
(b) Average Bottom Story Shear per Column. Run W2. Acceleration Records vs Force Transducers. Southside Columns . . . . .	89



LIST OF FIGURES (Continued)

<u>Figure</u>	<u>Page</u>
4.22(a) Average Bottom Story Shear per Column. Run W3. Acceleration Records vs Force Transducers. Northside Columns . . . . .	90
(b) Average Bottom Story Shear per Column. Run W3. Acceleration Records vs Force Transducers. Southside Columns . . . . .	91
4.23 Bottom Story average Shear per Column. Run W3. Northside vs Southside . . . . .	92
4.24 Average Bottom Story Shear per Column. Run R3. Northside vs Southside . . . . .	93
4.25 Load-Deformation Relationship. Actual Static Test Results . . . . .	94
4.26 Deformation of Structure Midway through the Static Test . . . . .	95
4.27 Damage Pattern at Bottom Story Girder - Column Joint . .	96
4.28 Transverse View of Frame Showing Pattern and Extent of Cracking of Columns . . . . .	97
4.29 Extension and Widening of the Vertical Cracks, which Developed in the Column during Dynamic Testing, Shown Midway Through the Static Test . . . . .	98
4.30 Girder - Column Joint. Extent of Damage . . . . .	99
4.31 Damage of Columns towards Loading Actuator after "Functional" Failure . . . . .	100
4.32 Damage of Slab above Transverse Girder . . . . .	101
4.33 Transverse Girder which "Failed" due to Fracture of Reinforcement . . . . .	102
5.1 Bilinear Model (Model B) . . . . .	117
5.2 Correlation for Run W1. Top Story Displacement. Model B . . . . .	118
5.3 Correlation for Run W1. Top Story Displacement. Model B . . . . .	119



LIST OF FIGURES (Continued)

<u>Figure</u>	<u>Page</u>
5.4	Correlation for Run W1. Top Story Displacement. Model B Including Stiffness Deterioration Mechanism . . . . . 120
5.5	Correlation for Run W1. Top Story Displacement. Model B Including Stiffness Deterioration Mechanism . . . . . 121
5.6	Bilinear Stiffness Degrading Model (Model D). . . . . 122
5.7	Correlation for Run W2. Top Story Displacement. Model D . . . . . 123
5.8	Correlation for Run W3. Top Story Displacement. Model D . . . . . 124
5.9	Bilinear, Stiffness Degrading and Deteriorating Models (Models E and F) . . . . . 125
5.10	Correlation for Run W2. Top Story Displacement. Model E . . . . . 126
5.11	Correlation for Run W2. Top Story Displacement. Model E . . . . . 127
5.12	Correlation for Run W2. Top Story Displacement. Model E . . . . . 128
5.13	Correlation for Run W3. Top Story Displacement. Model E . . . . . 129
5.14	Correlation for Run W3. Top Story Displacement. Model E . . . . . 130
5.15	Correlation for Run W2. Top Story Displacement. Model F . . . . . 131
5.16	Correlation for Run W3. Top Story Displacement. Model F . . . . . 132
5.17	Correlation for Run W3. Cracked Section Properties. Top Story Displacement. Model F . . . . . 133
5.18	Correlation for Run W3. Cracked Section Properties. Top Story Displacement. Model F . . . . . 134
5.19	Correlation for Run W10, First Structure. Cracked Section Properties. Model F . . . . . 135



LIST OF FIGURES (Continued)

<u>Figure</u>		<u>Page</u>
5.20	Correlation for Run W2. Top Story Displacement. Cracked Section Properties. Model F. . . . .	136
5.21	Correlation for Run W2. Cracked Section Properties. Top Story Displacement. Model F. . . . .	137



## 1. INTRODUCTION

### 1.1 BACKGROUND

The investigation described in this report is part of the research program "Energy Absorption Characteristics of Structural Systems Subjected to Earthquake Excitation," which has been in progress at the Earthquake Engineering Research Center since the organization of that research unit. The specific objective of the research described herein was to continue the study of reinforced concrete frames subjected to simulated earthquake motions by the EERC shaking table.

The first stage of this study which involved the design, construction and testing of a two-story concrete frame structure was described completely by Pedro Hidalgo<sup>(1)</sup>. That test served as a pilot model for the earthquake simulator testing of reinforced concrete frames, and it demonstrated conclusively

(1) that typical structures could be subjected to base motions intense enough to cause significant damage, and

(2) that dynamic response data could be obtained which would serve to verify the validity of assumed mathematical models and analytical procedures.

However, two features of that test were not typical of expected field conditions, as follows:

(1) The most prominent damage observed in the first test structure was a crack in the first floor slab above the transverse girder, extending the full width of the structure; subsequent examination revealed that the crack resulted from a construction error--the wire mesh in the slab having been terminated at this section.

(2) The testing sequence which had been adopted for the first structure provided a gradual increase of earthquake intensity, requiring five tests to proceed from the weakest to the strongest level of excitation. Thus the strongest shake was applied to a structure which already had been significantly damaged by the preceding tests and it is believed that this damage had an important effect on the resulting response behavior.

These deviations from normal conditions suggested that a second test should be performed on another frame built in accordance with the design plans and specifications of the first test structure. In this second frame, the construction would be inspected continuously, and the testing sequence would be planned to apply a maximum intensity earthquake to an essentially undamaged structure. This present report describes the construction and testing of Frame 2. It is an independent report, giving complete experimental results and a full account of the correlation of analysis with experiment. However, because of the great similarity between Frames 1 and 2, extensive reference is made here to the report on the testing of Frame 1<sup>(1)</sup> in order to avoid excessive duplication. In general only specific differences between the construction and tests of Frames 1 and 2 are discussed in detail here. The organization of this report follows its predecessor in order to emphasize and take advantage of the similarities between the two studies.

## 1.2 REVIEW OF OTHER RESEARCH

An extensive list of references to research work related to the seismic response of concrete frames was given by Hidalgo<sup>(1)</sup>, together with brief descriptive comments on each entry. Similar references and comments on work which has appeared since that report was written (1973) are presented here.

### 1.2.1 Dynamic Tests

K. Muto, T. Hisada, M. Yamamoto, T. Tsugawa, S. Bessho of the Kajima Corporation in Japan (1973), carried out experimental studies to improve reinforcement procedures for concrete structures. The reinforcing method was intended to be applicable to field construction. From the point of view of damage control, they established necessary seismic criteria for structural design.

R. Shepherd and D. A. Ross (1973) tested a full scale reinforced concrete frame, subjected to lateral loading into the inelastic range. The inelastic structural behavior was induced dynamically using an exciter mounted on a frame. The dynamic lateral load at which significant inelastic behavior was induced was found to be significantly less than the equivalent static load on which the elastic seismic design was based. The frame also exhibited marked torsional response despite the fact that the excitation was applied along the plan center line of the slabs.

### 1.2.2 Dynamic Analysis

R. D. Sharpe and A. J. Carr (1974) describe the problems encountered in writing a comprehensive computer program with which the deformation sensitivity of a two dimensional inelastic frame can be measured. These difficulties arise from the fact that there is a need to simplify computer input data, as well as the selection of an economic and accurate numerical integration technique which can remain stable over a reasonable and realistic frequency range. The difficulties met in designing a beam model for the moment-curvature relationship are also described and a recommendation made as to the method that can best be used. The sensitivity of the frames to modelling is also discussed.



## 2. THE TEST STRUCTURE

### 2.1 SELECTION AND DESIGN OF TEST STRUCTURE

The basis for selection and design of the test structure was that described for Frame 1<sup>(1)</sup>, except that the defect in the slab reinforcement would be avoided for Frame 2 by adequate inspection during construction. However, for convenience, the principal features of the test structure will be described again here.

Figures 2.1 and 2.2 show the dimensions, reinforcing, and general arrangement of the test structure, which was intended to represent a two-bay segment of a long narrow building subjected to an earthquake in the short axis direction. For economy and convenience in testing, it was built to a length scale of 0.7; in addition, the span in the direction perpendicular to the excitation axis was reduced drastically. Other deviations of the test structure from the prototype configuration were the introduction of force transducers at mid-height in each column, and the addition of heavy concrete weights on each floor. The force transducers were intended to provide direct measurements of the dynamic axial force, shear, and moment developed in the columns during the test; their location at mid-height insured that they would not influence the dynamic response behavior. The weights served to increase the forces induced during the test, and also to provide an appropriate frequency of vibration in the model.

In addition, 1"  $\phi$  steel cable bracing (shown in Fig. 2.1) was provided in the transverse direction to constrain the structure against transverse or torsional motion. These cables were tightened enough to prevent out-of-plane motions, but did not induce any significant static

or dynamic stresses in the columns. Figure 2.3 shows the test structure mounted on the shaking table ready for testing.

## 2.2 MATERIAL PROPERTIES

Sample specimens of both the reinforcing steel and the concrete were tested to determine their structural properties. Average stress-strain curves were then constructed for each type of material, and these average properties were used in establishing the mathematical models formulated to represent the structure in computer analyses. Test data obtained for each type of material are discussed in the following paragraphs.

### (a) Reinforcing Bars

Figure 2.4 is the stress-strain curve obtained in testing a typical bar of the ASTM A615 grade 40 reinforcing steel used in the test frame. Also tabulated in the figure are the yield stress, ultimate strength, and other relevant properties measured in each bar test. All bars were deformed except the #2 bars which were used for ties and stirrups.

### (b) Wire Mesh Reinforcement

Both floor slabs were reinforced with 4"x4" welded wire mesh. During tensile tests of the mesh, it was found to be quite brittle, generally breaking at the welded intersection points. Also it was found that the strength of the mesh used in Frame 2 was noticeably lower than that used in Frame 1. A typical stress-strain curve, the corresponding idealized curve, and average values obtained from the wire mesh tests are shown in Fig. 2.5.

### (c) Concrete

The readymix concrete used in the test structure was proportioned to provide 4000 psi compressive strength. Six 6"x12" test cylinders

were cast during the concreting of the structure, and were stored in conditions similar to those of the test structure. These were subjected to compressive stress-strain tests just before the shaking table test of the frame was performed. Stress and strain properties measured during these tests are listed in Table 2.1, together with average values for all the tests.

Stress-strain curves obtained from these cylinder tests are shown in Fig. 2.6. Also shown on this graph is Hognestad's parabolic curve<sup>(2)</sup> which was used in the analysis to approximate the stress-strain behavior. Note that the ultimate strain assumed for analysis was

$$\epsilon_{c \text{ ult}} = 0.005 .$$

### 2.3 SECTION PROPERTIES

The effective cross-section properties of the test structure column and girders were evaluated on the basis of three different behavior hypotheses, as follows:

#### (a) Transformed Area Section

In this case, the concrete is assumed to function as a linear elastic material in both tension and compression, with a modulus of elasticity  $E_c$ . The steel in the section is assumed to contribute additional stiffness in accordance with its transformed area  $A_s(n-1)$ , where  $A_s$  is the actual area of steel and  $n = E_s/E_c$  in which  $E_s$  is the modulus of elasticity of steel.

#### (b) Gross Section

In this case, the concrete is assumed to contribute in tension and compression but no additional stiffness is attributed to the steel.

(c) Cracked Area Section

In this case, the concrete is assumed to function in compression, but not in tension. No additional stiffness in compression is attributed to the steel, but it is assumed fully effective in tension.

Based on these hypotheses and using the properties measured for the steel and concrete materials, the effective section properties of both columns and girders were calculated. The actual locations of the steel in the sections (as measured before pouring of the concrete) shown in Fig. 2.7 were used in these calculations. Details of the calculations are shown in Appendix A; results are listed in Tables 2.2 and 2.3. Cracked section yield moments for the girders were evaluated taking account of the wire mesh reinforcement in the slab. The mesh contributed little to the positive moment capacity, but made a significant difference in the negative yield moment at which tensile yield occurs in the top layer of steel. For use in a computer program which does not distinguish between moment of inertia values corresponding to the positive and negative values of the yield moments, the moment of inertia of the cracked section was defined to be the average of these values. Idealized yield surfaces for the columns and bilinear moment-curvature relations for the girders are shown in Fig. 2.8.

2.4 STRUCTURAL PROPERTIES

The dimensions of the test frame were measured, and its dead weight as well as the weight of the concrete blocks supported by the floor slabs were evaluated before the test program was initiated. Results of these measurements, shown in Fig. 2.9, were used in calculating the stiffness and vibration properties of the structure.

Based on these dimensions and the section properties discussed

above, the flexibility coefficients of the frame and its vibration mode shapes and frequencies were calculated. Three sets of results were obtained corresponding to the three hypotheses used in evaluating the section properties: gross, transformed area, and cracked sections. The basic section properties and corresponding frame property results are listed in Table 2.4. It should be noted that the frequencies were evaluated for the structure without the concrete blocks added; the column lengths were measured with the force transducers installed.

In addition to the frame's vibration properties, its static load carrying capacity also was evaluated. For this purpose, a computer program based on a simple elastic - perfectly plastic moment yield mechanism was used<sup>(3)</sup>. The plastic moments assumed for the girder sections were their ultimate capacities calculated using an ultimate strain in the concrete of  $\epsilon_{c_{ult}} = 0.005$ . Contributions of both compression steel and slab mesh were included in the analyses. The yield moment capacity of the column sections was determined including the effect of axial force. The axial force used for this purpose was that produced by the dead load, plus the maximum dynamic load achieved during the test program. Details of the evaluation of these yield moment capacities are presented in Appendix A.

Two different analyses of static load capacity were carried out using these member moment capacities, for the two cases discussed in the following paragraphs:

#### Case 1

This was intended to approximate the strength of the frame during its earthquake simulator testing. Loads applied to the structure in the computer program included the gravity loads of Fig. 2.9 combined with a first mode distribution of lateral loads. If an assumed unit

lateral load was applied at the first floor level, the corresponding load at the top floor was given by the ratio

$$\frac{M_T \phi_{T1}}{M_B \phi_{B1}} = \frac{(0.0352)(1.000)}{(0.0572)(0.553)} = 1.13$$

in which  $M$  is the story mass,  $\phi_1$  is the first mode shape, and the subscripts T and B refer to the top and bottom stories, respectively. The initial yield and collapse values of the story shears, moments and displacements computed by this program are discussed in Chapter 4.

### Case 2

After the structure had been tested on the earthquake simulator, repaired and then tested again, it was subjected to a final static test to determine its ultimate load carrying capacity. In this final phase of testing, the concrete blocks were taken off the structure, and also the force transducers were removed to avoid any possible damage to them. Accordingly in the second case considered by the elasto-plastic frame analysis program, the dead load and column lengths of the frame were adjusted appropriately. Results of this analysis are presented in Fig. 2.10 which shows both the lateral load capacity and the order of appearance of plastic hinges as predicted by the computer program. In addition, the load-deformation behavior calculated for both cases 1 and 2 is listed in Table 2.5. Correlation of these analytical results with the observed static test behavior is discussed in Chapter 4.

## 2.5 CONSTRUCTION AND REPAIR OF TEST STRUCTURE

In most respects, the construction of Frame 2 was similar to that of Frame 1 as described in Reference 1. A major difference was that care was taken to ensure that the wire mesh in the floor slabs was

extended over the top of the transverse girders, to avoid the slab cracking over the girder which was so prominent in Frame 1. A second important difference was that special care was taken in curing Frame 2 to avoid shrinkage cracks. The model was kept in the laboratory under controlled temperature conditions and the forms were not stripped before 28 days. Testing was then started within three weeks, with the result that the frame was essentially free of cracks and consequently very stiff at the beginning of testing. At that time it was decided that this nearly perfect structure was not typical of normal construction in the field. A typical structure would have numerous minor cracks due to shrinkage and variable live loads, which would reduce its stiffness. Accordingly Frame 2 was subjected to a small intensity earthquake as the first step in its testing sequence; this caused sufficient cracking so that its stiffness was then representative of normal field conditions.

After completion of the first major test sequence, the test frame was removed from the shaking table and repaired by epoxy injection. The repair technique was the same as that employed with Frame 1, and is described in Reference 1.

TABLE 2.1 RESULTS FOR 6" x 12" CONCRETE CYLINDER TESTS

LOADING RATE = 1000 lbs/sec.

SPECIMEN NUMBER	AGE OF SPECIMEN (DAYS)	$f'_c$ (psi)	$\epsilon_{co}$ (in/in)	$\epsilon_{0.45f'_c}$ (in/in)	$E_c = \frac{0.45f'_c}{\epsilon_{0.45f'_c}}$ (ksi)
1	91	4465	0.00330	0.000750	2680
2	91	4395	0.00344	0.000745	2610
3	91	4430	0.00338	0.000755	2640
4	91	4465	0.00350	0.000780	2580
5	91	4320	0.00330	0.000750	2590
6	91	4285	0.00318	0.000700	2760
AVERAGE VALUES FOR ANALYTICAL STUDIES		4395	0.00335		2640

TABLE 2.2 COLUMN SECTION PROPERTIES

YIELD SURFACE PROPERTIES (1)							TRANSF. AREA (2)		GROSS-SECTION (3)	
$P_o$ (kips)	$P_T$ (kips)	$P_B$ (kips)	$M_B$ (in-kips)	$M_o$ (in-kips)	$\phi_y$ (1/in)	$I_{CR}$ (in <sup>4</sup> )	$A_{TR}$ (in <sup>2</sup> )	$I_{TR}$ (in <sup>4</sup> )	$A_g$ (in <sup>2</sup> )	$I_g$ (in <sup>4</sup> )
260.9	51.5	98.4	352.1	148.8	0.000354	159.0	61.25	371.6	48.88	294.3

(1) Compression reinforcement included in computations  
 cracked section assumed, i.e. concrete does not contribute in tension

$$\text{cracked section moment of inertia} = I_{CR} = \frac{M_o}{E_c \phi_y}$$

(2) Transformed area section assumes concrete contributing in tension

$$E_c = 2640 \text{ ksi} \quad E_s = 29000 \text{ ksi} \quad n = 10.98$$

(3) Gross section neglects contribution of steel.

TABLE 2.3 GIRDER SECTION PROPERTIES

SLAB WIRE MESH REINFORCEMENT INCLUDED											
STORY	YIELD SURFACE PROPERTIES (1)									TRANSFORMED AREA (2)	GROSS SECTION (3)
	TENSION AT BOTTOM FIBRE			TENSION AT TOP FIBRE			$I_{CR.AVG}$ (in <sup>4</sup> )				
	$M_Y^+$ (in-k)	$\phi_y^+$ (1/in)	$I_{CR}^+$ (in <sup>4</sup> )	$M_Y^-$ (in-k)	$\phi_y^-$ (1/in)	$I_{CR}^-$ (in <sup>4</sup> )					
TOP	205.5	0.000246	317.0	640.0	0.000400	575.0	446.0	1650.0	1440.0		
BOTTOM	232.1	0.000177	497.0	720.0	0.000400	670.0	583.5	1749.0	1440.0		

(1) Compression reinforcement included in computations.  
Cracked section assumed i.e. concrete does not contribute in tension.

$$\text{Cracked Moment of Inertia } I_{CR} = \frac{M_Y}{E_C \phi_C} ; I_{CR.AVG} = 1/2 (I_{CR}^+ + I_{CR}^-)$$

(2) Transformed area section assumes concrete contributing in tension.

$$E_C = 2640 \text{ ksi}, E_S = 29000 \text{ ksi}, n = 10.98.$$

(3) Gross section neglects the contribution of steel.

TABLE 2.4 VIBRATION PROPERTIES OF THE TEST STRUCTURE  
 UNDER DIFFERENT STIFFNESS FORMULATIONS  
 (STRUCTURE WITHOUT CONCRETE BLOCKS)

$$E_c = 2640 \text{ KSI}$$

			STIFFNESS FORMULATION		
			GROSS SECTION	TRANSFORMED AREA SECTION	CRACKED SECTION
I (in <sup>4</sup> )	TOP STORY	COLUMN	294.3	371.60	159.0
		GIRDER	1440.0	1650.0	446.0
	BOTTOM STORY	COLUMN	294.3	371.6	159.0
		GIRDER	1440.0	1749.0	583.5
FIRST MODE	NATURAL FREQUENCY (Hz)		6.66	7.42	4.63
		$\phi_{T1}$	1.000	1.000	1.000
		$\phi_{B1}$	0.499	0.495	0.476
SECOND MODE	NATURAL FREQUENCY (Hz)		18.28	20.36	13.09
		$\phi_{T2}$	1.000	1.000	1.000
		$\phi_{B2}$	-1.826	-1.842	-1.920
FLEXIBILITY MATRIX COEFFICIENTS (in/kip)		$F_{BB}$	0.0124	0.0099	0.0240
		$F_{BT}$	0.0145	0.0116	0.0294
		$F_{TT}$	0.0347	0.0280	0.0730
		$F_{TT}/F_{BB}$	2.800	2.820	3.042
		$F_{BT}/F_{BB}$	1.170	1.172	1.225

TABLE 2.5 VALUES FOR LOAD-DEFORMATION CURVES FOR  
A SINGLE FRAME USING ELASTO-PLASTIC ANALYSIS

BASE SHEAR V (kips)	LOAD FACTOR γ (kips)	DISPLACEMENTS (inches)		PLASTIC HINGE NUMBER
		BOTTOM STORY	TOP STORY	
CASE 1 (*)				
7.045	3.334	0.380	0.744	1
7.588	3.591	0.426	0.819	2
8.346	3.950	0.508	0.940	3
9.000	4.260	0.791	1.266	4
9.061	4.289	0.818	1.300	5
9.276	4.390	0.927	1.450	6
CASE 2 (*)				
7.650		0.452	1.126	1
7.781		0.460	1.154	2
7.961		0.477	1.199	3
8.226		0.537	1.303	4
8.502		0.599	1.426	5
8.567		0.615	1.480	6

(\*) Cases 1 and 2 are explained in Fig. 2.10.



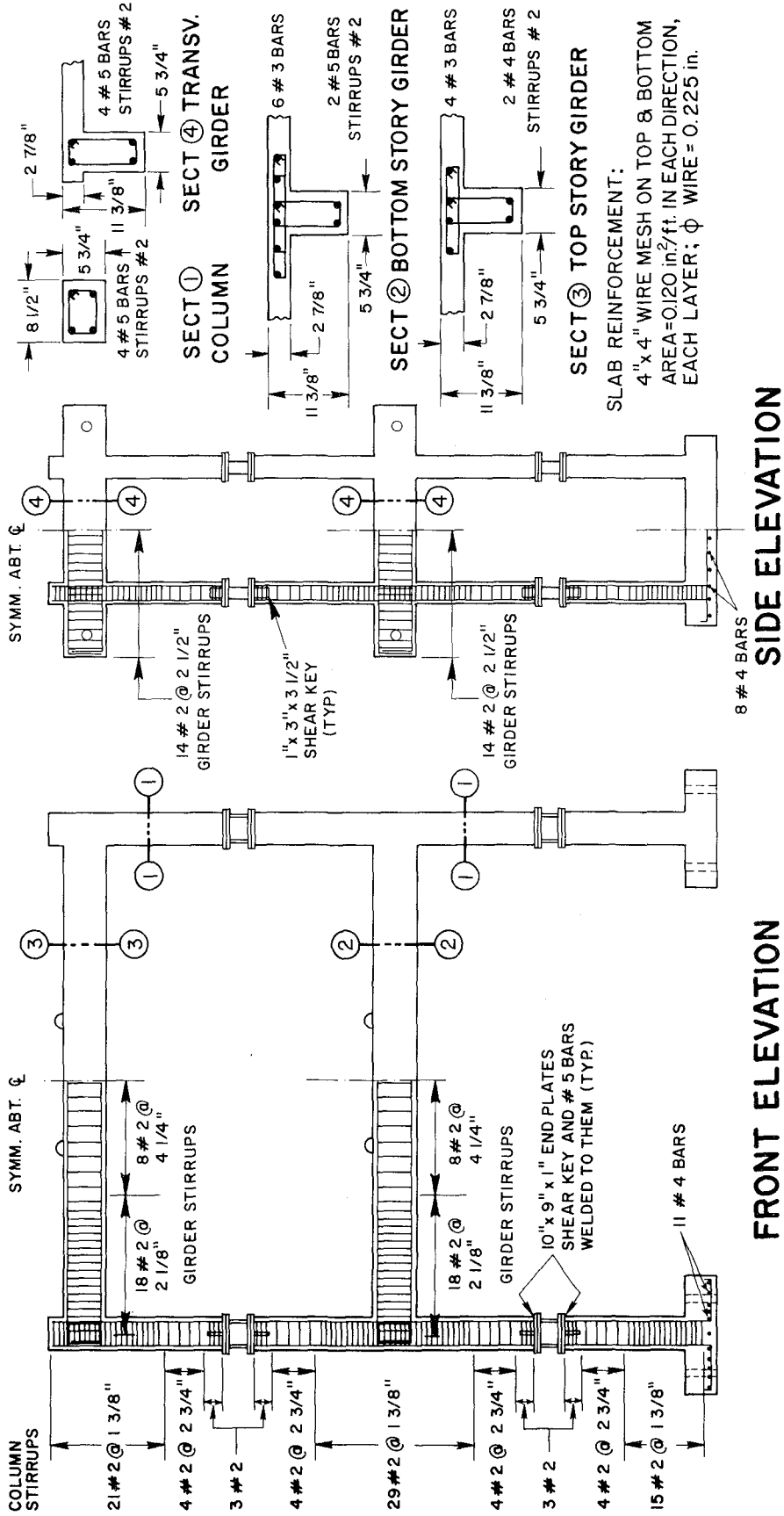


Fig. 2.2 TEST STRUCTURE - DETAILS OF REINFORCEMENT

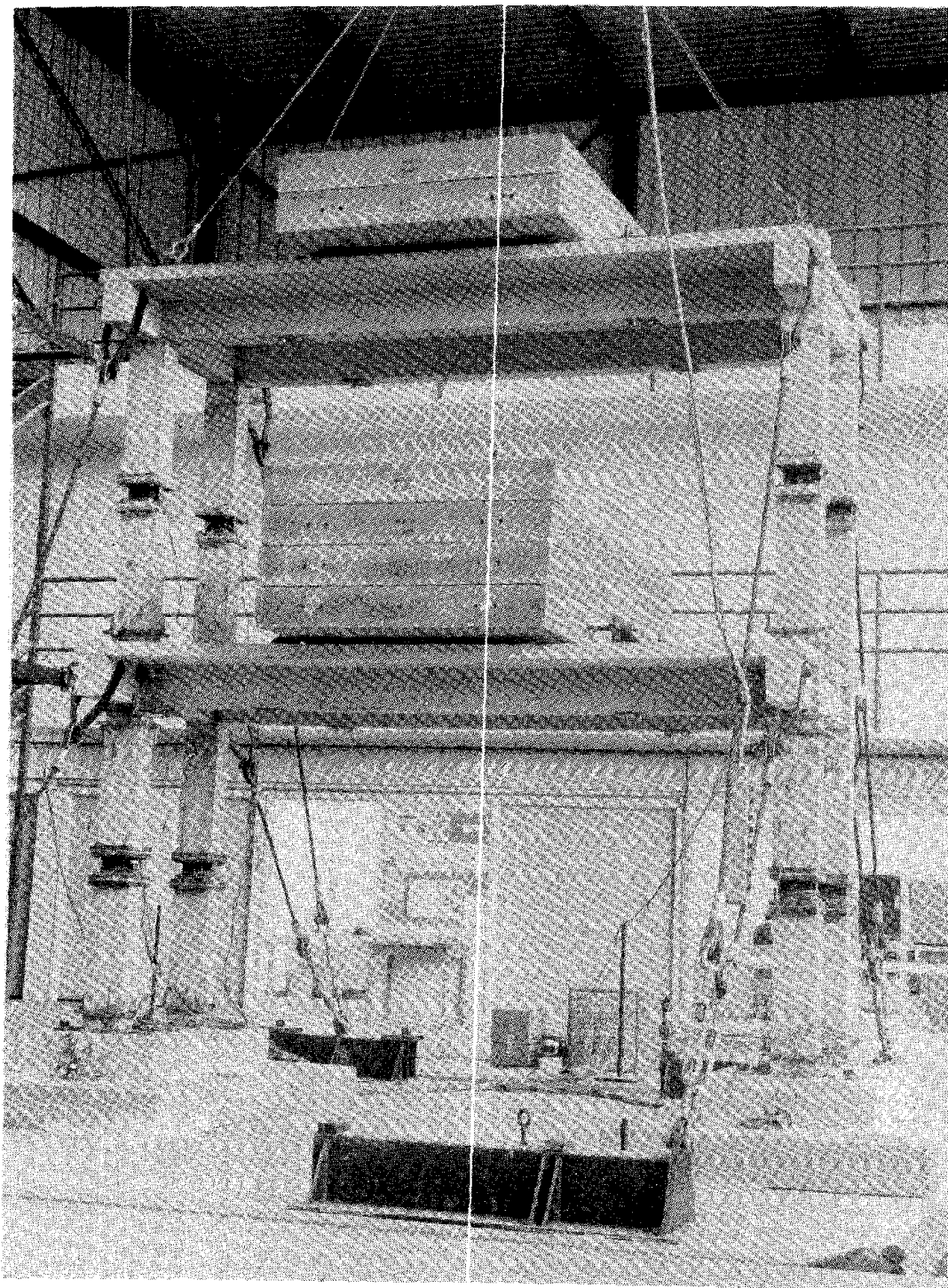


Fig. 2.3 TEST STRUCTURE ON SHAKING TABLE

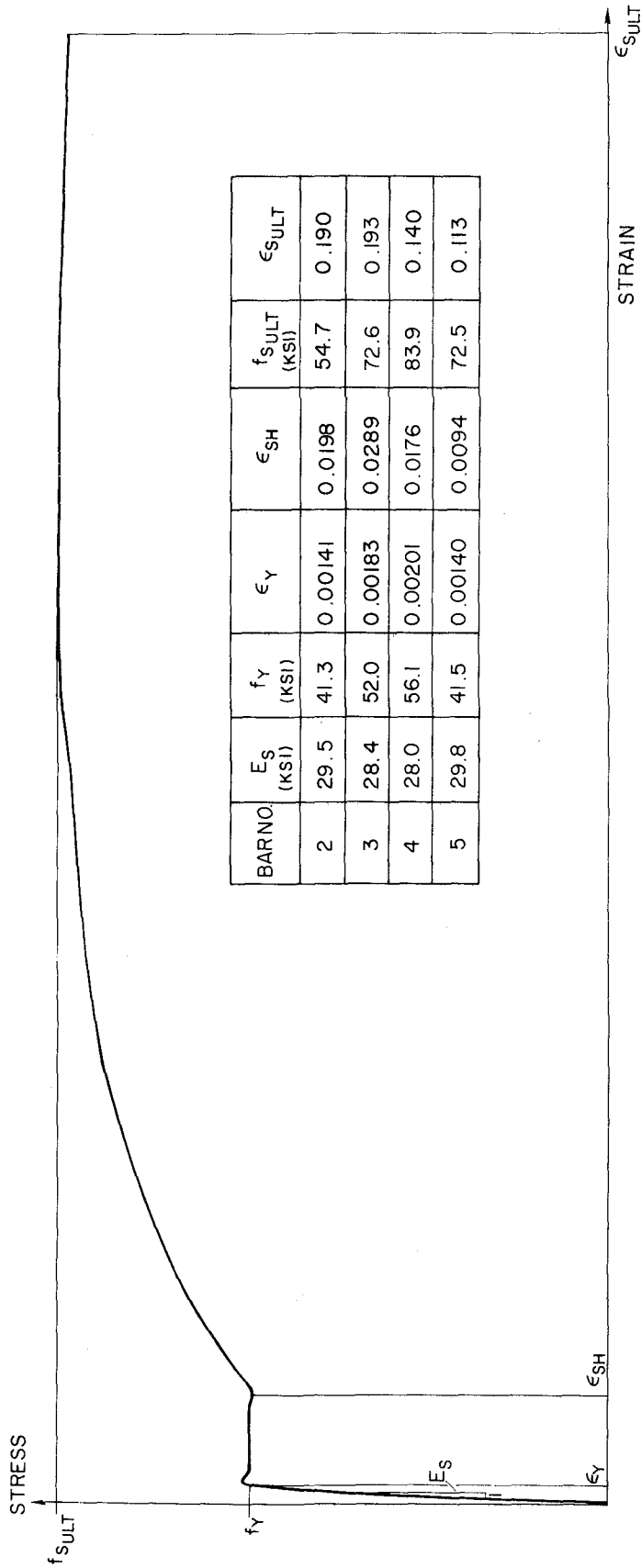


Fig. 2.4 TYPICAL STRESS-STRAIN CURVE OF A REINFORCING STEEL BAR.  
AVERAGE VALUES OBTAINED FROM TESTS.

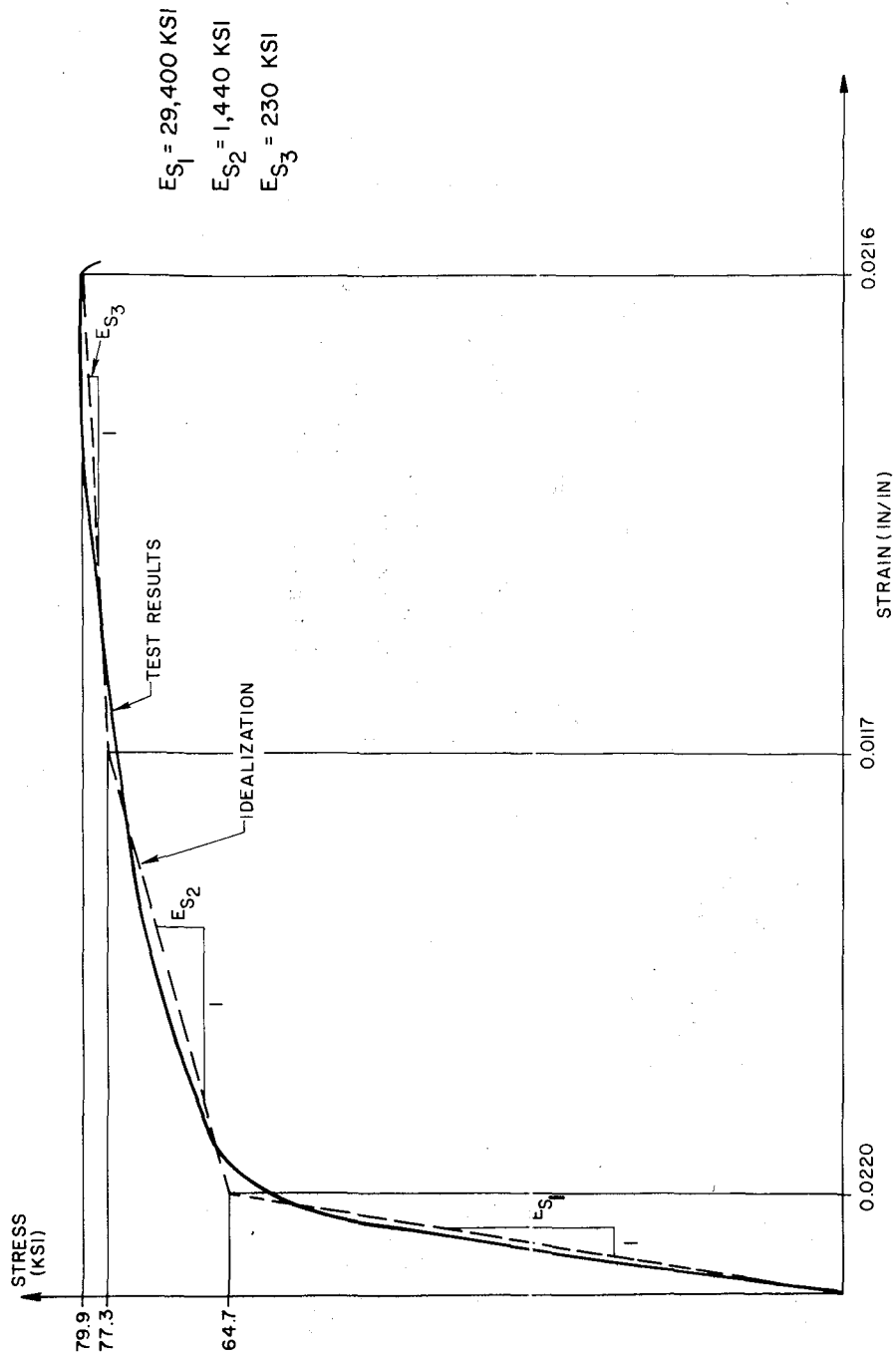


Fig. 2.5 STRESS-STRAIN RELATIONSHIP OF WIRE MESH REINFORCEMENT. AVERAGE VALUES OBTAINED FROM TESTS.

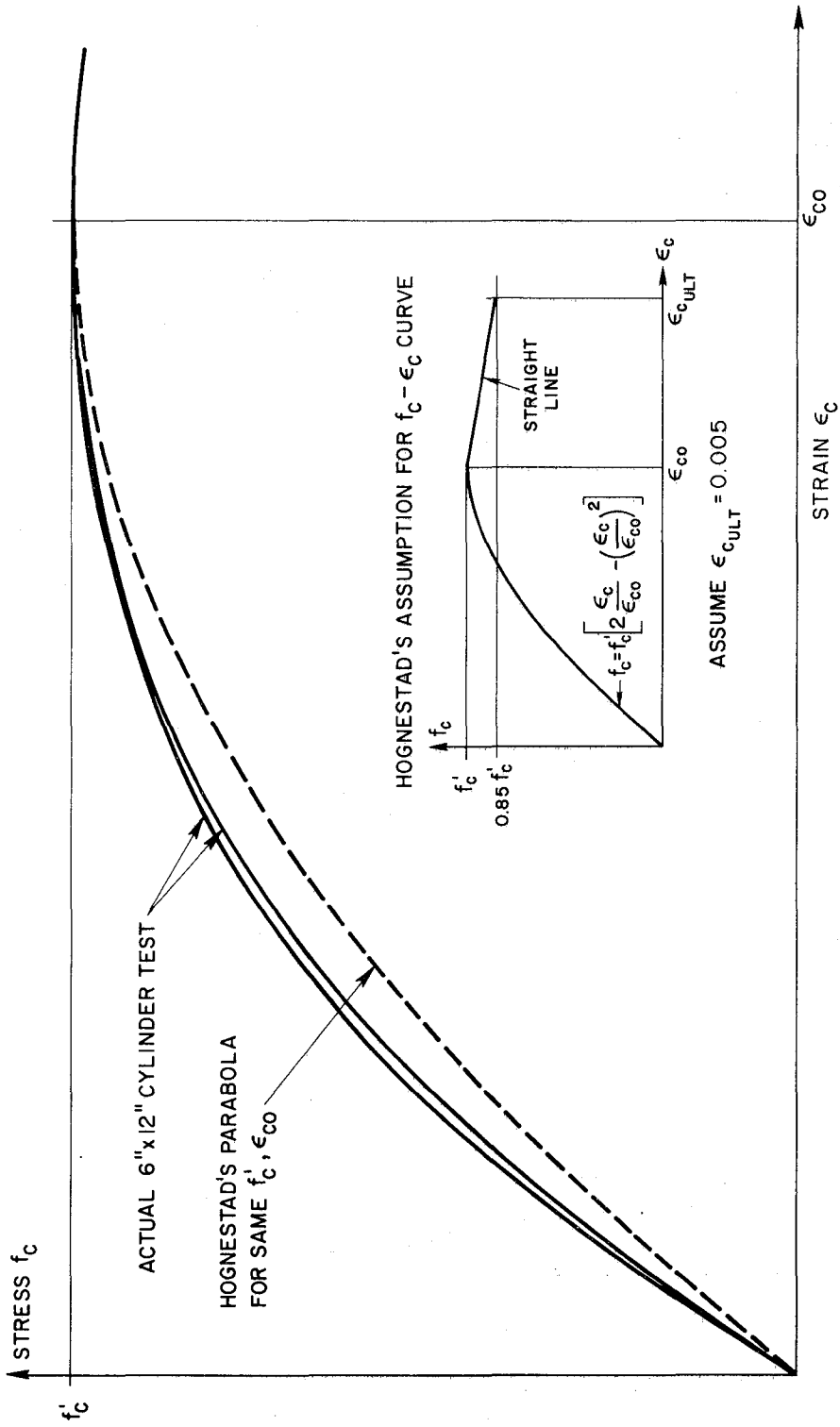
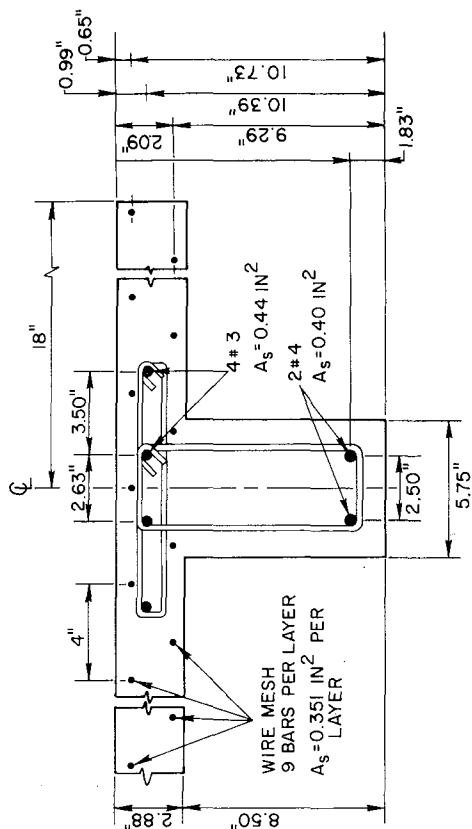
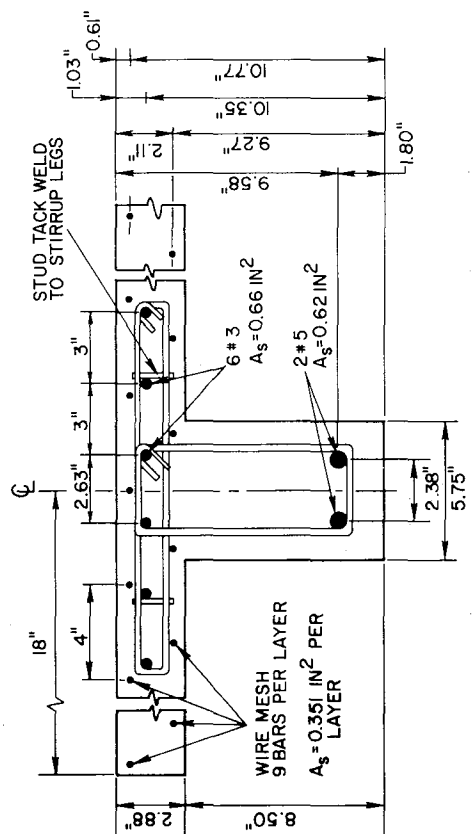


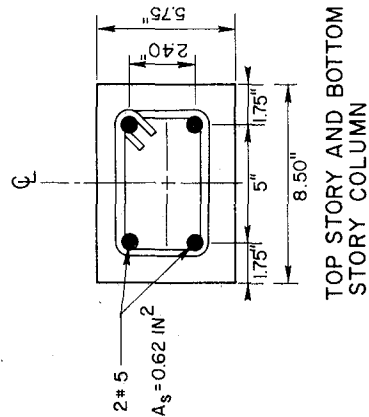
Fig. 2.6 STRESS-STRAIN CURVES FOR CONCRETE



TOP STORY GIRDER



BOTTOM STORY GIRDER



TOP STORY AND BOTTOM STORY COLUMN

Fig. 2.7 ACTUAL REINFORCEMENT LAYOUT OF VARIOUS SECTIONS.

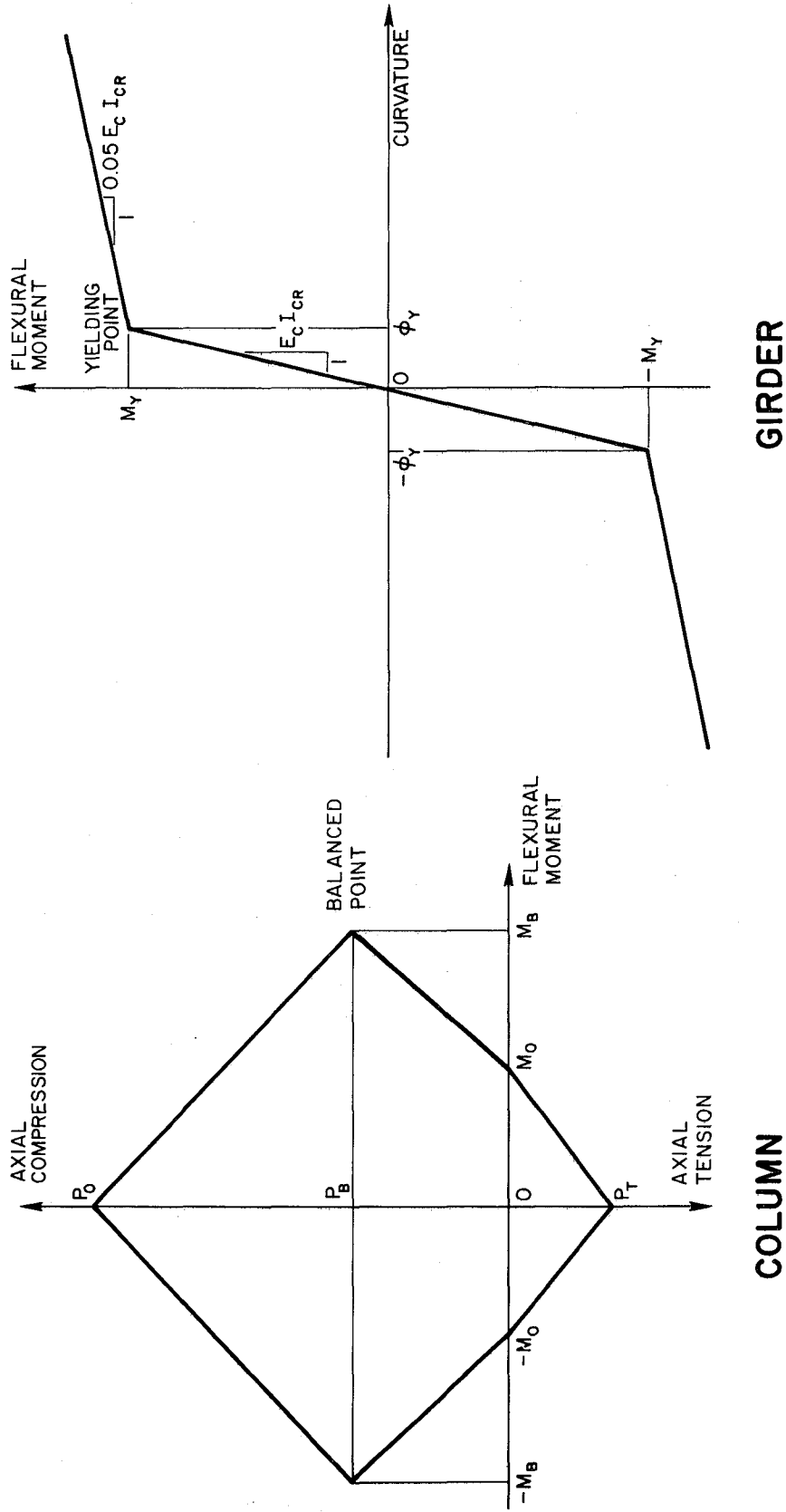
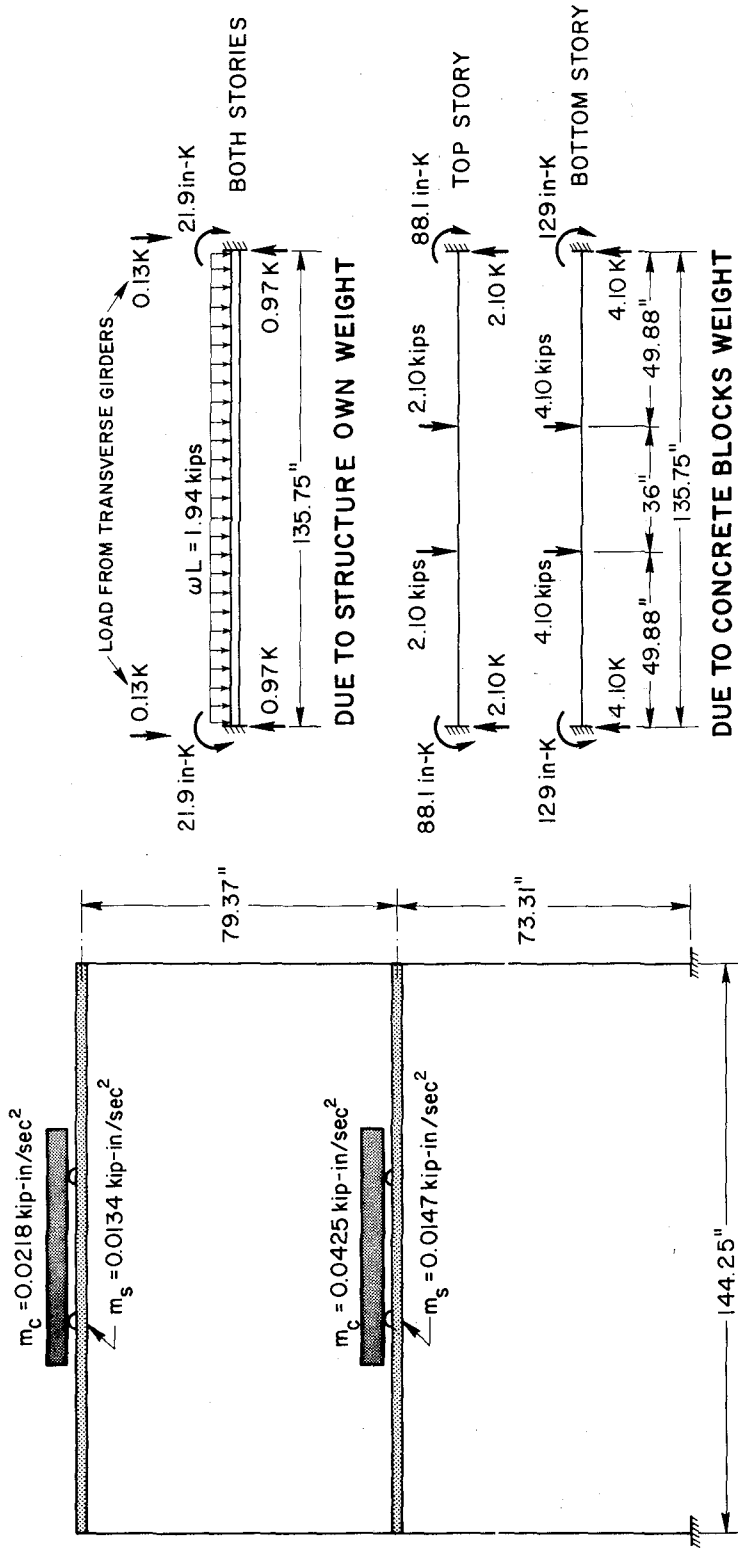


Fig. 2.8 IDEALIZED YIELD SURFACES FOR COLUMN AND GIRDER SECTIONS.

GIRDER

COLUMN



**GRAVITY LOAD FOR EACH GIRDER**

ASSUME CLEAR DISTANCE DIMENSIONS TO COMPUTE MOMENTS

**STRUCTURE IDEALIZATION**

ASSUME AXIS TO AXIS DIMENSIONS FOR STRUCTURAL ANALYSIS

$m_s$  = STRUCTURE STORY MASS, ASSUMED TO BE LUMPED AT FLOOR LEVEL

$m_c$  = MASS FROM CONCRETE BLOCKS AND ATTACHEMENTS

Fig. 2.9 ACTUAL DIMENSIONS, MASS DISTRIBUTION AND GRAVITY LOADS OF THE TEST STRUCTURE.

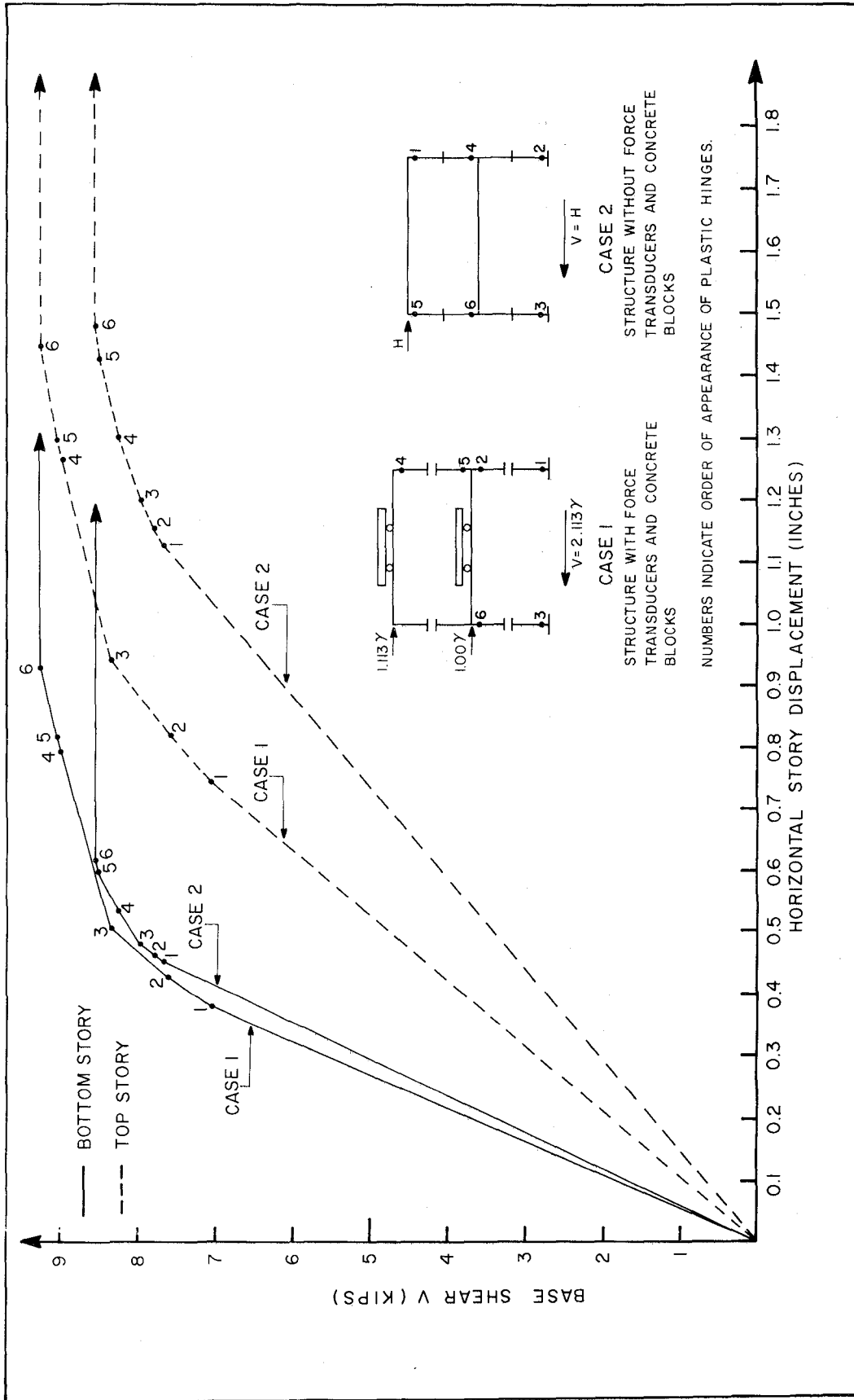


Fig. 2.10 ELASTO PLASTIC ANALYSIS RESULTS

### 3. TEST PROCEDURES AND INSTRUMENTATION

#### 3.1 EARTHQUAKE EXCITATION

The ground motion used for the testing of Frame 1 was the N69W accelerogram recorded at Taft during the Arvin-Tehachapi earthquake of 1952. In general, the generated response in the test structure seemed to be suitable, so it was also selected as the basic excitation of Frame 2. However as was mentioned earlier (see section 1.1), the extended sequence of shakes with gradually increasing intensity which was adopted for testing of Frame 1 did not seem to be a realistic form of excitation. Instead for Frame 2 a very high intensity earthquake was applied directly to the undamaged structure.

The test sequence included a preliminary very low intensity shake which was intended to induce a normal degree of cracking in the frame, and thus to reduce its stiffness to a representative level. The change of stiffness which occurred during this test induced an interesting response which is discussed in Chapter 5. The intensity of excitation for the major earthquake input was determined on the basis of experience gained in testing Frame 1. From those earlier results, it appeared that the Taft earthquake with a peak acceleration of 50 to 60 percent of gravity could cause extensive damage; it was predicted that this intensity would be obtained with a control "span" setting of 850. For completeness, this first high intensity quake was followed by a second one of similar intensity simulating a severe aftershock in the field. A comparison of the results of these two tests would demonstrate how the stiffness of a structure before an earthquake can influence the behavior of the structure during the earthquake. The control span

settings and the peak input accelerations obtained in the tests of Frame 2 are listed in Table 3.1. The accelerogram of the actual Taft earthquake record and of the table motions induced using the Taft record and a span setting of 850 are shown in Fig. 3.1. The response spectra for the corresponding accelerogram and the table motions are shown in Figs. 3.2 and 3.3, respectively. Slight differences are apparent in the shapes of the spectra; also the great increase of the test intensity over the recorded motion is obvious.

After the second high intensity test, the frame was repaired by epoxy injection and was then subjected to a second sequence of tests similar to those applied before repair. The control span settings and peak input accelerations of these tests are also listed in Table 3.1.

### 3.2 INSTRUMENTATION

The instrumentation used in testing Frame 2 was basically similar to that used with the first frame<sup>(1)</sup>. Hence only the various types of transducers employed, and the changes that were made from the instrumentation of Frame 1 are described.

#### 3.2.1 Accelerometers

Three accelerometers were attached to the floor slabs of the frame to measure horizontal accelerations developed during the tests. Two were mounted on the top floor slab--one at each side--so that any deviation from symmetric translation could be observed; one was mounted at the centerline of the first floor slab. These measured accelerations when multiplied by the story masses, provided a direct indication of the earthquake forces developed at each story.

### 3.2.2 Potentiometers

Potentiometers were connected at each side of the two floor slabs so as to measure the displacements of the floors relative to the reference frame which is located on the floor of the laboratory outside the shaking table. Relative displacements measured by the two gages at a given floor level indicate the torsional response tendencies of the structure; differences between the shaking table displacements and the story displacements indicate the relative story displacements due to the deformation of the frame.

### 3.2.3 Linear Variable Differential Transformers (LVDT)

LVDTs mounted on column frames cemented to the structure were used to measure the curvature developed at critical sections of the frame beams and columns. Two frames were used at each section, and two LVDTs were arranged to measure the relative rotation of the two frames (i.e. the difference between the LVDT readings divided by the distance between them). The average curvature of the member section is given by the relative rotation divided by the distance between the mounting frames.

Details of the LVDT mounting frames for the columns and girders are shown in Figs. 3.4 and 3.5, respectively, while photographs of typical installations at column base and column girder joint are presented in Figs. 3.6 and 3.7. The main difference between the installation of these transducers in Frame 2, as compared with Frame 1, was in the girder-column joint region. During the tests of Frame 1, it was apparent that the principal cracking occurred at the plane where the column top met the bottom surface of the girder. In order to account for this cracking in the curvature measurement, the column target frame was cemented directly to the bottom of the girder, as shown in Fig. 3.7. Similarly

the girder target frame was cemented to the face of the transverse girder, in order to take account of cracking in the plane of the girder end; this is also shown in Fig. 3.7.

#### 3.2.4 Force Transducers

Force transducers were installed at mid-height of the columns of Frame 2 to measure the axial force, shear, and moment developed in the columns, in the same way as was done for Frame 1. Details concerning these transducers are presented in Reference 1. The only difference in the present case is that the transducers were recalibrated; results of the new calibration tests are listed in Table 3.2. The shear forces indicated by the force transducers provided a direct measure of the inertial forces developed in the frame during dynamic testing, hence the consistency of the experimental data could be checked by comparison of the accelerometer results with the force transducer results, as explained in Chapter 4.

#### 3.2.5 Strain Gages in Reinforcing Bars

Resistance wire strain gages were cemented to the longitudinal reinforcing bars at certain critical sections of the columns, specifically at top and bottom of the bottom story columns and at the bottom of the top story columns. Post-yield gages were used having a strain capacity of 30 mils per inch so that significant ductile deformations could be recorded. All columns were gaged, but only those on one side of the frame were connected to the data acquisition system because the number of channels of data that could be recorded was limited.

At each section that was to be measured, the gages on two bars were connected in a single circuit for measuring curvature directly, while

the gages on the remaining two bars were connected separately so as to measure their strains independently. The curvature indicated by the reinforcing bar gages provided a check on the curvature measured by the LVDTs at the same section.

### 3.2.6 LVDTs for Static Displacements

LVDT gages having a maximum travel of one inch were mounted between the reference frame and each floor slab. These were in parallel with the displacement potentiometers, and were used in static measurements of the flexibility influence coefficients of the frame, because of their greater precision.

## 3.3 FREE VIBRATION PROPERTIES

The free vibration mode shapes and frequencies of the test frame provide a direct indication of its dynamic properties. They were measured before and after each simulated earthquake test to monitor the cumulative damage effects induced by severe shaking. Two different procedures were employed to determine the free vibration properties, as described below.

### 3.3.1 Snap Tests

The most direct measure of the free vibration properties was given by snap tests, which were conducted by loading the structure laterally at the first floor level and then releasing the load suddenly. The resulting dynamic response of the structure was measured by accelerometers at each floor level; the accelerometer records were passed through narrow band filters to separate the first and second mode response components. Frequencies and damping values could then be obtained from

the filtered records, treating them as single degree of freedom systems. Details of the procedure are given in Reference 1; results are presented in Chapter 4.

### 3.3.2 Flexibility Matrix Measurements

The free vibration properties also were evaluated by measuring directly the flexibility of the frame and then using these measurements together with the known mass properties to formulate the vibration eigen problem of the structure. The flexibility coefficients of the frame were obtained by applying a horizontal load first to one story and then to the other story, and measuring the resulting displacements of both stories. The load was applied in increments of 200 lbs, and the corresponding displacements were recorded during both the increasing and decreasing sequence. The force-displacement relationship obtained at each story was plotted as a hysteresis loop; the slope of the increasing load branch was taken as the flexibility coefficient.

The measurement procedure was essentially the same as described in Reference 1 except that LVDT gages rather than potentiometers were used to measure displacements. Results of the tests, which are presented in Chapter 4 demonstrate the improved accuracy obtained with the LVDTs in that there is better agreement between the cross-flexibility coefficients; however, it was still necessary to average these values before formulating the vibration eigen problem from which mode shapes and frequencies were calculated.

### 3.4 STATIC TEST

After the structure had been tested, repaired, and tested again, it was removed from the earthquake simulator and moved to the Structural

Research Laboratory to determine its remaining static load behavior and ultimate capacity. The test procedure was exactly the same as employed with Frame 1, and only a general outline of the procedure will be given here.

Instrumentation used in the static test included LVDTs for measuring curvature at the column bases, and at the same sections strain gages on reinforcing bars were connected to measure both curvature and direct strain. In addition, the horizontal static force applied to the top story and the displacements produced at both stories were measured. All static test data were recorded on direct writing oscillographs; hence the number of channels available was quite limited.

The test was performed by applying the static load in increments, recording all gage readings at each step. When the displacement capacity of the actuator was reached, the structure was unloaded, a spacer block inserted, and then the loading was continued until the displacement capacity was again reached. Static test results are presented in Chapter 4.

TABLE 3.1 EARTHQUAKE SIMULATOR TEST PROGRAM

TEST STRUCTURE CONDITION	RUN NO.	GROUND MOTION ACCELEROGRAM RECORD	SHAKING TABLE SPAN SETTING	SCALED PEAK ACCELERATION	RUN IDENTIFI- CATION
WITH CONCRETE BLOCKS	1	TAFT (1)	100	0.097g	W1
WITH LATERAL BRACING	2	TAFT	850	0.57g	W2
	3	TAFT	850	0.65g	W3
REPAIRED WITH CONCRETE BLOCKS WITH LATERAL BRACING	4	TAFT	50	0.07g	R1
	5	TAFT	850	0.78g	R2
	6	TAFT	850	0.82g	R3

(1) TAFT = TAFT, JULY 21, 1952 N69W COMPONENT

TABLE 3.2 CALIBRATION VALUES FOR FORCE TRANSDUCERS

TRANSDUCER NUMBER IDENTIFICATION	FLEXURAL MOMENT (in - lbs) $\epsilon_{T1}$	SHEAR FORCE $\frac{\text{lbs}}{\epsilon_{T2}}$	AXIAL COMPRESSION $\frac{\text{lbs}}{\epsilon_{T3}}$
2	122	26.5	66.4
3	118	26.7	63.0
4	117	25.0	63.0
5	120	29.1	62.4
6	118	21.4	63.2
7	116	22.6	61.3
8	118	21.8	63.2
9	119	26.7	61.3

$$\epsilon_{T1} = 1/2 \text{ [TOP FLANGE STRAIN-BOTTOM FLANGE STRAIN]} (10^{-6} \text{ in/in})$$

$$\epsilon_{T2} = \text{[SHEAR BRIDGE STRAIN]} (10^{-6} \text{ in/in})$$

$$\epsilon_{T3} = 1/2 \text{ [TOP FLANGE STRAIN + BOTTOM FLANGE STRAIN]} (10^{-6} \text{ in/in})$$

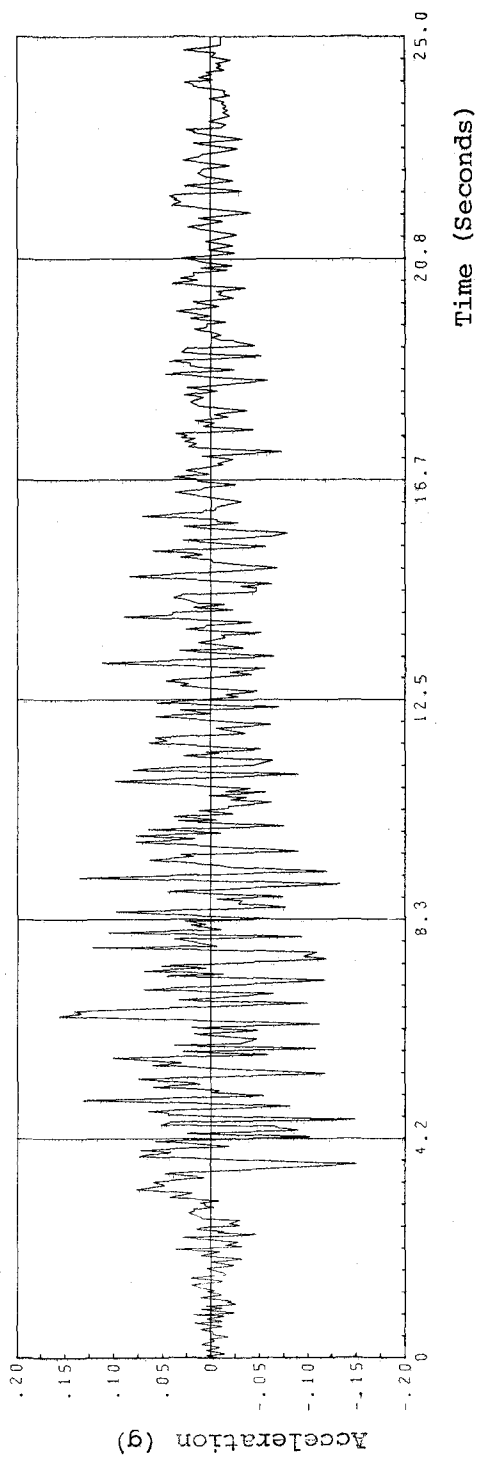


Fig. 3.1 (a) TAFT 1952 N69W ACCELEROGRAM.

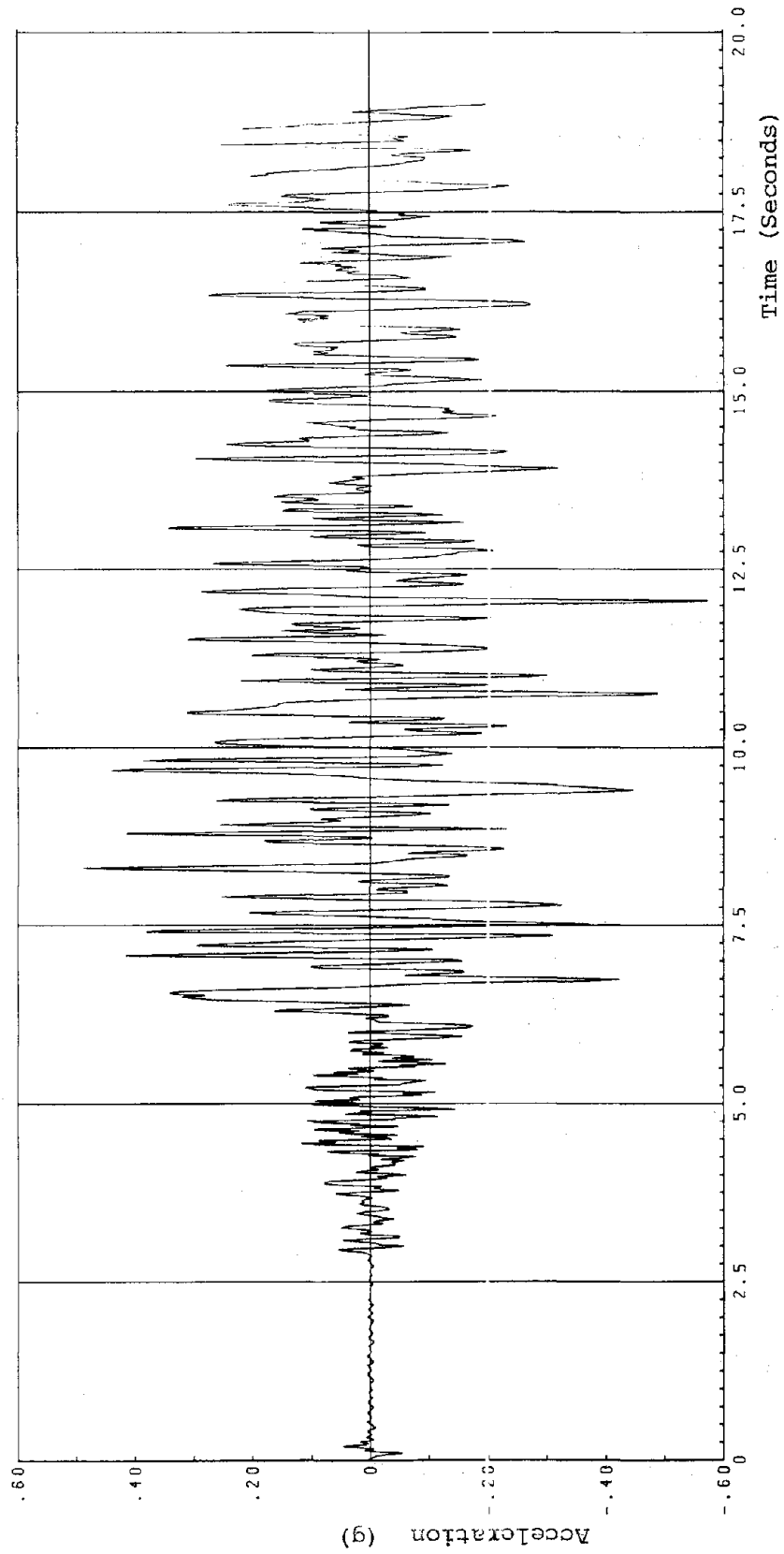


Fig. 3.1 (b) TAFT SIMULATED TABLE ACCELERATION. RUN W2.

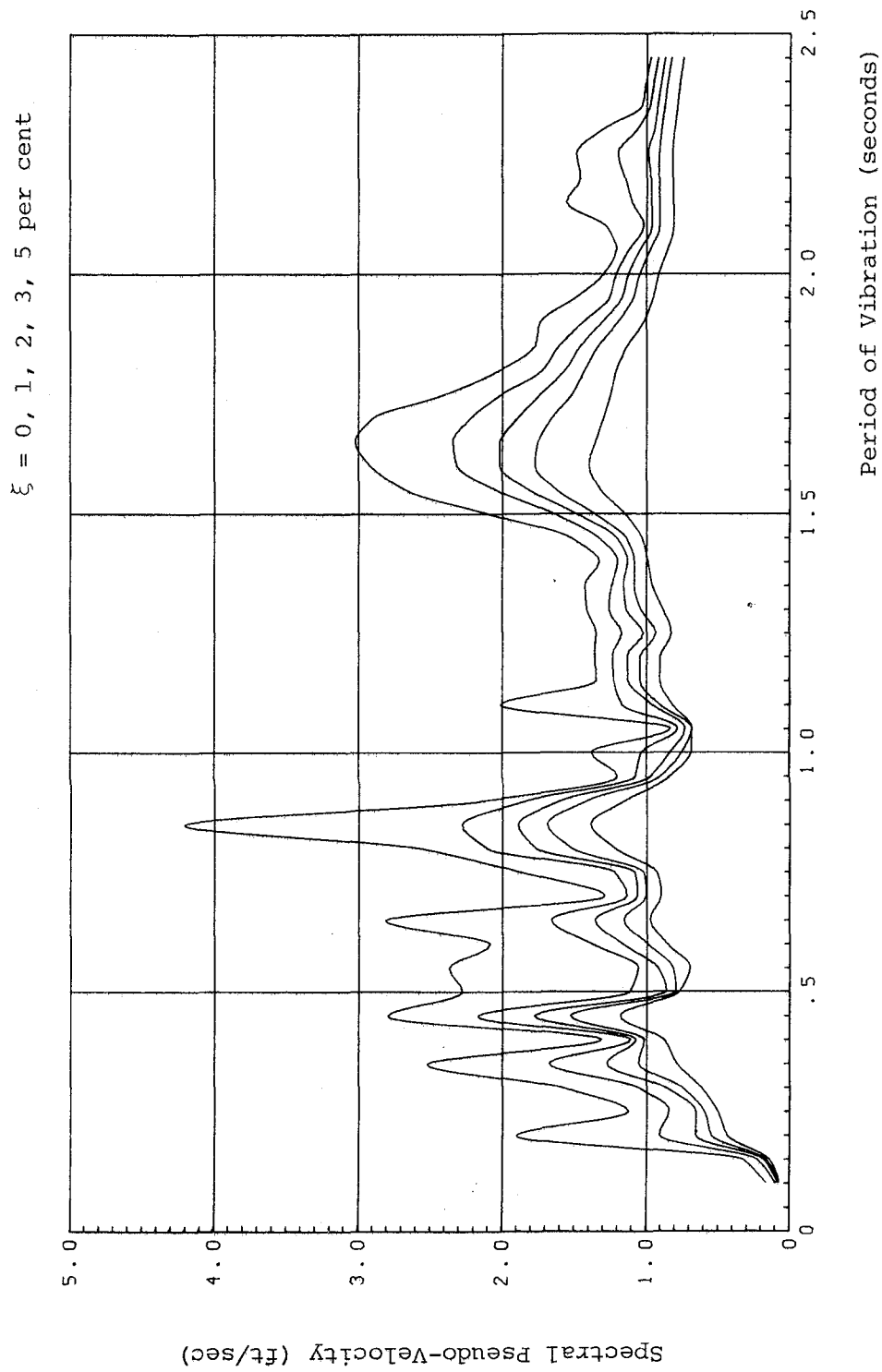


Fig. 3.2 PSEUDO-VELOCITY RESPONSE SPECTRA  
FOR TAFT N69W, JULY 21, 1952

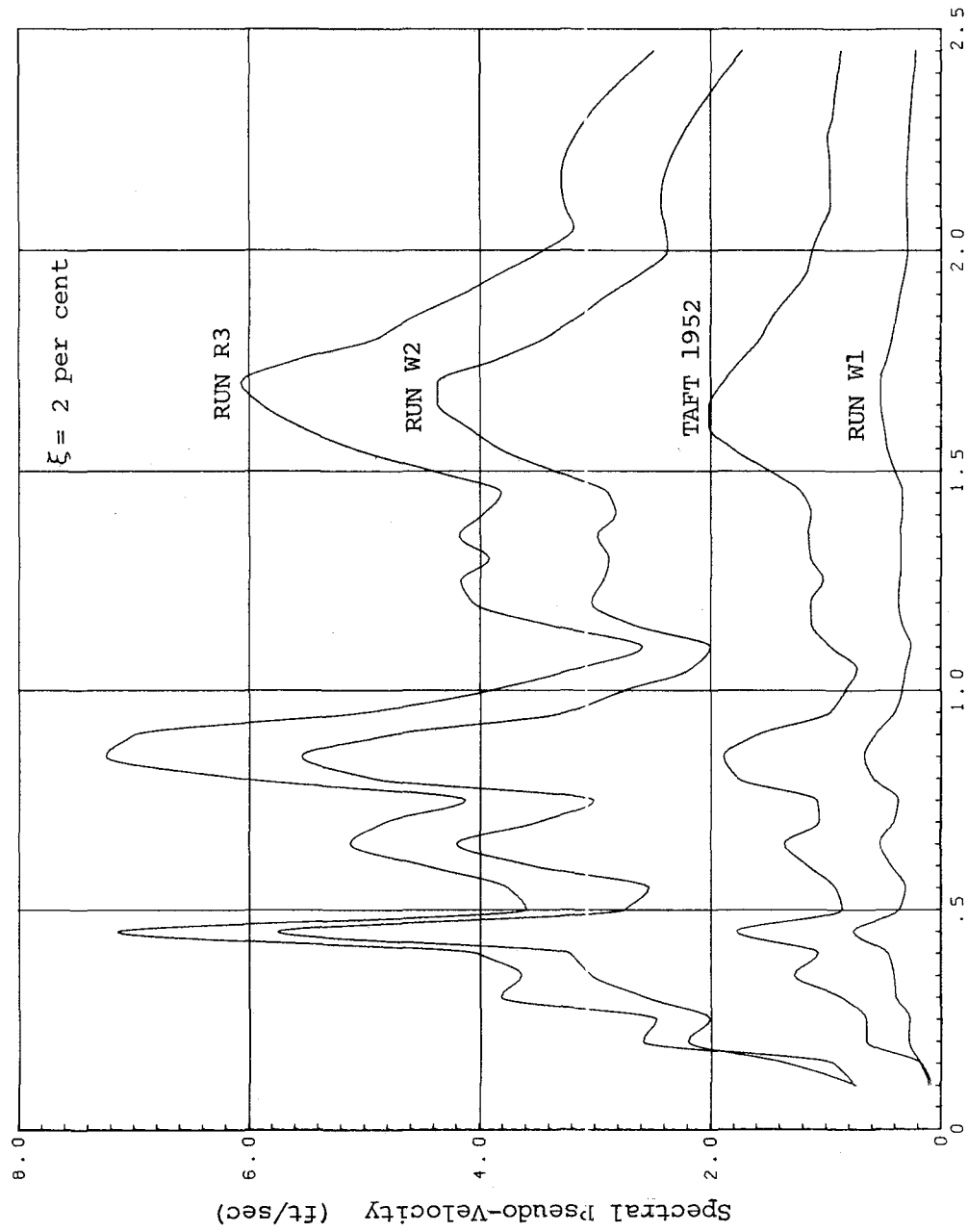


Fig. 3.3 PSEUDO-VELOCITY RESPONSE SPECTRUM FOR TAFT N69W, JULY 1952, AND TABLE ACCELERATION FOR RUNS W1, W2, and R3.



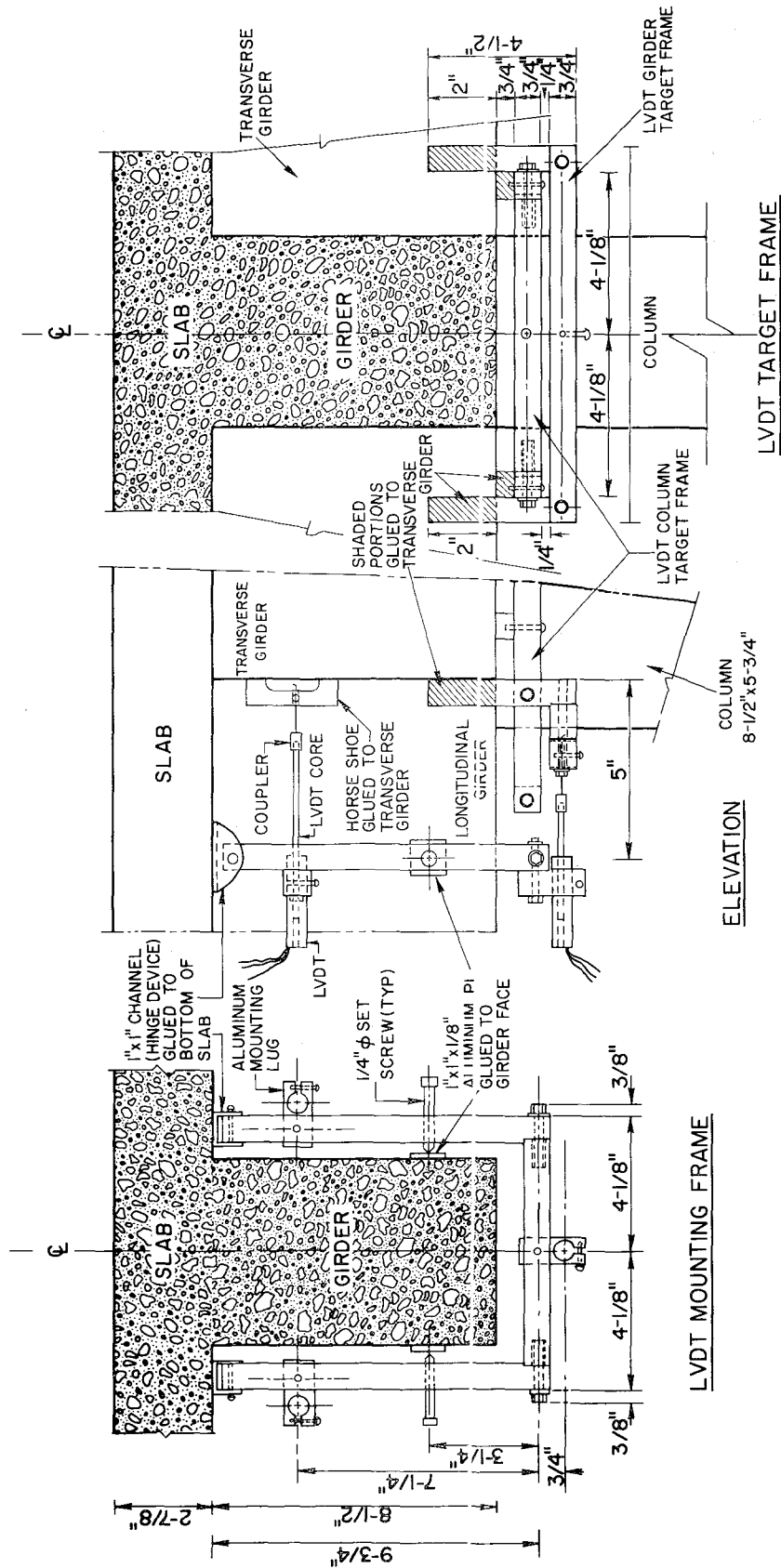


Fig. 3.5 GIRDER LVDT MOUNTING AND TARGET FRAME DETAILS TO MEASURE GIRDER END ROTATIONS AT BEAM-COLUMN JOINT.

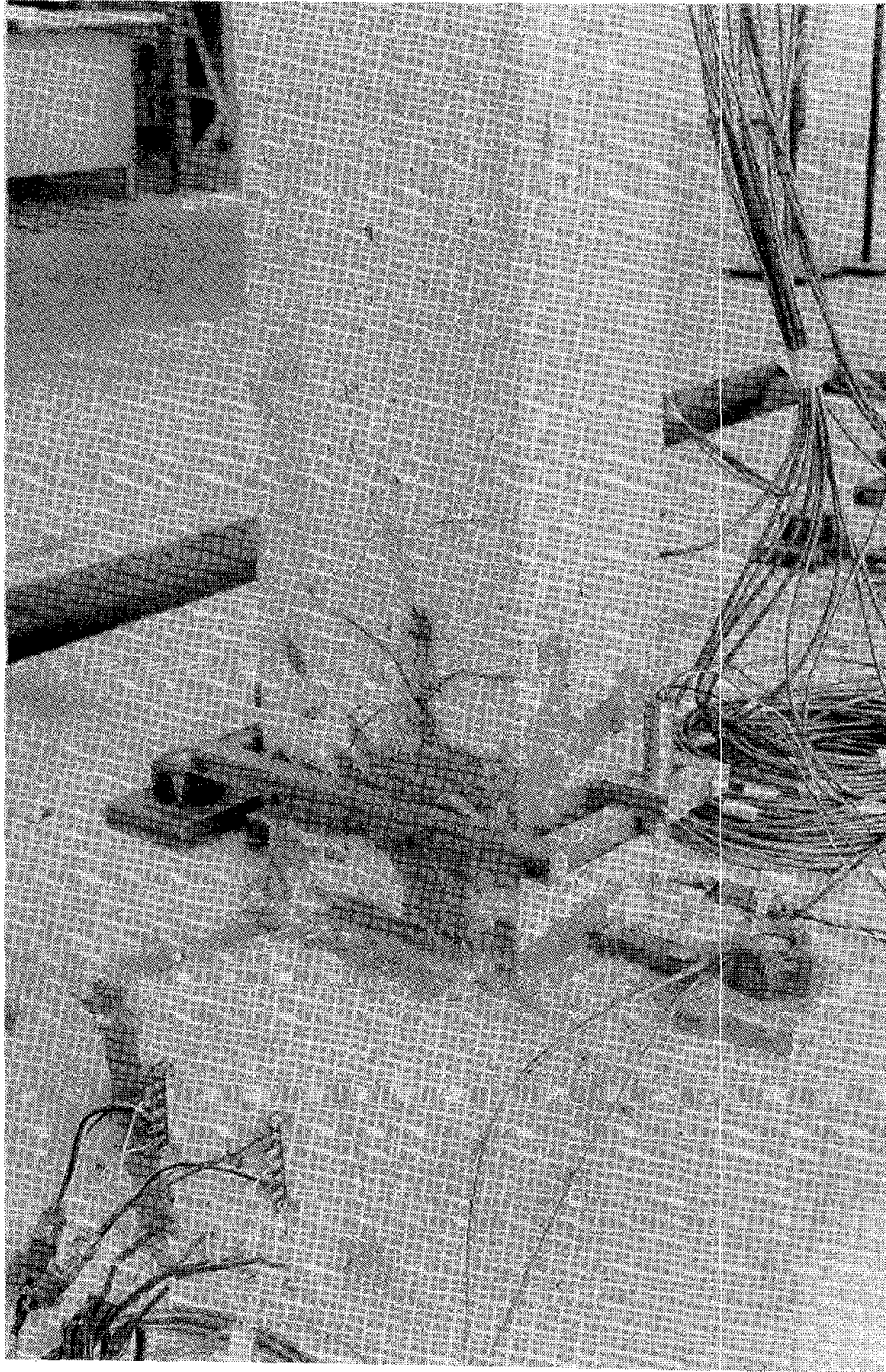


Fig. 3.6      LVDTs, MOUNTED ON FRAME,  
TO MEASURE COLUMN END ROTATION.

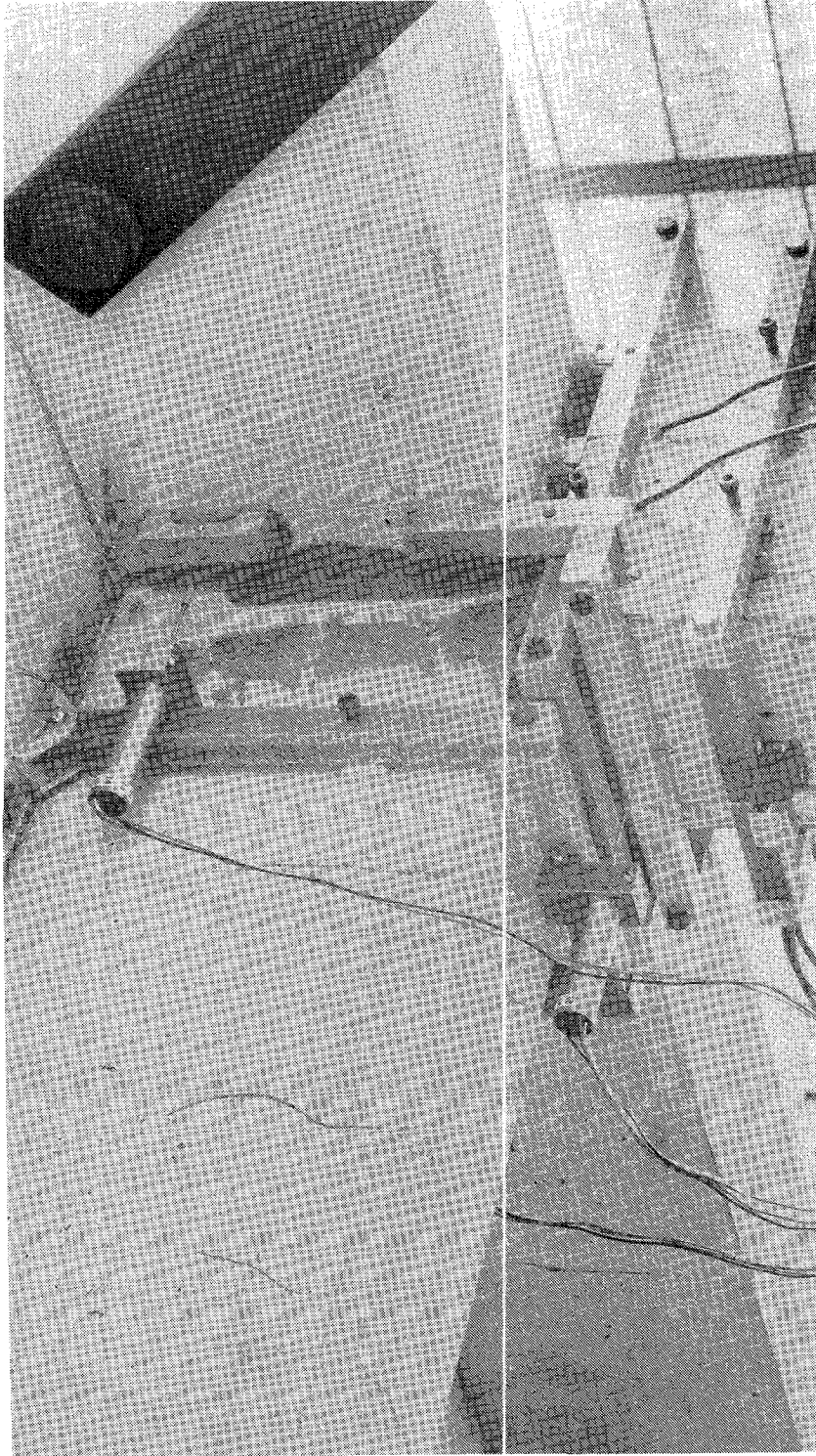


Fig. 3.7 LVDTs, MOUNTED ON FRAMES, TO MEASURE ROTATIONS AT THE GIRDER-COLUMN JOINT.



#### 4. TEST RESULTS

##### 4.1 DAMAGE OBSERVATIONS

One of the most important indications of the response of structures to damaging earthquakes is the appearance of the structure after the event. In the case of real structures subjected to real earthquakes, generally no instrumentation has been provided to record the response, so the only available measure of the response characteristics is provided by the observed damage patterns. For earthquake simulator studies such as that described herein, extensive instrumentation provides rather complete quantitative evidence concerning the response, but even in this case the damage patterns observed in the structure provide additional evidence of the response intensity. Accordingly, the structure was inspected carefully after each test for evidence of damage, and a summary of these observations is presented here.

In general, the extent and type of damage induced in Frame 2 by the three simulated earthquakes applied before its repair were very similar to those observed in Frame 1 after its much more extensive test sequence before repair. Of course the peak accelerations applied in two tests of Frame 2 (0.57g and 0.65g) were significantly greater than the two largest accelerations achieved in the tests of Frame 1 (0.30g and 0.44g), so this observed equivalence of damage is probably due to the increased intensity in the one case compensating for the greater number of tests in the other.

As was mentioned earlier, the main difference between the two structures was that Frame 2 was essentially uncracked before testing. Even though some cracks were observed when the concrete blocks were

installed, these dead load cracks were not closely related to the lateral deformation patterns. The minor earthquake which was applied to induce a more realistic degree of cracking caused a noticeable reduction of vibration frequency and some minor increase in visible cracking in the bottom story members; however, the structure still appeared to be essentially undamaged after this test.

During the first major earthquake test (accel. = 0.57g) the steel at the first story column bases and tops yielded, and many significant flexure cracks could be seen in these regions. Also, cracks developed in the longitudinal girders near the column joints, extending from the bottom surface to the base of the slab. Some minor cracking occurred at the top of the first floor slab along the line of the transverse girder, but no major crack developed equivalent to that observed in Frame 1 because the slab reinforcing mesh was continued across the top of the transverse girder. The base of the top story column also cracked at its junction with the first floor slab. In general, it may be said that during this quake the structure was significantly cracked and underwent several cycles of plastic deformation in the reinforcing steel, but that its strength was not reduced.

During the next major test (accel. = 0.65g) the cracking patterns were extended, but not changed in character. Cracking at the column bases became somewhat inclined, showing the influence of shear, and some spalling and crushing of column concrete occurred at the juncture with the footing. The bottom story girders showed some minor shear cracking, and the slab cracks over the transverse girders were enlarged.

After the structure was repaired, the preliminary low intensity earthquake caused some minor new cracking. The two high intensity

earthquakes then produced additional cracking which was generally similar to that incurred in the tests before repair. However, the shear cracks in the columns became more prominent, as can be seen in Fig. 4.1. Also, the cracking and spalling of the concrete at the column bases again was quite evident, and was accompanied by significant cracking of the footing, as may be seen in Fig. 4.2. Similar spalling is shown in column tops at the beam-column joint in Fig. 4.3. Another interesting crack pattern is shown in Fig. 4.4, starting in the top of the bottom story slab and continuing vertically into the second story column. This may be due to some type of torsional deformation, but the source of the torsion is unclear.

One feature of these final two tests on Frame 2 which should be discussed is the fact that the overturning moment capacity of the shaking table was exceeded. The horizontal inertia forces developed at the two floors of the frame in response to the high base accelerations applied to the repaired structure (peak values of 0.78g and 0.82g) induced very large overturning moments which exceeded the dynamic capacity of the vertical actuators. As a result, the overload bypass valves of the actuators operated, allowing the system to move vertically. Significant vertical accelerations having a peak value of 0.60g accompanied this vertical motion, and of course the observed structural response therefore was caused by the combination of vertical and horizontal acceleration. The vertical direction accelerogram is shown in Fig. 4.5.

An important observation drawn from the test of Frame 2 was that the structure did not appear to be more sensitive to damage when the high intensity earthquake was applied to a completely undamaged structure than was Frame 1 which had been strained extensively in low intensity earthquake tests before the maximum test was applied. The damage effects are

cumulative, so that a sequence of tests produce more damage than a single test of like intensity. Also, the degree of damage during any test is proportional to the intensity of that test. But there was no evidence that an undamaged structure is more "brittle" or damage-prone than one which had been cracked and strained significantly before a major earthquake was applied.

#### 4.2 VARIATION OF FREE VIBRATION FREQUENCY AND DAMPING

Free vibration frequencies of the test structure, as determined from the snap tests and the flexibility matrix measurements are listed in Table 4.1 and are depicted graphically in Fig. 4.6. It is of interest to note that the second mode frequency is about three times the first mode value during all stages of the test; this same ratio was observed in the test of Frame 1. The fact that Frame 2 was stiffer before testing than was Frame 1 is apparent from the first mode frequency of Frame 2 (without blocks) of 6.58 Hz, as compared with 5.01 Hz of Frame 1<sup>(1)</sup>. This demonstrates the essentially uncracked condition of Frame 2 before testing.

The fundamental mode frequency of the frame with blocks is shown in Table 4.1 to have changed during testing from 3.80 to 1.88 Hz, the damaged structure having only half the frequency of the original frame. Thus it may be deduced that the stiffness of the frame was reduced by a factor of 4 during the testing before repair. After repair, the frequency was increased to 2.58 Hz, or 68% of the original value; hence the repaired stiffness was about 46% of the original value. During subsequent testing, the frequency was reduced to only one third of the original value; this corresponds to an ultimate stiffness of only one-ninth of the original. These changes demonstrate clearly the great stiffness degradation suffered by concrete frames during severe earthquake loadings. By way of comparison,

the frequency of Frame 1 just before repair was 58% and just after repair was 77% of its original value, hence it may be concluded that Frame 2 suffered more damage during testing than did Frame 1. This fact is a direct consequence of the essentially virgin quality of Frame 2--it had more stiffness to lose. However, it is significant that the frequencies of the two frames were quite similar after each had been subjected to the first test which caused yielding of the steel. Similar correspondence was also observed after completion of testing before repair of the structures. The greater loss of stiffness after repair of Frame 2 is attributable to the extremely severe shaking it was given during these final tests.

Another feature of the vibration properties apparent in Table 4.1 is that the frequencies computed from the flexibility coefficients are generally lower than the values obtained directly from the snap tests. The discrepancy averages about 6 per cent implying that the flexibility coefficients (which are listed in Table 4.2) are about 12 per cent too high; no explanation can be offered for this deviation.

The damping ratios measured in the snap tests of Frame 2 also are listed in Table 4.1 and are plotted in Fig. 4.7. These values, which range from about 2 to 7 per cent in the first mode and from about 1 to 3.5 per cent in the second mode, are generally similar to those observed in Frame 1. The much greater increase of damping in the first mode shown during the tests of both structures demonstrates that the damage was primarily concentrated in the first mode deformation pattern. Another aspect of the damping behavior, which is evident both in Fig. 4.7 and in Table 4.1, is the decrease of damping ratio which accompanies the addition of the concrete blocks to the structure. A decrease of frequency also accompanied the addition of the blocks, and since the frequency changed proportionately more than the damping ratio, it may be argued that the stiffness was reduced at the

same time that the mass was added. (If stiffness and damping are unchanged while the mass of a single degree of freedom system is changed, both damping ratio and frequency should be changed by the same percentage.) The argument is supported by the lateral flexibility coefficients listed in Table 4.2, so it is probable that the cracking, resulting from the gravity load of the concrete blocks, did actually reduce the lateral frame stiffness.

A similar argument can be applied to the comparison of changes of frequency and damping that occurred during the epoxy repair of the frame. The resulting reduction of damping was much greater than the increase of frequency, hence the material damping factor must have been changed as well as the stiffness. Of course, it is reasonable to assume that less energy is lost when the cracks are fully cemented so the test data seem consistent in this regard.

#### 4.3 LATERAL FLEXIBILITY MATRIX

A main point of interest of the lateral flexibility matrix coefficients which are presented in Table 4.2 is the relative flexibility indicated for the two stories, i.e. the ratios  $F_{TT}/F_{BB}$  and  $F_{BT}/F_{BB}$ . These ratios remained reasonably constant during the testing of the structure before repair, even though the flexibility coefficients themselves were changing by factors of four or more. Similar behavior is also apparent during testing after the epoxy repair of the frame, although the ratios are slightly higher during this sequence than before the repair. The significance of this observation is that the damage done during the testing sequence can be represented reasonably by a single stiffness degradation parameter (such as a change of modulus of elasticity); it is not necessary to completely reformulate the flexibility matrix. Advantage is taken of this fact in the analytical prediction of dynamic response,

as is described in Chapter 5.

#### 4.4 GLOBAL RESPONSE BEHAVIOR

The general nature of the dynamic response of this frame to the earthquake simulator inputs is depicted effectively by time history plots of the story displacements relative to the base. A series of such plots is presented in Figs. 4.8 through 4.16; in each figure graph "a" shows the bottom story response and graph "b" the top story motion. A general conclusion which may be drawn from all of these figures is that the displacement response of the frame is essentially a first mode motion; very little contribution is seen at the second mode frequency. Another basic fact is that the type of response depends strongly on the fundamental frequency of the frame at the time of the test. A direct demonstration of this phenomenon is shown in Fig. 4.8 which compares the responses during runs W2 and W3; the change of frequency resulting from the damage done during run W2 leads to a significantly different response history in run W3. A similar plot for runs R2 and R3 after the structure was repaired is shown in Fig. 4.16.

The fact that the response is similar for two structures having similar periods is demonstrated by Fig. 4.9 which compares the response of Frame 2 during test W1 with the response of Frame 1 during its test, W2. The earthquake intensity was small in both cases, so the response was essentially linear, and the "beating" phenomenon which is characteristic of a high frequency linear response, is evident in both structures. A second comparison of similar structures, but demonstrating nonlinear response, is shown in Fig. 4.10. Figure 4.10 shows the response of Frame 2 during test W3 and the response of Frame 1 to its test W6. The frequencies of the two structures were very nearly the same before these

two similar tests, and the responses are seen to be very similar, even though yielding of the steel occurred in both cases. A similar comparison of the behavior of the first and second frames after repair is given by Figs. 4.11, 4.12 and 4.13 which show the responses during tests R1, R2 and R3 of each structure, respectively. A comparison of response of the structure before and after repair to similar simulated earthquakes is shown in Figs. 4.14 and 4.15, which show comparisons for runs W2, R2 and runs W3, R3, respectively.

A summary of the response behavior during the entire test sequence of Frame 2 is presented in Figs. 4.17, 4.18 and 4.19, which show, respectively, the peak story displacements, story shears, and story overturning moments developed during each test. Also shown with the peak story displacements in Fig. 4.17 are values of displacement calculated by an elastoplastic static analysis<sup>(3)</sup> corresponding to first yield and full collapse mechanisms. The fact that the structure survived peak dynamic displacements which far exceed the so-called "collapse" value is evident in this figure. Clearly this simple analysis did not properly model the actual frame behavior, probably both because the yield capacity of both concrete and steel were under-estimated, and also because the frame does not develop true elasto-plastic hinges. Moreover, the dynamic resistance of the frame undoubtedly exceeds its static capacity. Similar comments apply to Figs. 4.18 and 4.19 which show the elasto-plastic predicted yield and collapse values as well as the observed peak story shears and story overturning moments, respectively. All observed peak response data also are summarized in Table 4.3.

#### 4.5 MEASURED COLUMN SHEAR FORCES

A comparison of the column story shear forces measured by the force transducers in the bottom story columns and the average column shear force computed from the accelerometer readings is presented in Fig. 4.20. It is seen in this plot of data from run W1 that there is a slight discrepancy in the results given by the original transducer calibration factors. Accordingly, correction factors were derived from this data to obtain agreement between the two types of measurement during test W1. These same correction factors were then applied to transducer data from runs W2 and W3, and plotted against the accelerometer derived results for those runs, as shown in Figs. 4.21 and 4.22. The agreement is considered to be adequate, but is not as good as was found in the test of Frame 1. It appears that the transducers may have been damaged slightly at some time in the testing procedure.

The plots of the average north side column shears and average south side column shears, which are shown in Figs. 4.23 and 4.24, demonstrate that the columns develop increased shear resistance on the side of the structure toward which it has moved. In other words, the columns subjected to compression due to dynamic overturning moments consistently carry the larger part of the shear force, as though the increased compression caused an increase of stiffness. This same type of behavior was observed in the analysis of results from Frame 1.

#### 4.6 STATIC TEST RESULTS

The static test was performed on Frame 2 after the frame was repaired and tested for dynamic tests, i.e. after run R3. The results will be presented in two parts:

- (1) the actual test load-deformation results compared to the

load-deformation relationship predicted by the elasto-plastic analysis, and

(2) damage after the test.

The actual test load-deformation relationship is shown in Fig. 4.25. The unloading branches during the test are due to the fact that the displacement capacity of the actuator was reached at these points; hence the frame had to be unloaded and spacers introduced before the frame could be loaded again. Comparing this result with the load-deformation relationship of Fig. 2.10, it can be seen that the actual capacity of the frame is much higher than predicted by computer analysis.<sup>(3)</sup> This increase in capacity is due to the reasons mentioned in section 4.4. to reiterate, the increased capacity is a result of the moment capacities being underestimated and the gross assumption that elasto-plastic hinges are formed. The important point to note is the significant displacement capacity of the frame. The maximum top story displacement reached during the test was 24" before "functional" failure of the frame occurred, due to failure of transverse girder reinforcement. This displacement capacity is due to good detailing of the sections, which provides a large amount of ductility.

The damage that occurred during various stages of testing is shown in Figs. 4.26 through 4.33. The deformation of the frame midway during the test is shown in Fig. 4.26 as 16 inches. The crushing and cracking at the ends of the columns was quite significant. Figure 4.27 shows the damage at the bottom story girder-column juncture, whereas a general view of the frame in the transverse direction is shown in Fig. 4.28. The crack that had developed in the slab and extended vertically into the column during the dynamic test (Fig. 4.4) was the key factor that promoted the failure of the frame. The widening of this crack and the extent

of the damage to the transverse girder can be seen in Fig. 4.29. Another view of the damage of the same girder-column juncture is shown in Fig. 4.30. As the deformation increased, the cracks widened and crushing of concrete continued until the steel in the transverse girder was fractured. The failure was due to the torsion developed in the transverse girder. The damage of the frame after "functional" collapse is shown in Figs. 4.31 through 4.33. The damage of the columns on the opposite side of the transverse girder in which the fracture of the bar occurred is shown in Fig. 4.31. Views of the extent of the damage to the slab and the transverse girder after "failure" are shown in Figs. 4.32 and 4.33.

Thus it is evident from this static test that the frame had significant deformation and load capacity beyond that estimated by the elasto-plastic analysis. Also the frame finally failed because of transverse girder torsion; if this could have been avoided, the ultimate capacity of the frame would have been still higher.

TABLE 4.1 VARIATION OF FREQUENCY AND DAMPING VALUES THROUGHOUT TEST HISTORY

TEST NO.	HORIZONTAL FORCE LEVEL H B (lbs)	LAST RUN BEFORE TEST	CONCRETE BLOCKS ON STRUCTURE	FREE VIBRATION TEST RESULTS				FREQUENCY AS COMPUTED FROM MEASURED FLEXIBILITY MATRIX (Hz)	
				NATURAL FREQUENCY(Hz)		DAMPING FACTOR (CRIT.)		FIRST MODE	SECOND MODE
				FIRST MODE	SECOND MODE	FIRST MODE	SECOND MODE		
1	1153	NONE	NO	6.58	20.58	1.55	2.09	6.75 (+2.6%)	21.04 (+2.2%)
2	1153	NONE	YES	3.80	9.80	1.28	1.59	3.64 (-3.9%)	8.95 (-8.7%)
3	1153	W1	YES	3.13	8.70	4.20	1.93	3.07 (-1.9%)	8.83 (+1.5%)
4	1153	W2	YES	2.03	6.70	5.77	2.99	1.92 (-5.4%)	6.06 (-9.6%)
5	1153	W3	YES	1.88	6.14	6.56	3.46	1.76 (-6.4%)	5.95 (-3.1%)
STRUCTURE REPAIRED									
6	1153	NONE	YES	2.58	7.22	2.67	2.00	2.40 (-7.0%)	7.18 (-0.6%)
7	1153	R1	YES	2.31	6.45	3.52	2.00	2.27 (-1.7%)	6.03 (-6.5%)
8	1153	R2	YES	1.49	5.77	5.40	2.78	1.38 (-7.4%)	4.43 (-23.2%)
9	1153	R3	YES	1.28	4.38	7.10	3.10	1.105 (-13.7%)	4.20 (-4.1%)
Average								-5.9%	-6.6%

\*Figures in parenthesis indicate the percentage deviation of the frequency as computed from the measured flexibility matrix as compared to the frequency computed from free vibration results.

TABLE 4.2 VALUES OF LATERAL FLEXIBILITY MATRIX THROUGHOUT TEST HISTORY

LAST RUN BEFORE TEST	CONCRETE BLOCKS ON STRUCTURE	HORZ. FORCE LEVEL		FLEXIBILITY MATRIX COEFFICIENTS (in/kip)			$F_{TT}/F_{BB}$	$F_{BT}/F_{BB}$
		$H_T$ max	$H_B$ max	$F_{BB}$	$F_{BT}$	$F_{TT}$		
NONE	NO	1049	1153	0.0138	0.0161	0.0305	2.21	1.17
NONE	YES	1049	1153	0.0148	0.0167	0.0393	2.65	1.13
W1	YES	1049	1153	0.0229	0.0260	0.0485	2.12	1.13
W2	YES	1049	1153	0.0563	0.0678	0.1235	2.19	1.20
W3	YES	1049	1153	0.0673	0.0819	0.1431	2.13	1.22
STRUCTURE REPAIRED								
NONE	NO	1049	1153	0.0330	0.0440	0.0800	2.42	1.33
NONE	YES	1049	1153	0.0316	0.0410	0.0870	2.64	1.30
R1	YES	1049	1153	0.0394	0.0455	0.0960	2.44	1.15
R2	YES	1049	1153	0.0940	0.1260	0.2590	2.76	1.34
R3	YES	1049	1153	0.1528	0.2090	0.3830	2.51	1.37

TABLE 4.3 PEAK VALUES OF STORY DISPLACEMENTS (1), STORY SHEARS (2),  
BASE OVERTURNING MOMENT (3) THROUGHOUT TEST HISTORY.

RUN IDENTIFICATION	SCALED PEAK ACCELERATION	STORY DISPLACEMENTS (inches)				STORY SHEARS (kips)				BASE OVERTURNING MOMENT (kip-ins)	
		BOTTOM STORY		TOP STORY		BOTTOM STORY		TOP STORY		POS.	NEG.
		POS.	NEG.	POS.	NEG.	POS.	NEG.	POS.	NEG.		
W1	0.097	0.272	0.261	0.432	0.393	7.98	7.46	2.65	2.37	1135	1057
W2	0.570	1.370	1.997	2.229	2.726	26.72	27.68	14.44	15.59	4722	4713
W3	0.650	1.885	1.790	2.770	2.450	26.45	24.67	15.45	12.58	4734	4008
R1	0.070	0.260	0.250	0.420	0.410	4.61	5.39	2.58	2.64	841	869
R2	0.780	2.510	2.920	2.700	4.280	29.08	28.79	18.08	17.16	5348	5402
R3	0.820	2.560	3.730	5.360	5.080	28.20	29.62	18.91	13.87	5441	4701

(1) Story Displacements measured relative to the table displacement.

(2) Story shears calculated from the measured inertia forces, i.e.  $f_I = m \cdot a$  where  $m$  = mass of the story and  $a$  = measured acceleration of the story.

(3) BASE OVERTURNING MOMENT evaluated from inertia forces (measured).

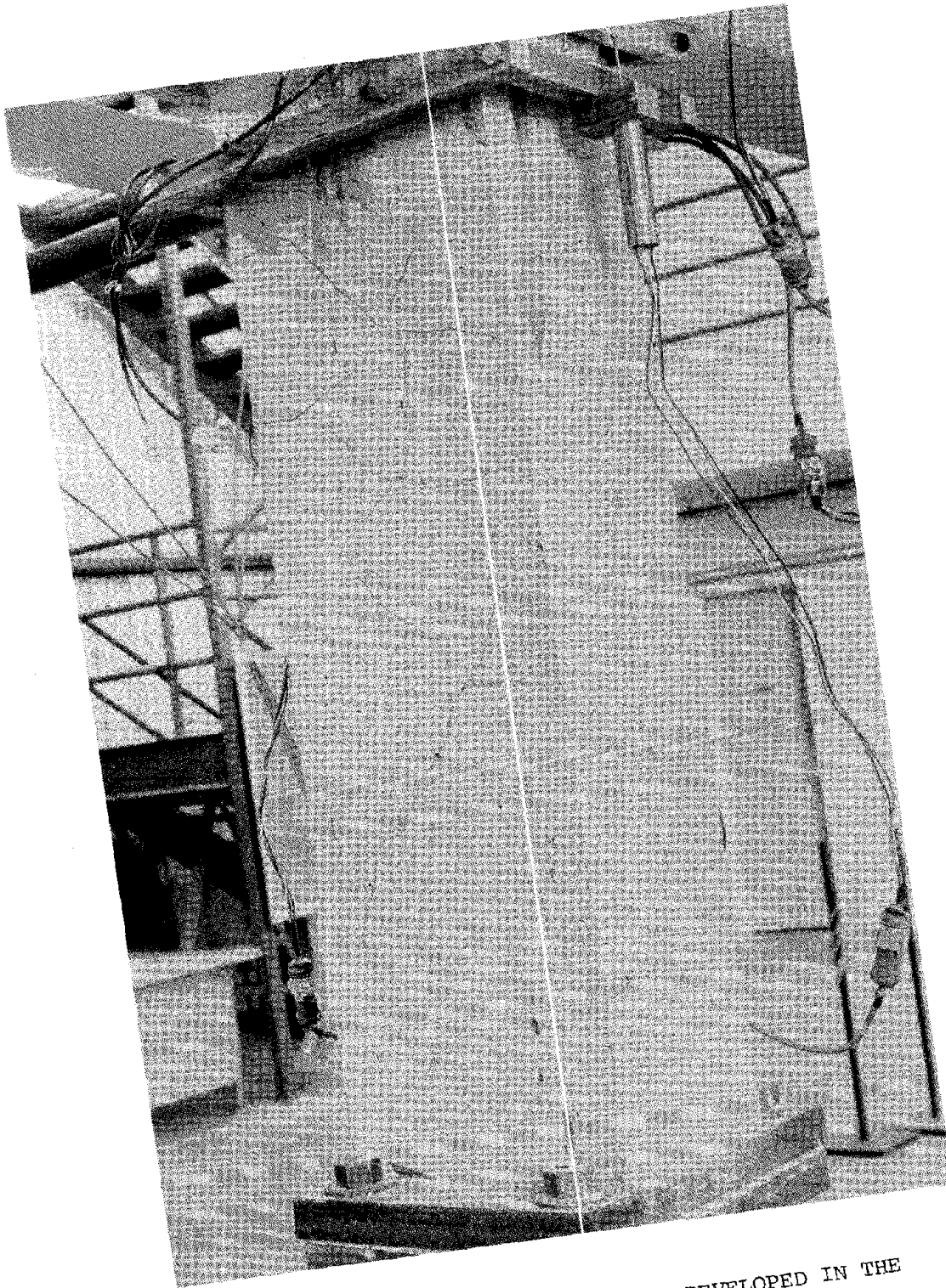


Fig. 4.1 SHEAR CRACKS DEVELOPED IN THE COLUMN AFTER TEST RUN W3.

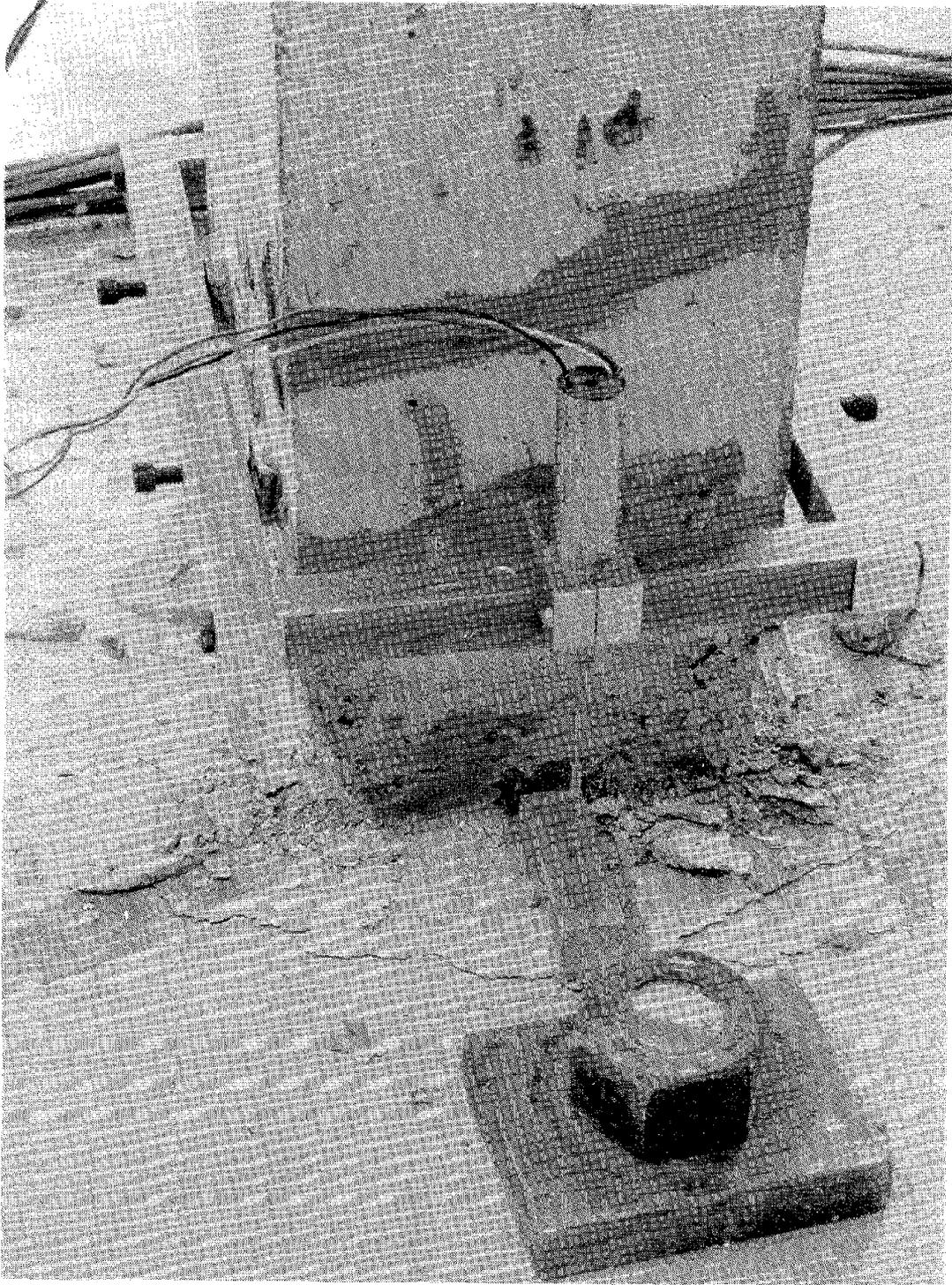


Fig. 4.2      CRACKING AND SPALLING OF CONCRETE AT  
THE COLUMN-FOOTING JUNCTURE.

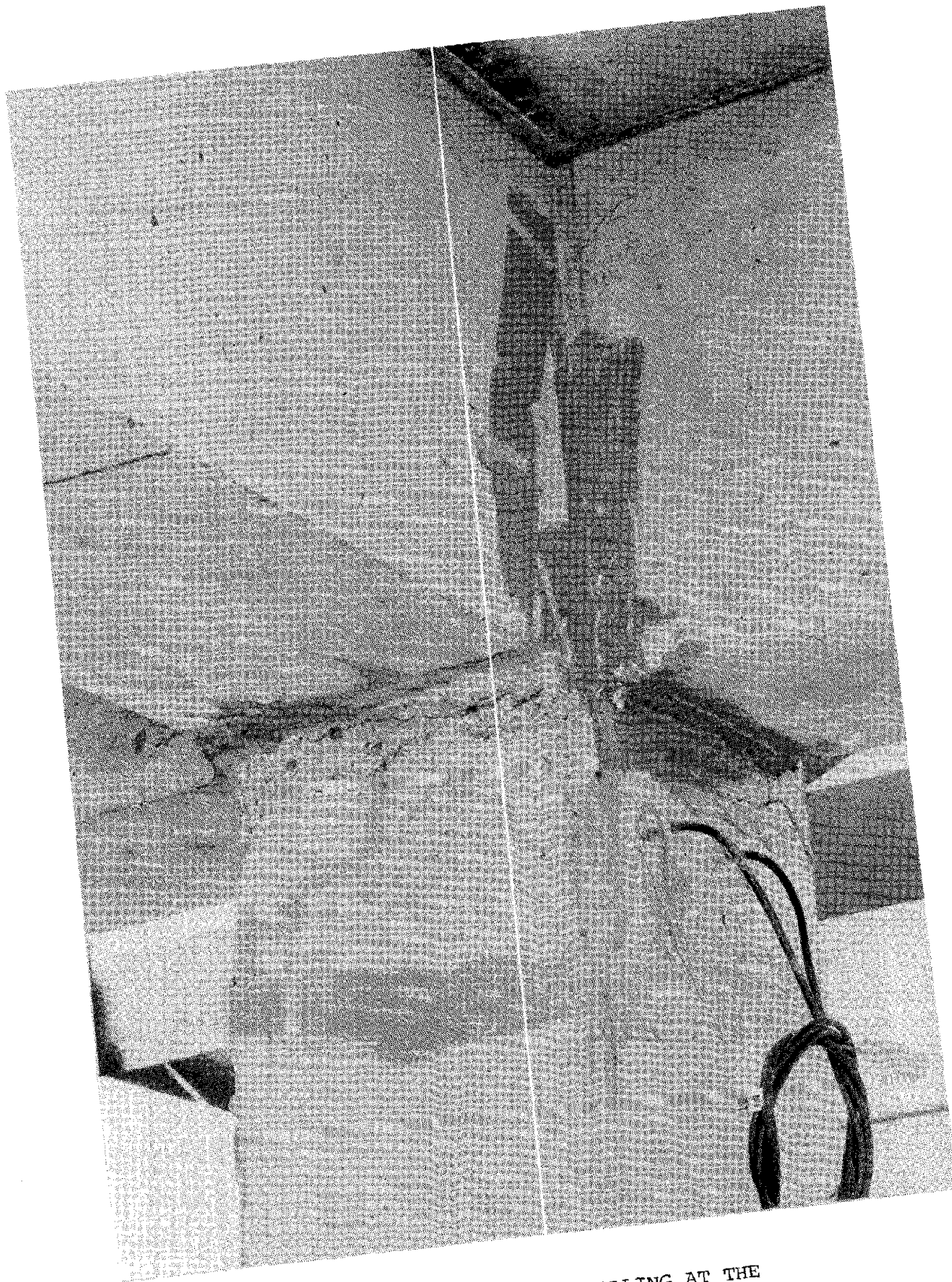


Fig. 4.3  
CRACKING AND SPALLING AT THE  
BOTTOM STORY COLUMN-GIRDER JUNCTION

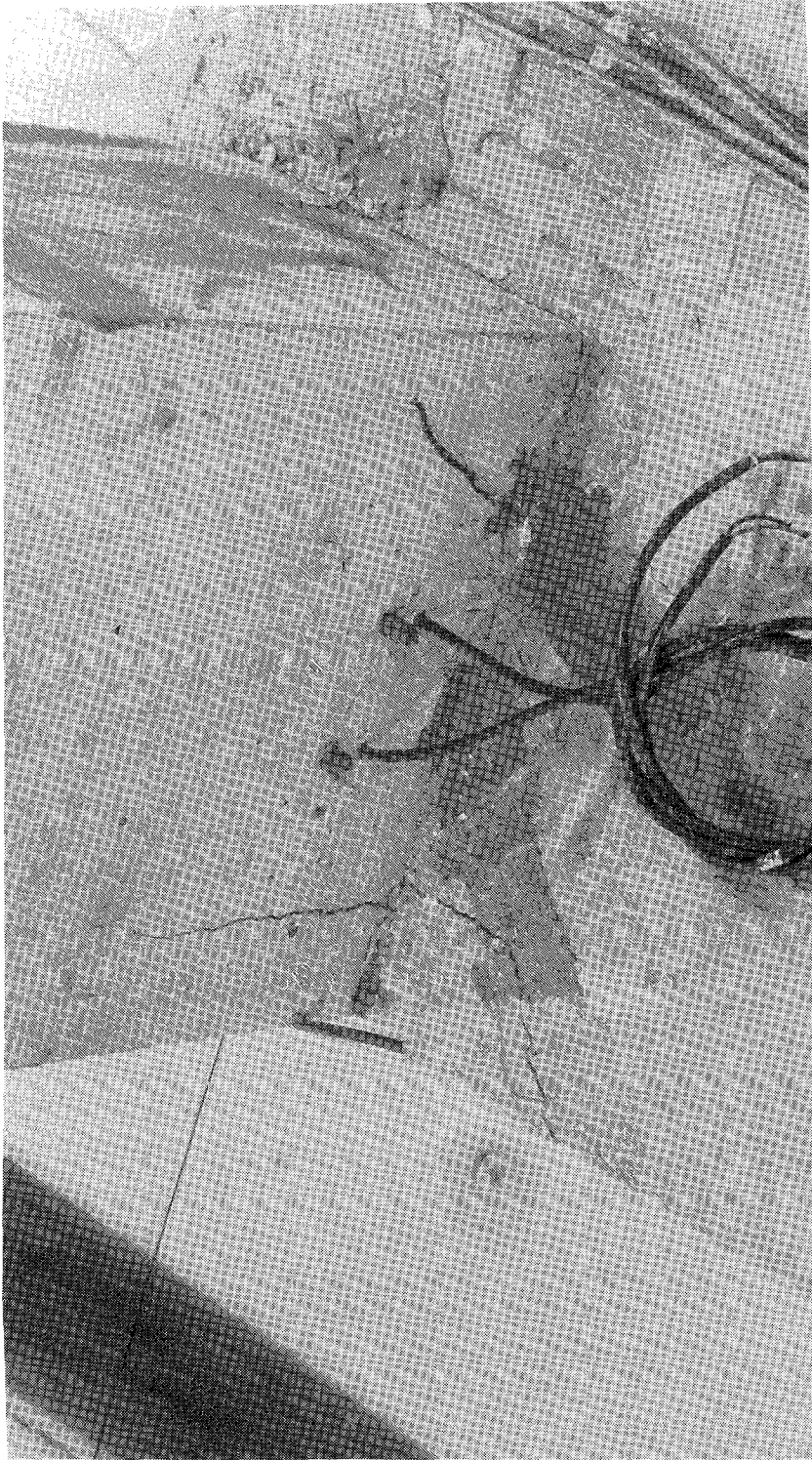


Fig. 4.4 CRACK PATTERN AT JUNCTION OF TOP STORY COLUMN WITH BOTTOM STORY SLAB.

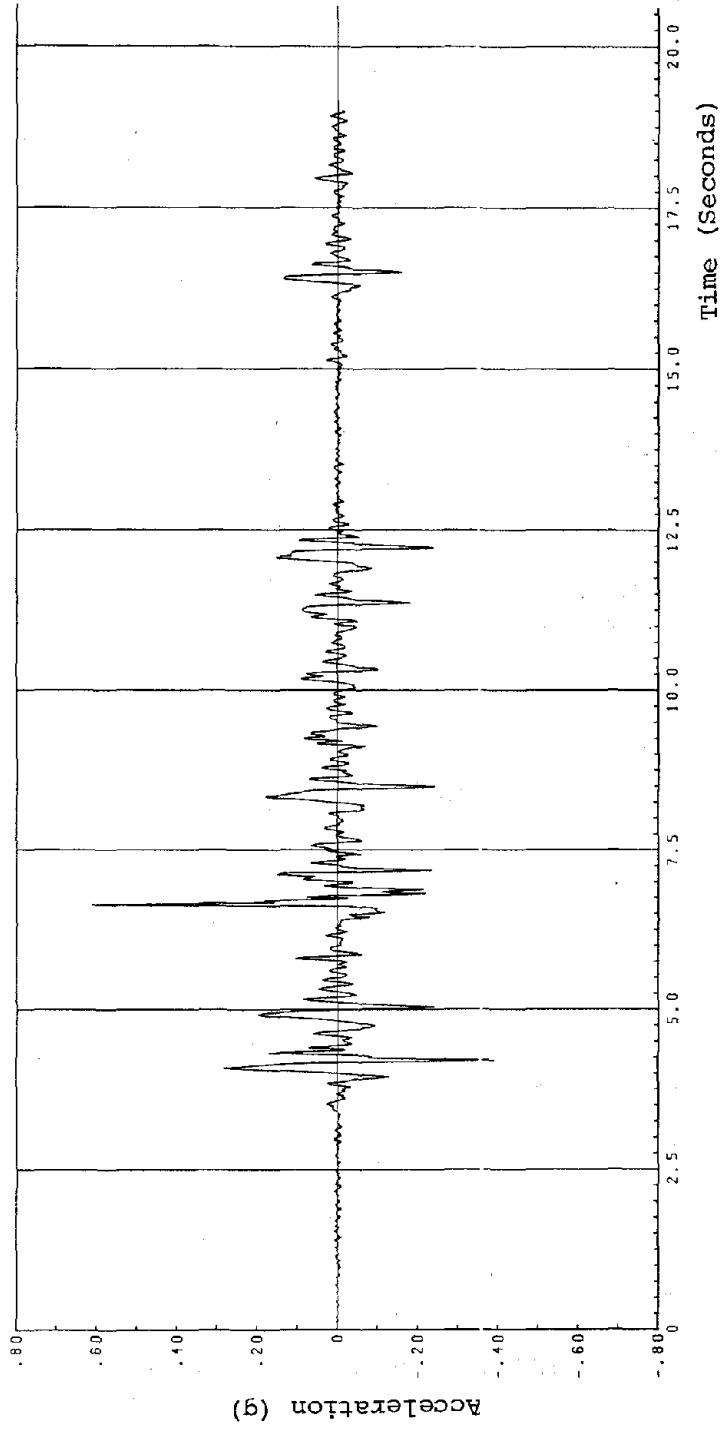


Fig. 4.5 VERTICAL TABLE ACCELERATION. RUN R3.

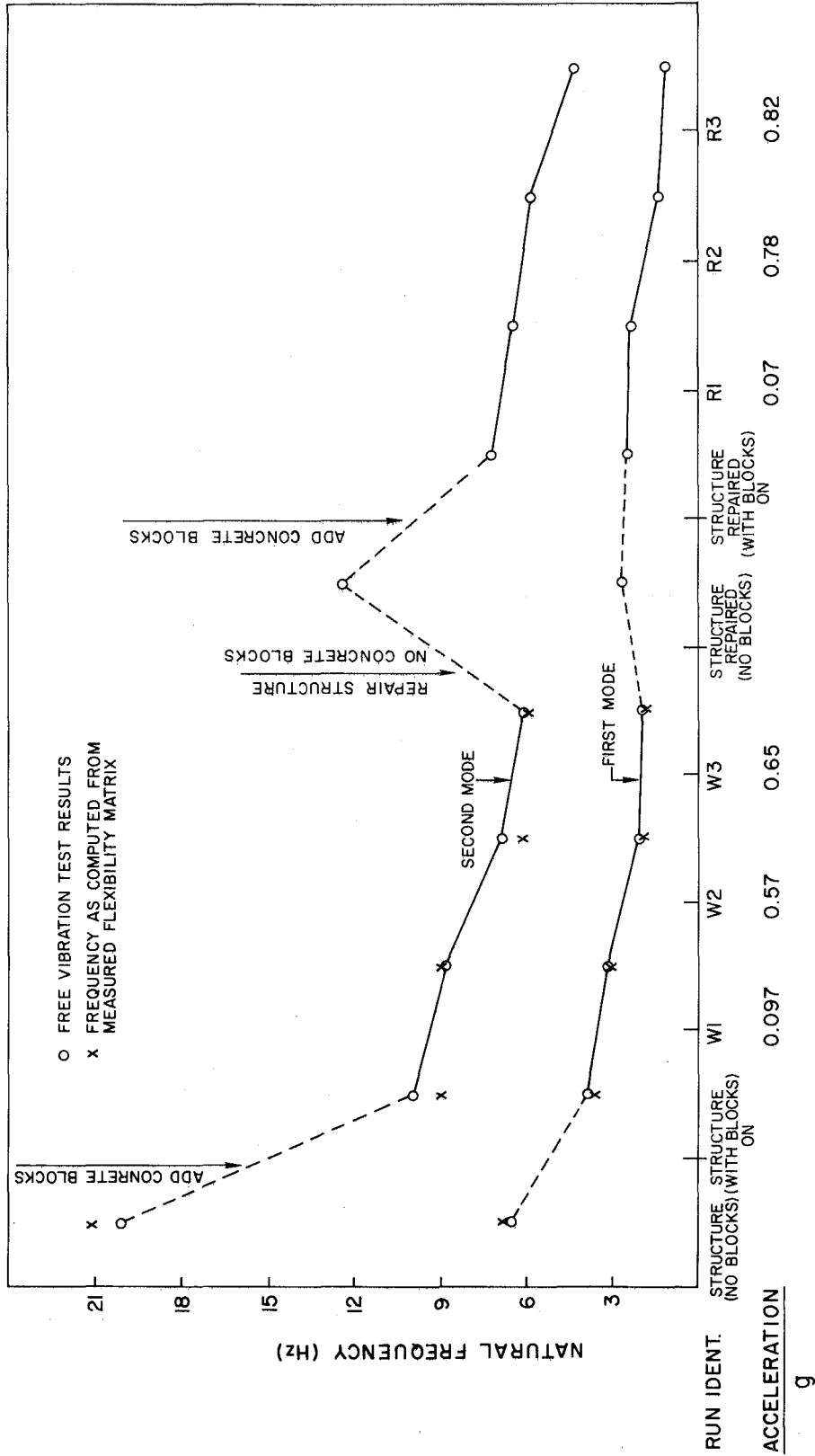


Fig. 4.6 FREQUENCY VARIATION THROUGHOUT TEST HISTORY.

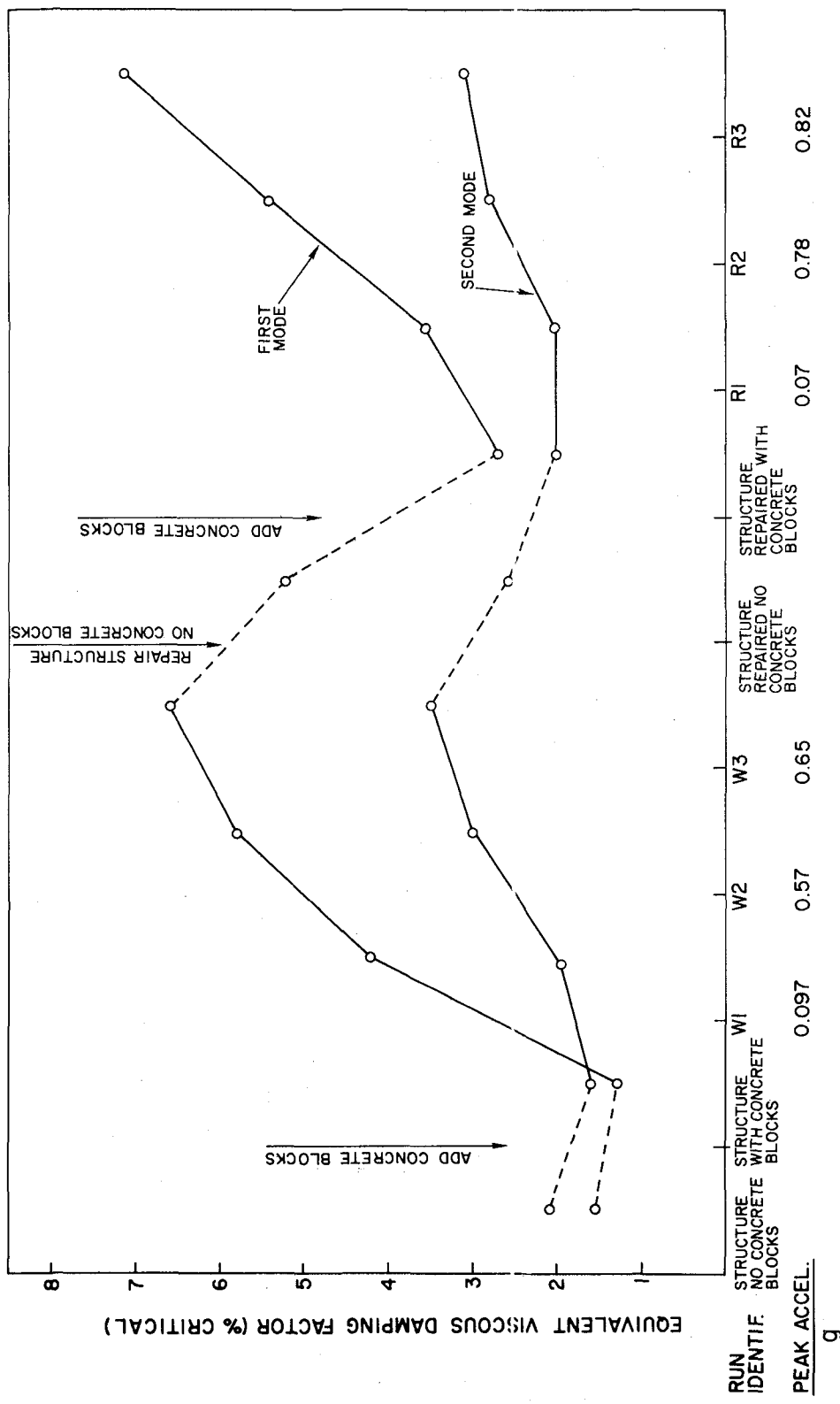


Fig. 4.7 VARIATION OF DAMPING THROUGHOUT TEST HISTORY AS EVALUATED FROM MEASURED FREE VIBRATION TESTS.

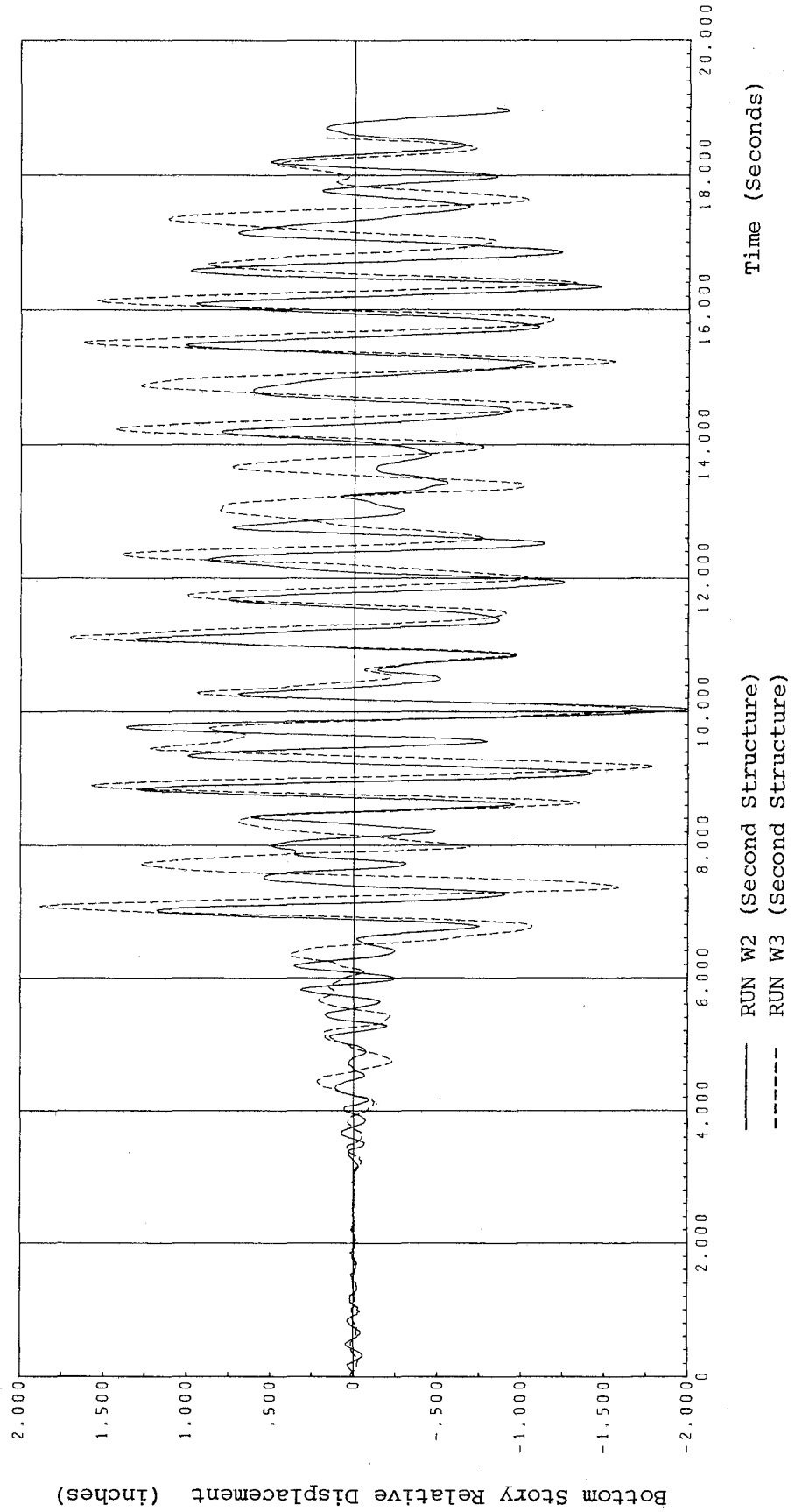


Fig. 4.8 (a) BOTTOM STORY RELATIVE DISPLACEMENT,  
RUNS W2 AND W3 OF SECOND STRUCTURE.

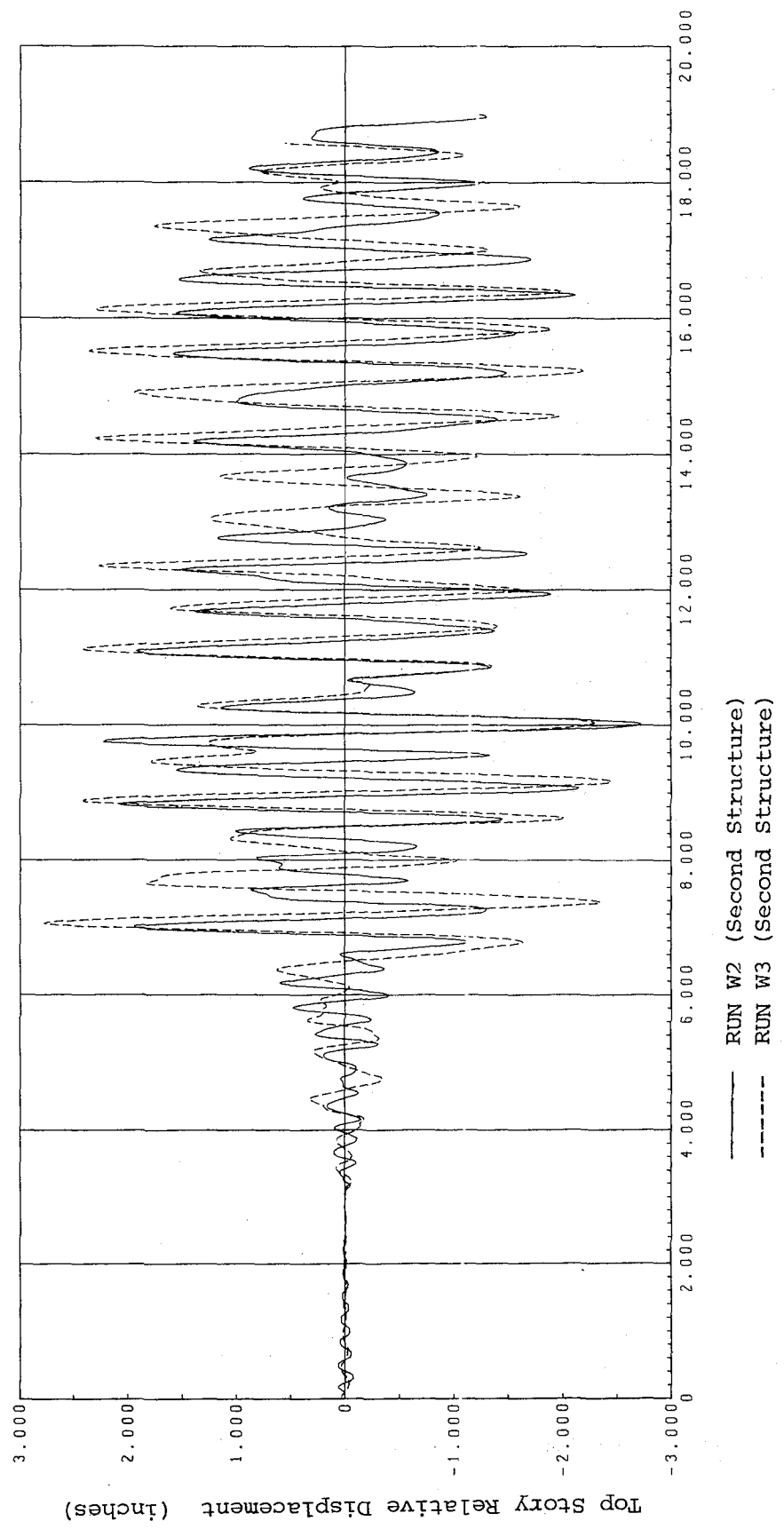


Fig. 4.8 (b) TOP STORY RELATIVE DISPLACEMENT,  
RUNS W2 AND W3 OF SECOND STRUCTURE.

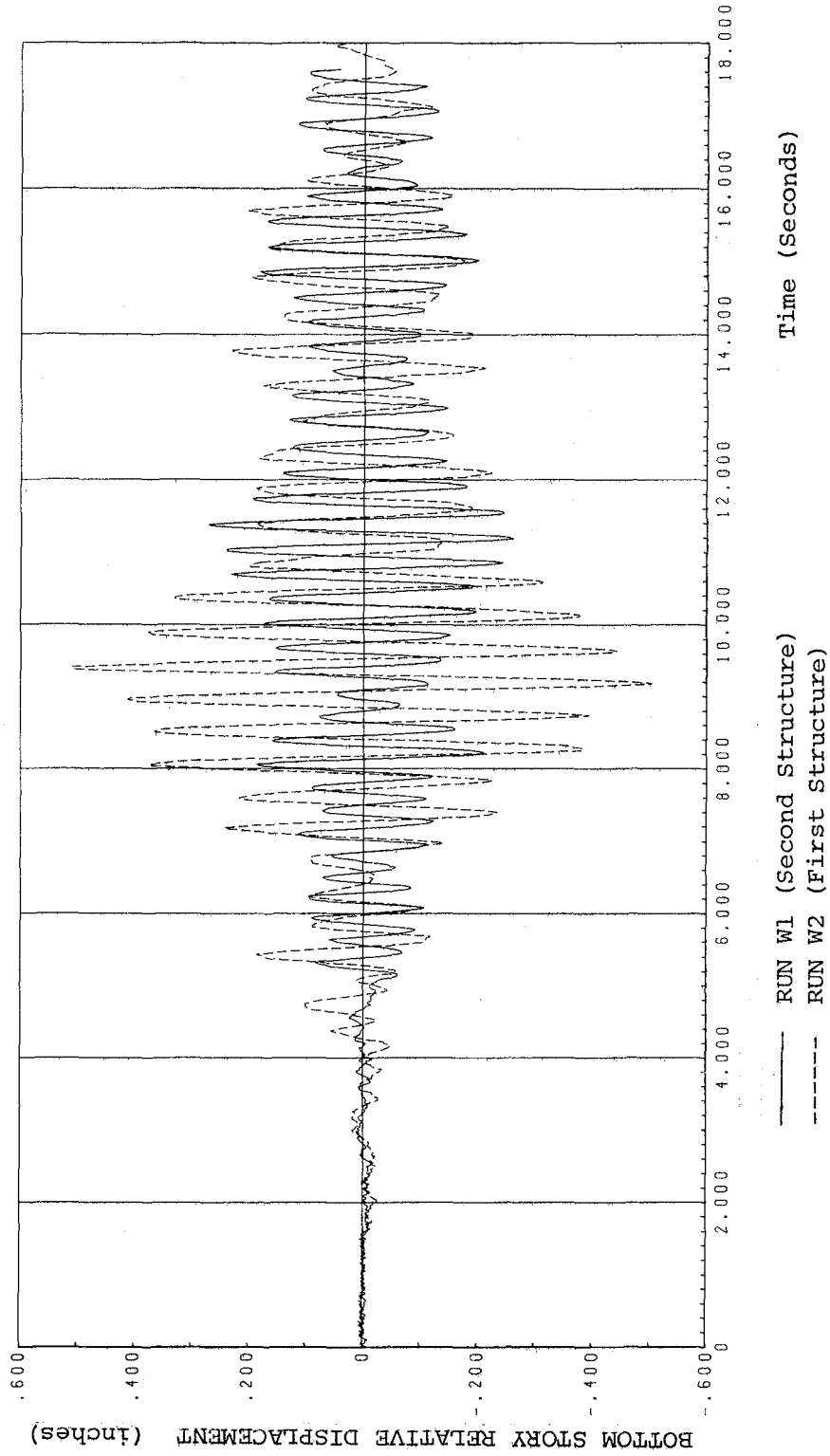


Fig. 4.9 (a) BOTTOM STORY RELATIVE DISPLACEMENT.  
RUN W1 OF SECOND STRUCTURE AND  
RUN W2 OF FIRST STRUCTURE.

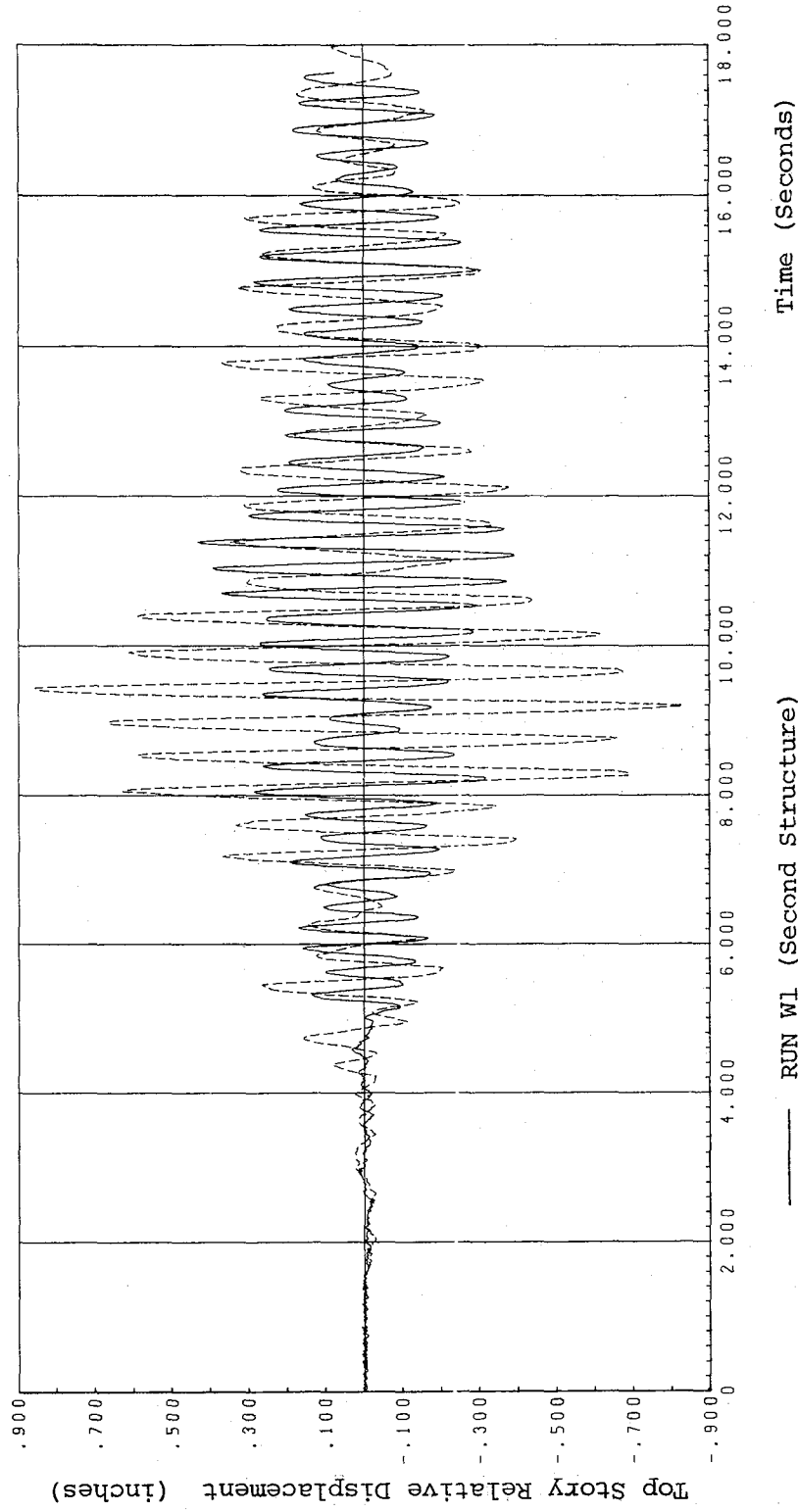


Fig. 4.9 (b) TOP STORY RELATIVE DISPLACEMENT.  
 RUN W1 OF SECOND STRUCTURE AND RUN W2 OF  
 FIRST STRUCTURE.

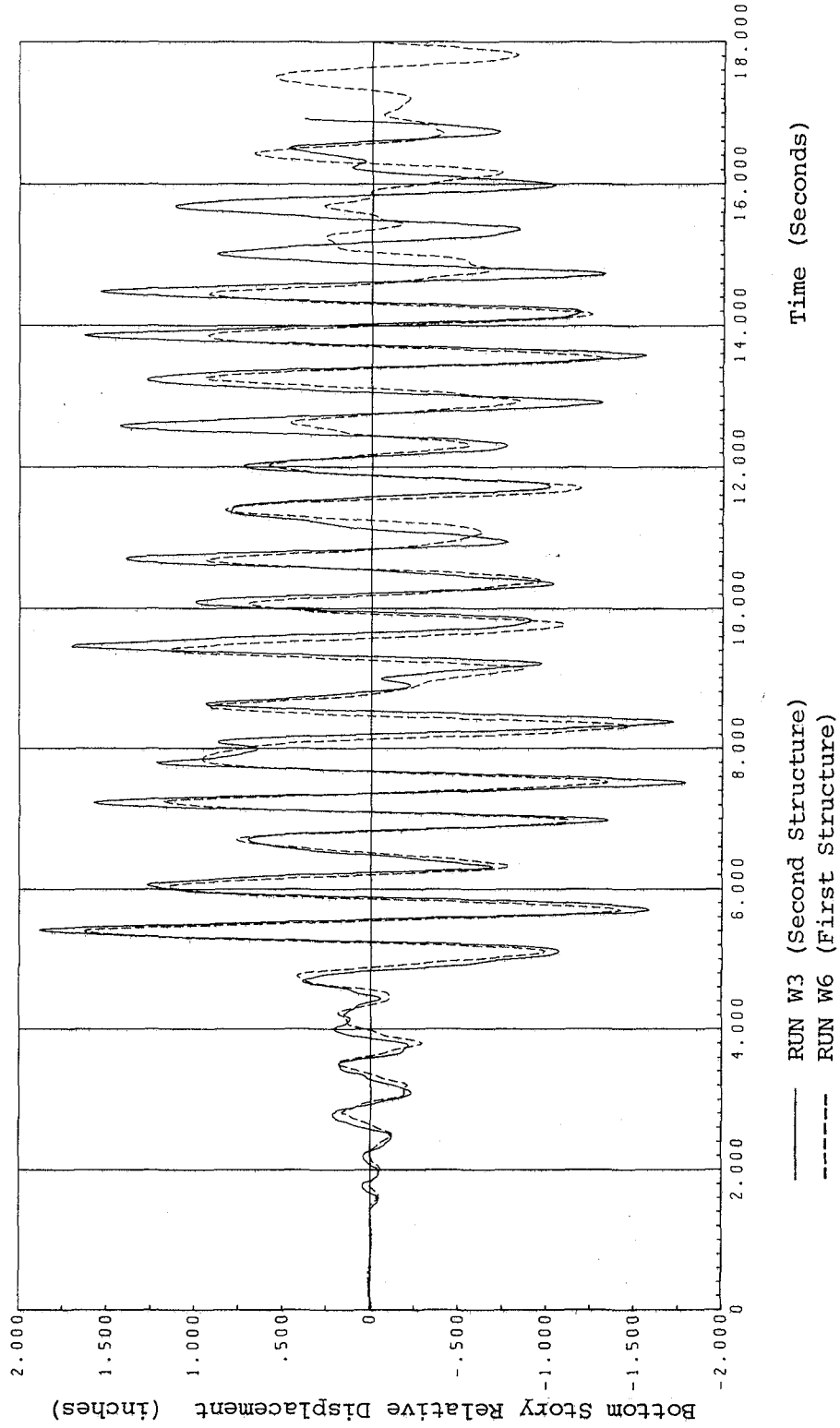


Fig. 4.10 (a) BOTTOM STORY RELATIVE DISPLACEMENT. RUN W3 OF SECOND STRUCTURE AND RUN W6 OF FIRST STRUCTURE.

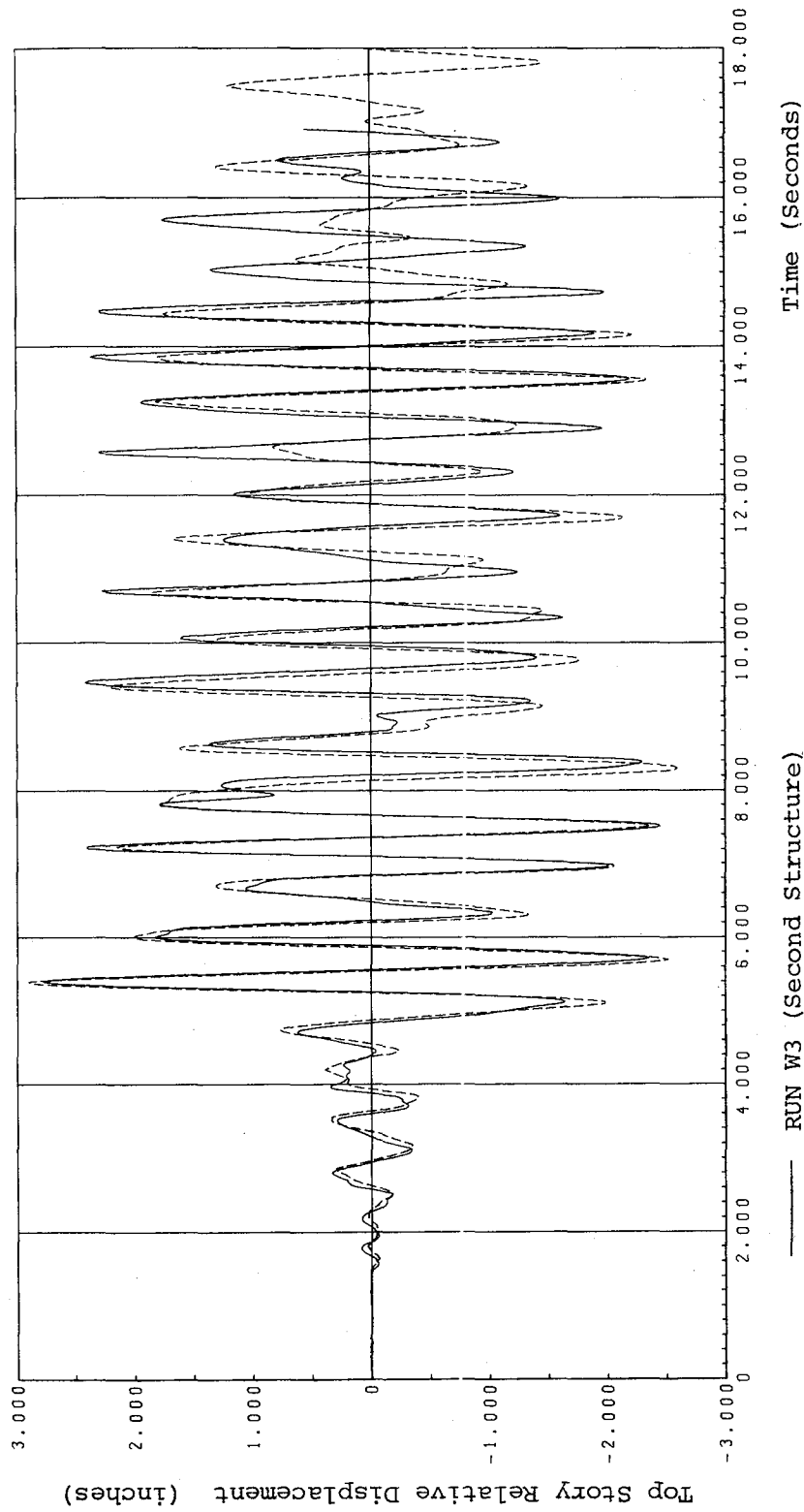


Fig. 4.10 (b) TOP STORY RELATIVE DISPLACEMENT. RUN W3 OF SECOND STRUCTURE AND RUN W6 OF FIRST STRUCTURE.

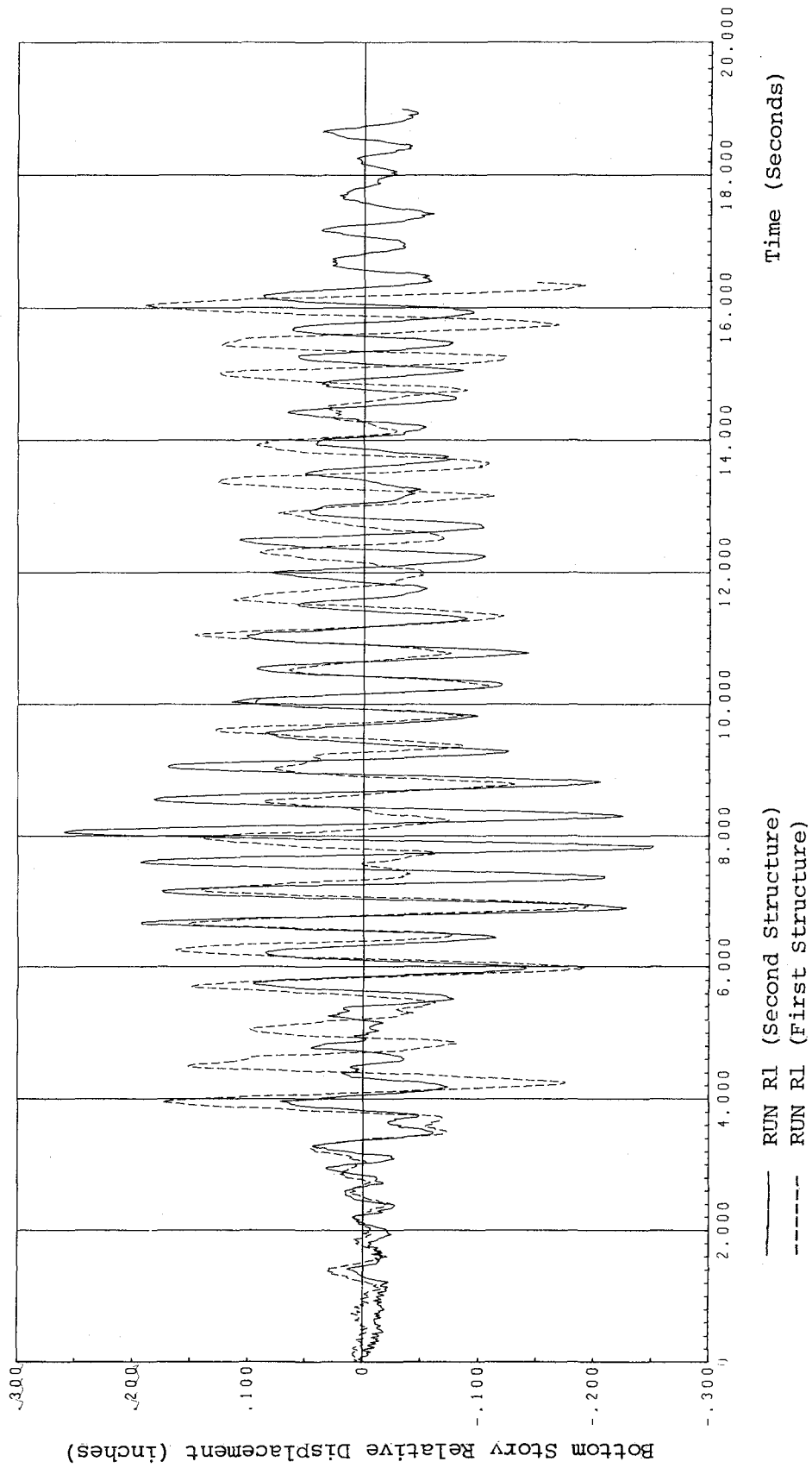


Fig. 4.11 (a) BOTTOM STORY RELATIVE DISPLACEMENT.  
RUNS R1 OF SECOND AND FIRST STRUCTURES.

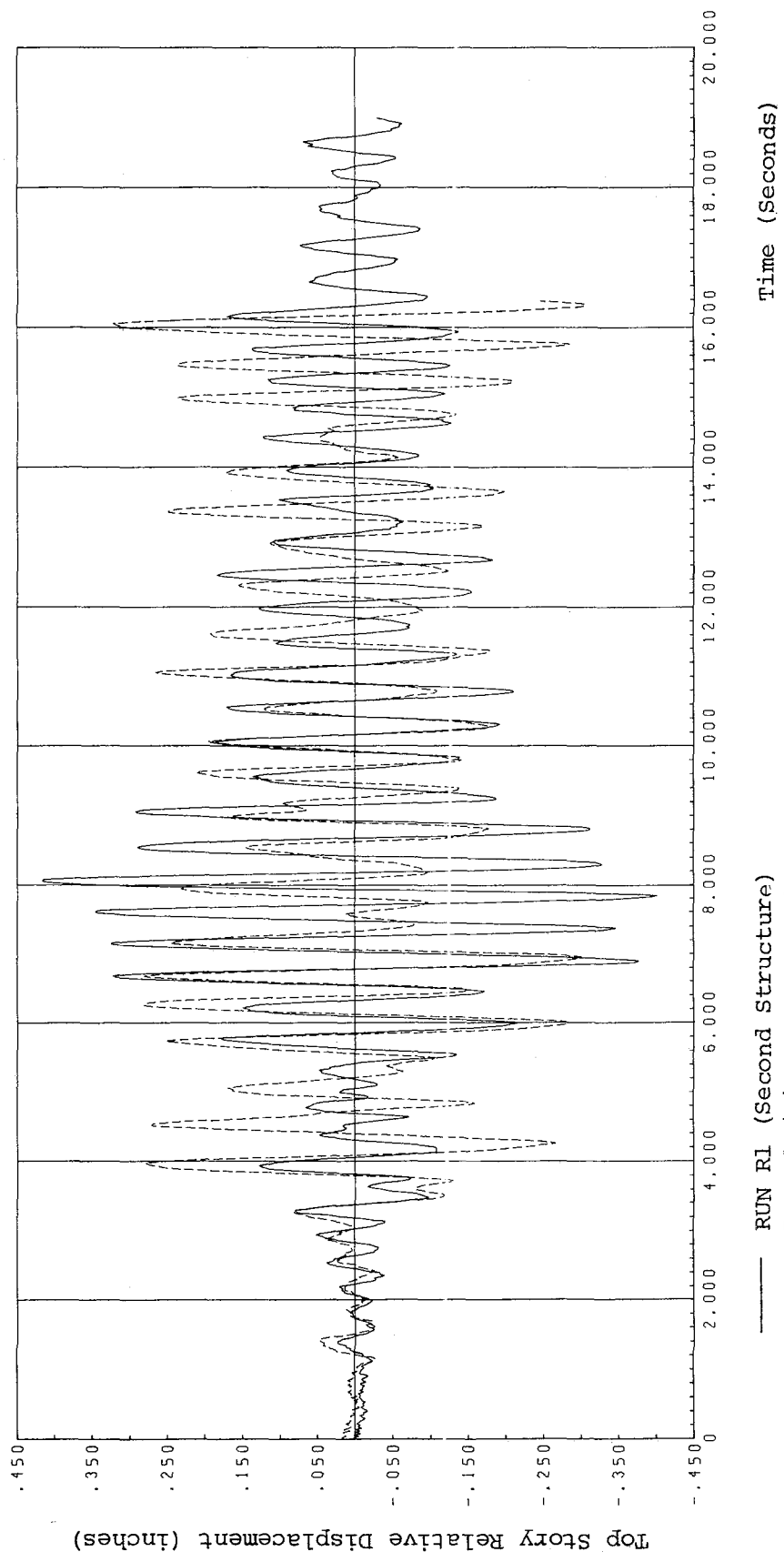


Fig. 4.11 (b) TOP STORY RELATIVE DISPLACEMENT.  
RUNS R1 OF SECOND AND FIRST STRUCTURES.

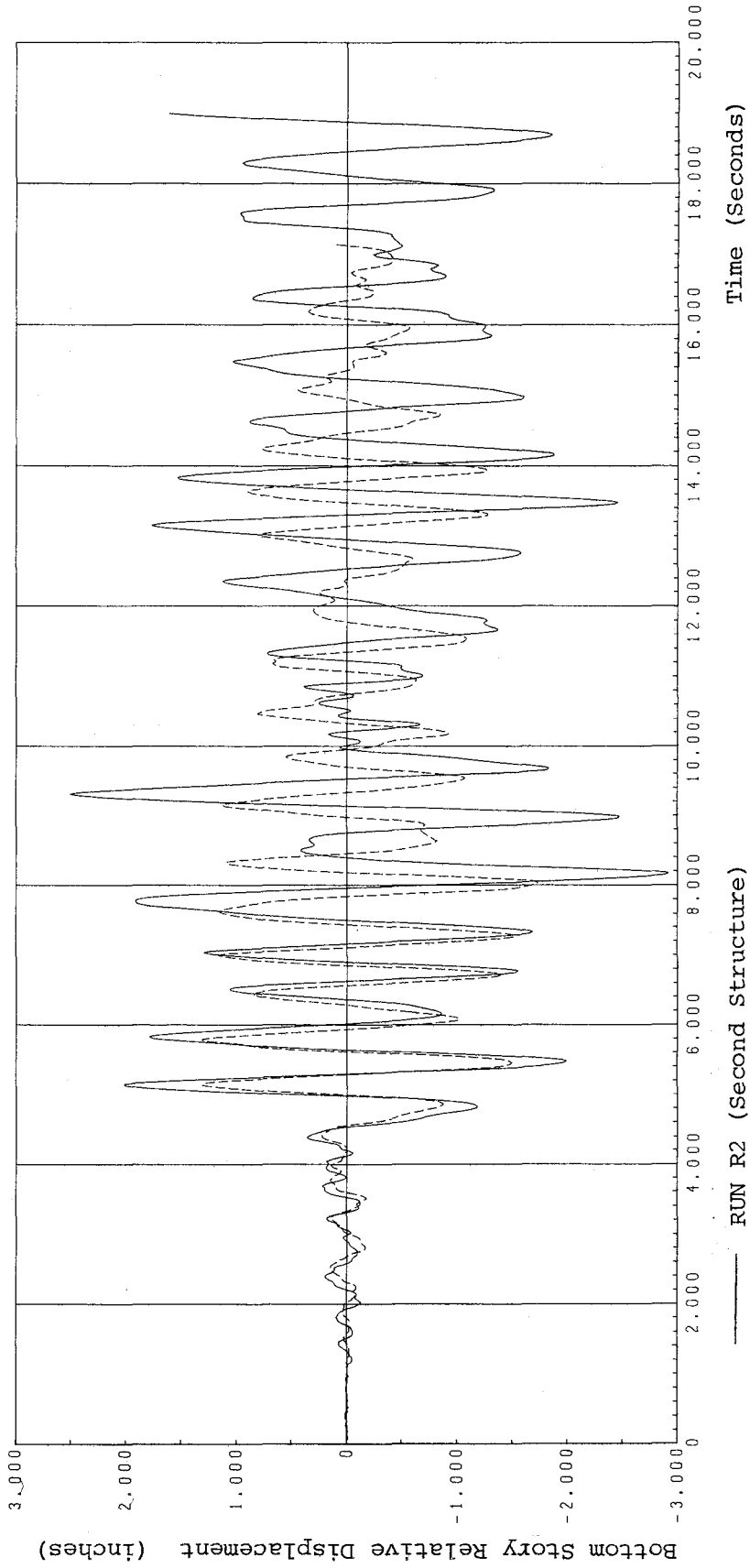


Fig. 4.12 (a) BOTTOM STORY RELATIVE DISPLACEMENT.  
RUNS R2 OF SECOND AND FIRST STRUCTURES.

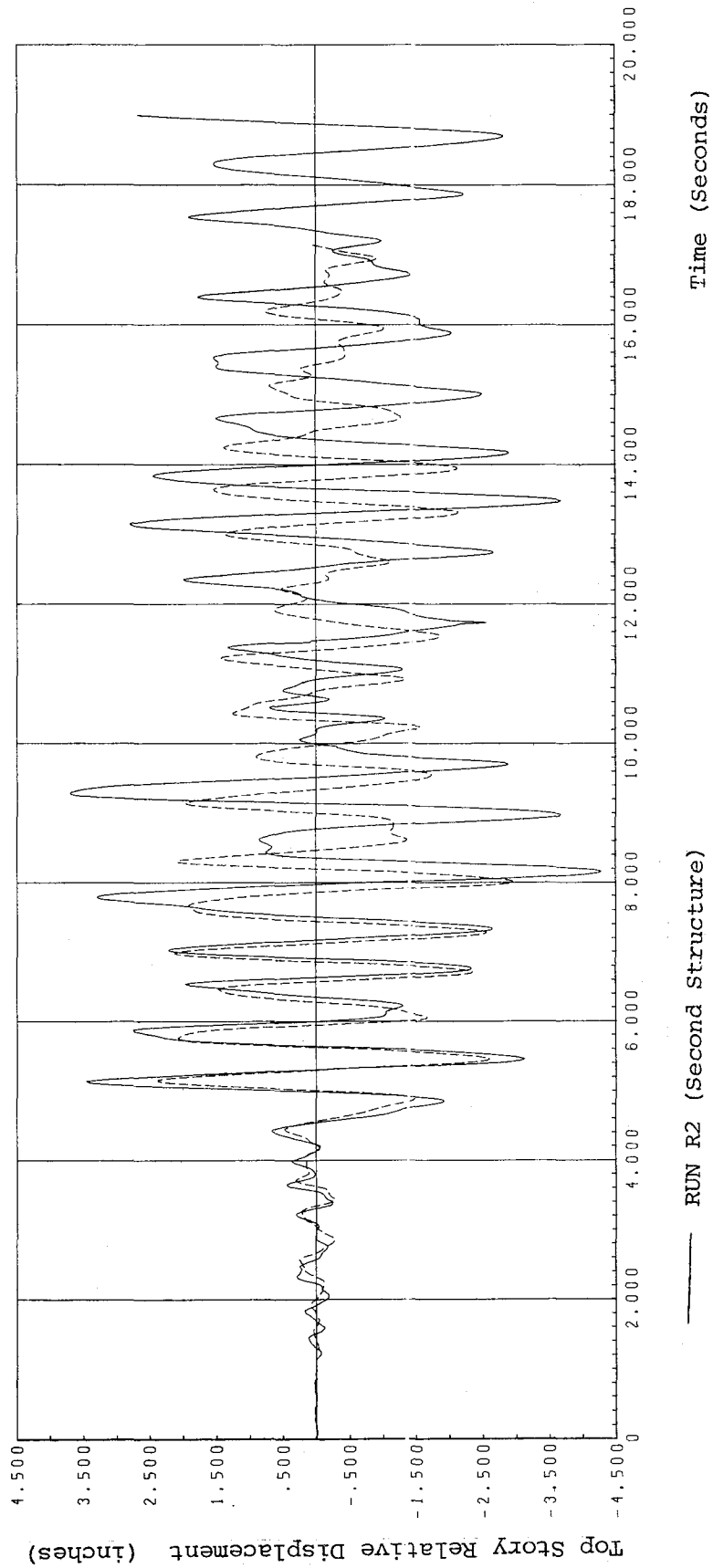


Fig. 4.12 (b) TOP STORY RELATIVE DISPLACEMENT.  
RUNS R2 OF SECOND AND FIRST STRUCTURES.

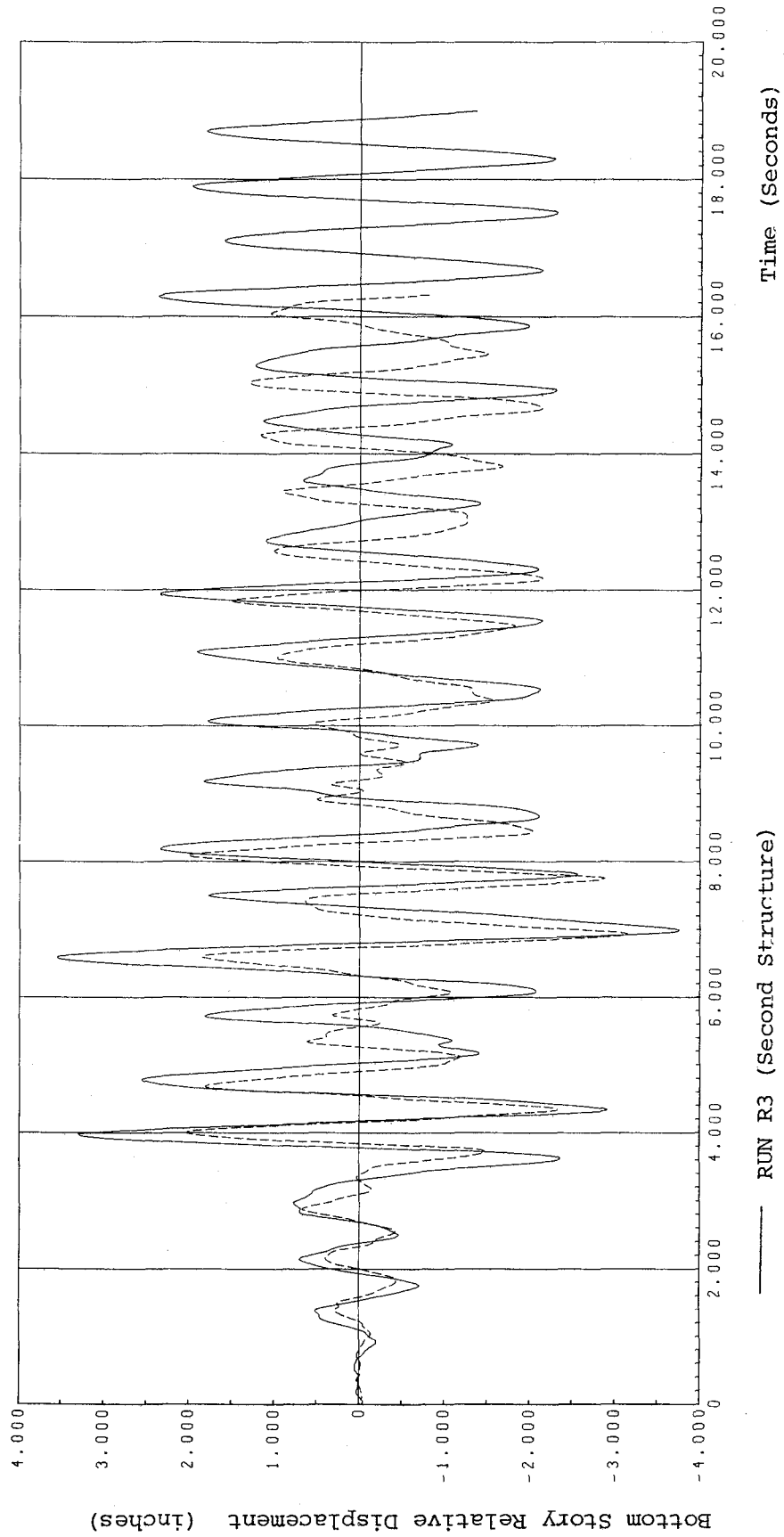


Fig. 4.13 (a) BOTTOM STORY RELATIVE DISPLACEMENT.  
RUNS R3 OF SECOND AND FIRST STRUCTURE.

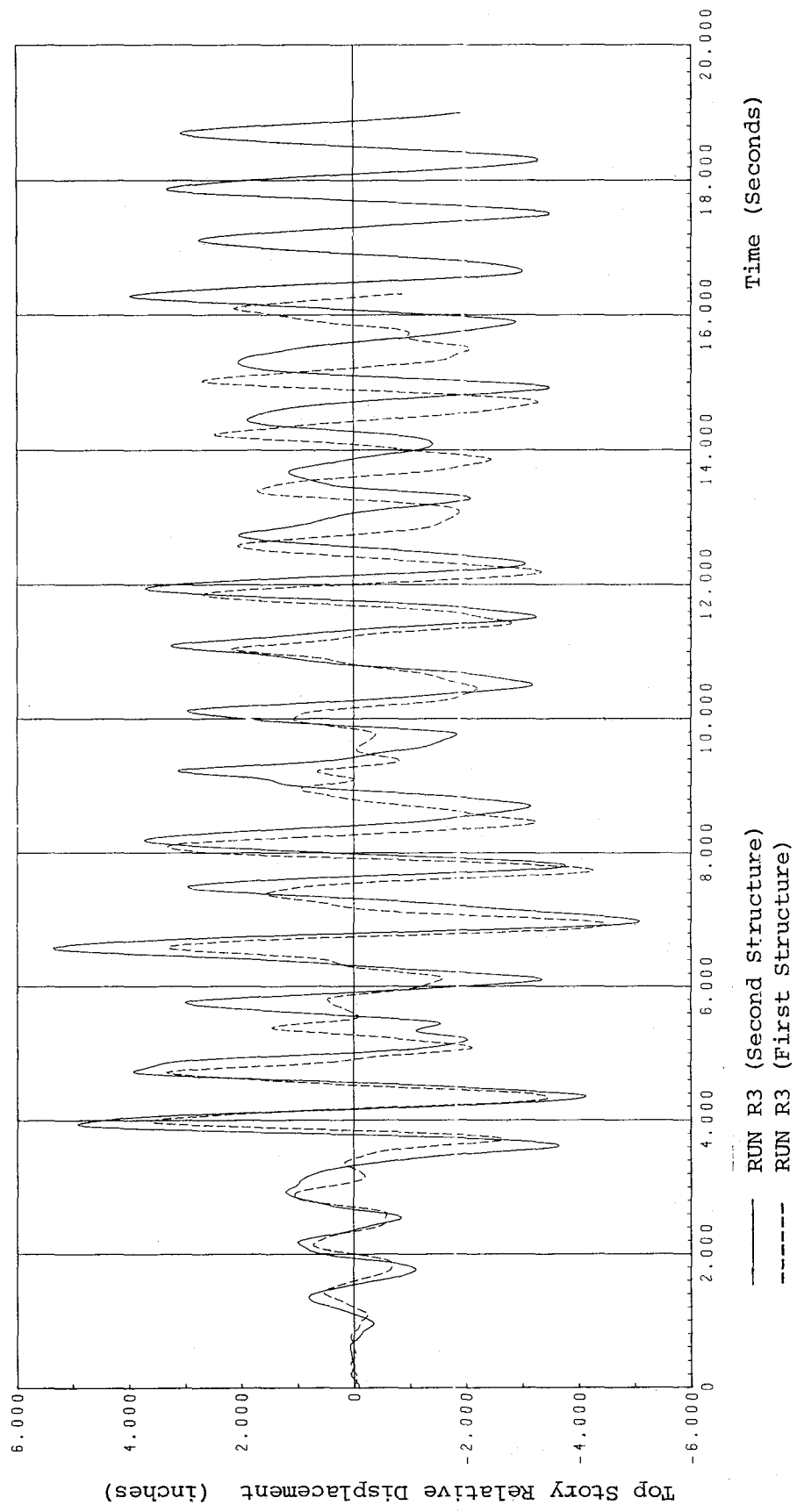


Fig. 4.13 (b) TOP STORY RELATIVE DISPLACEMENT.  
RUNS R3 OF SECOND AND FIRST STRUCTURE.

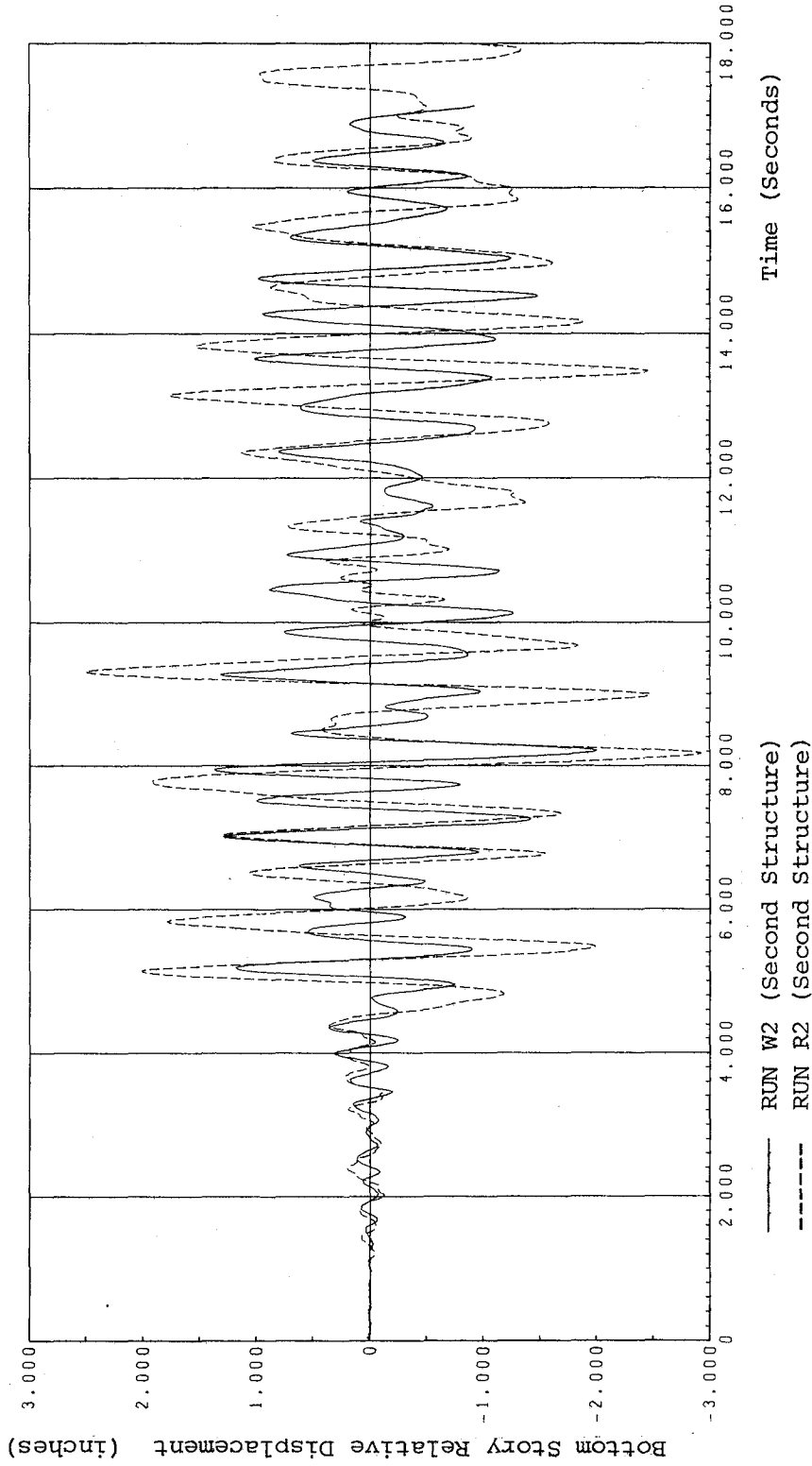


Fig. 4.14 (a) BOTTOM STORY RELATIVE DISPLACEMENT.  
RUNS W2 AND R2 OF SECOND STRUCTURE.

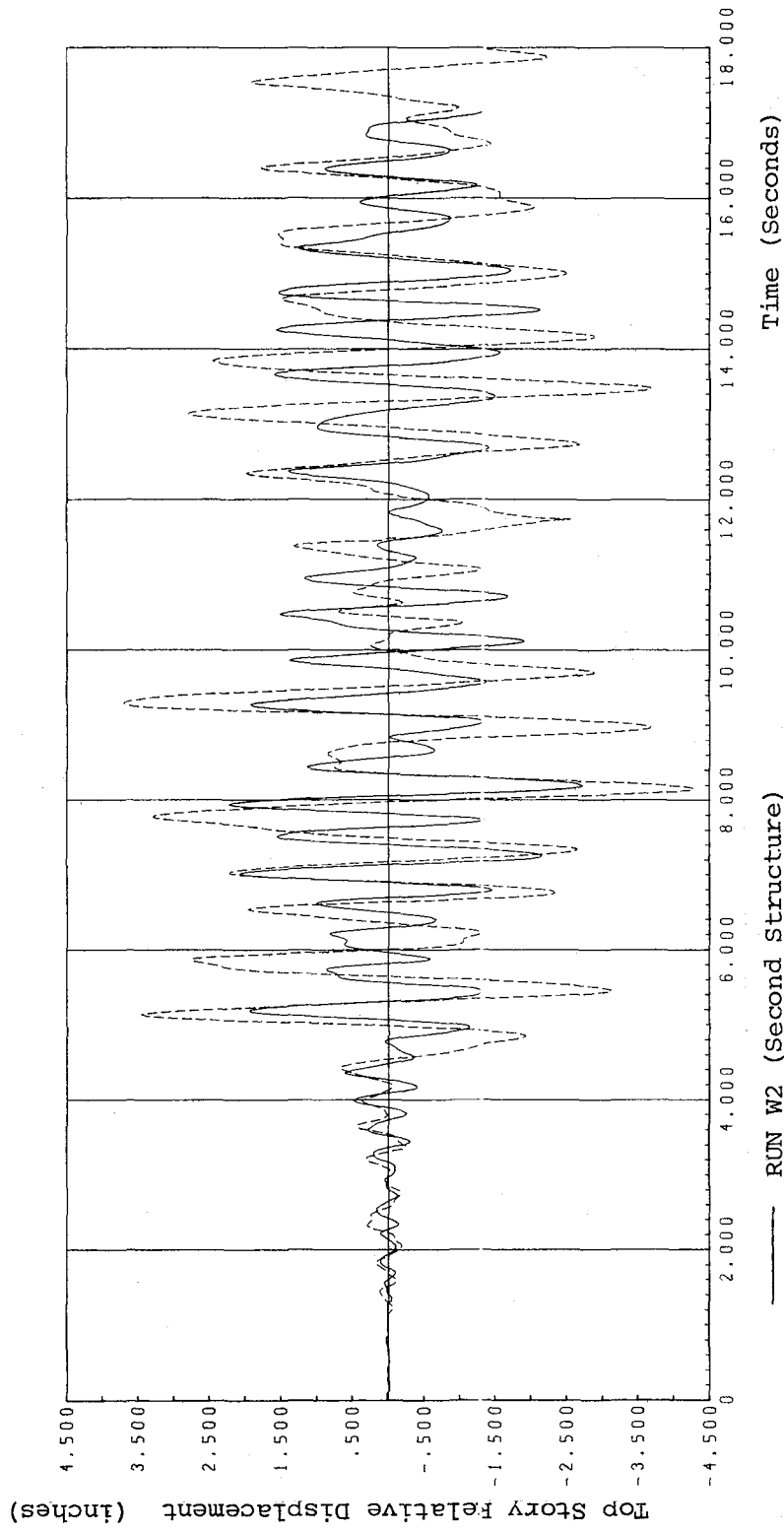


Fig. 4.14 (b) TOP STORY RELATIVE DISPLACEMENT.  
RUNS W2 AND R2 OF SECOND STRUCTURE.

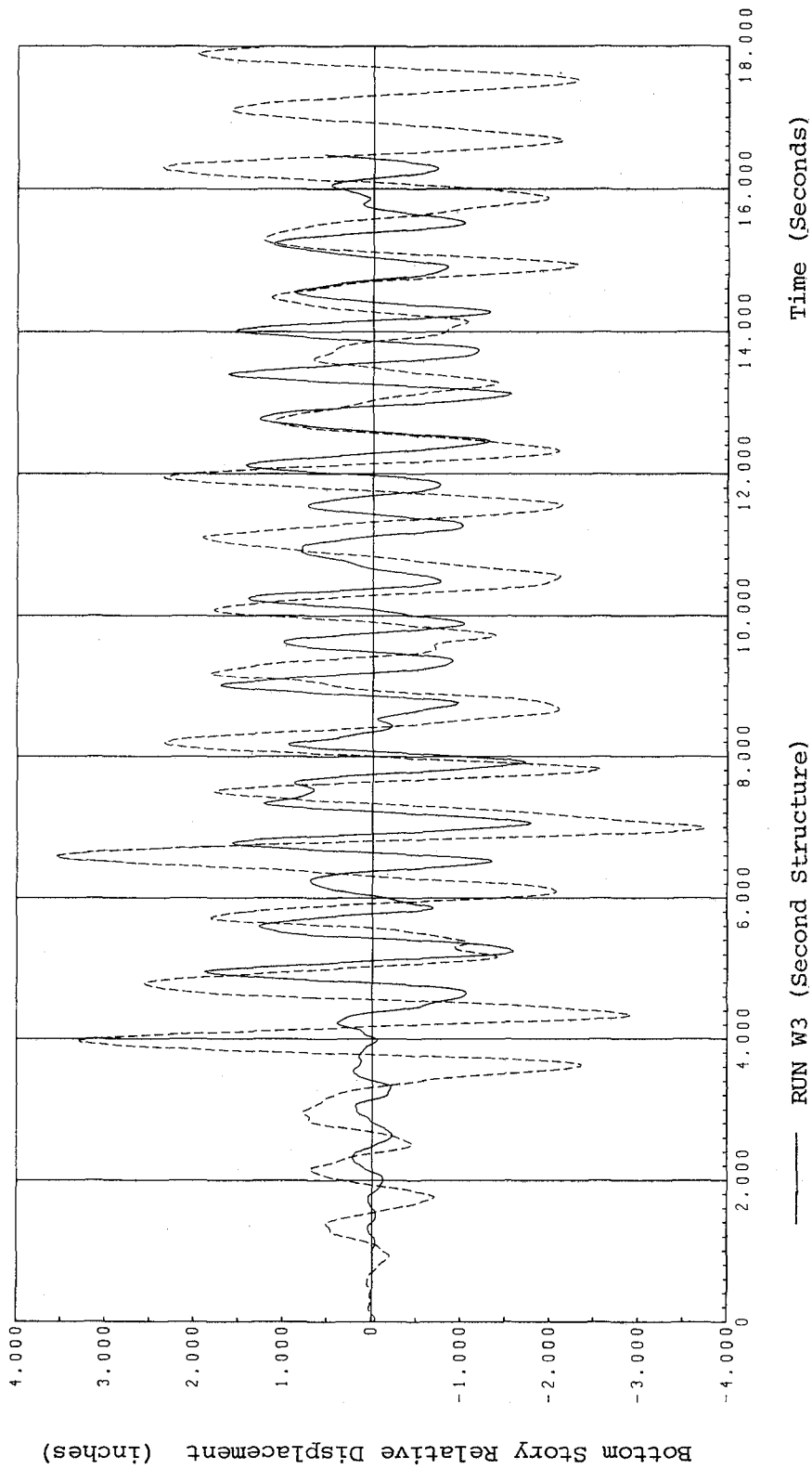


Fig. 4.15 (a) BOTTOM STORY RELATIVE DISPLACEMENT,  
RUNS W3 AND R3 OF SECOND STRUCTURE.

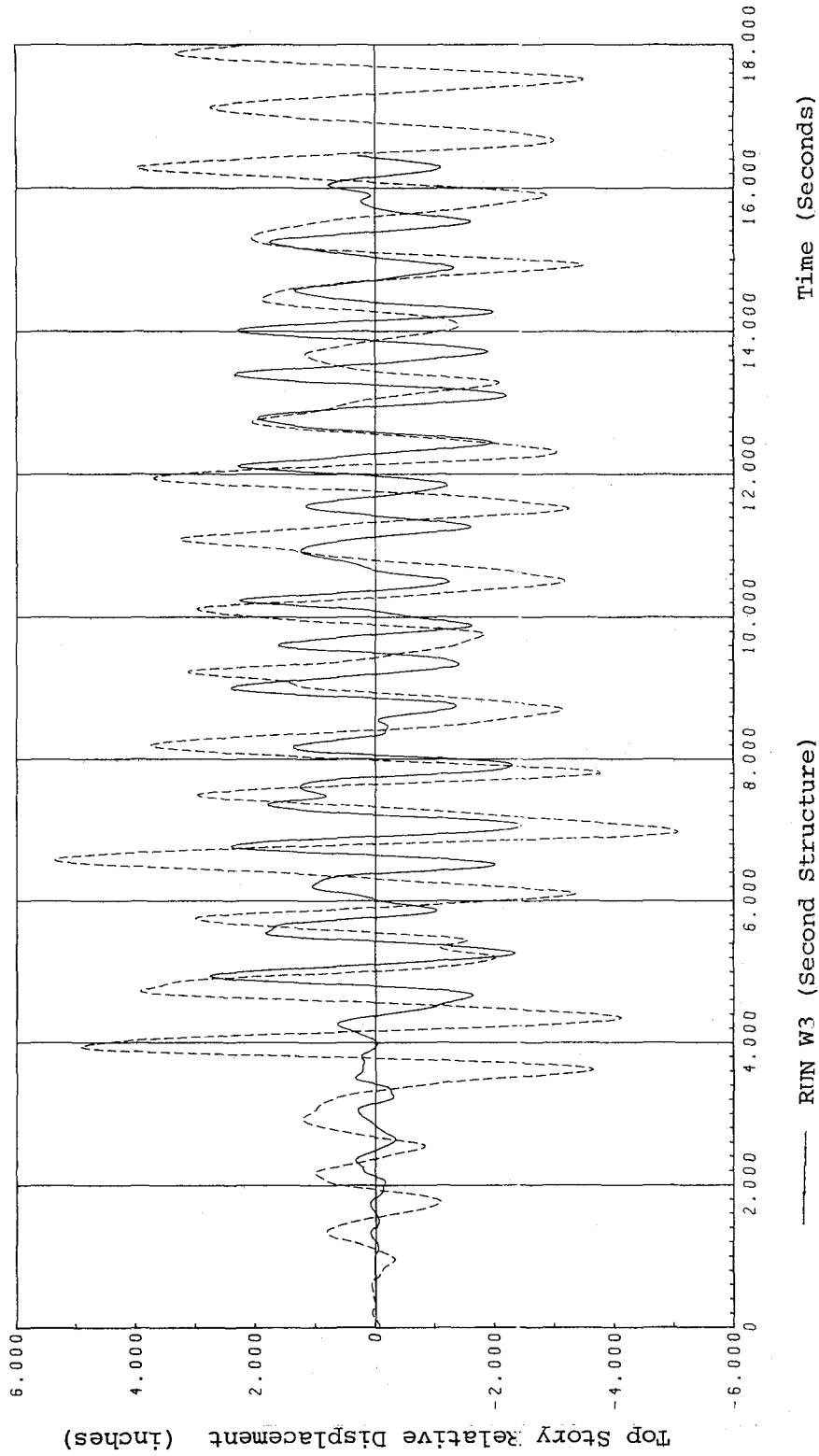


Fig. 4.15 (b) TOP STORY RELATIVE DISPLACEMENT.  
RUNS W3 AND R3 OF SECOND STRUCTURE.

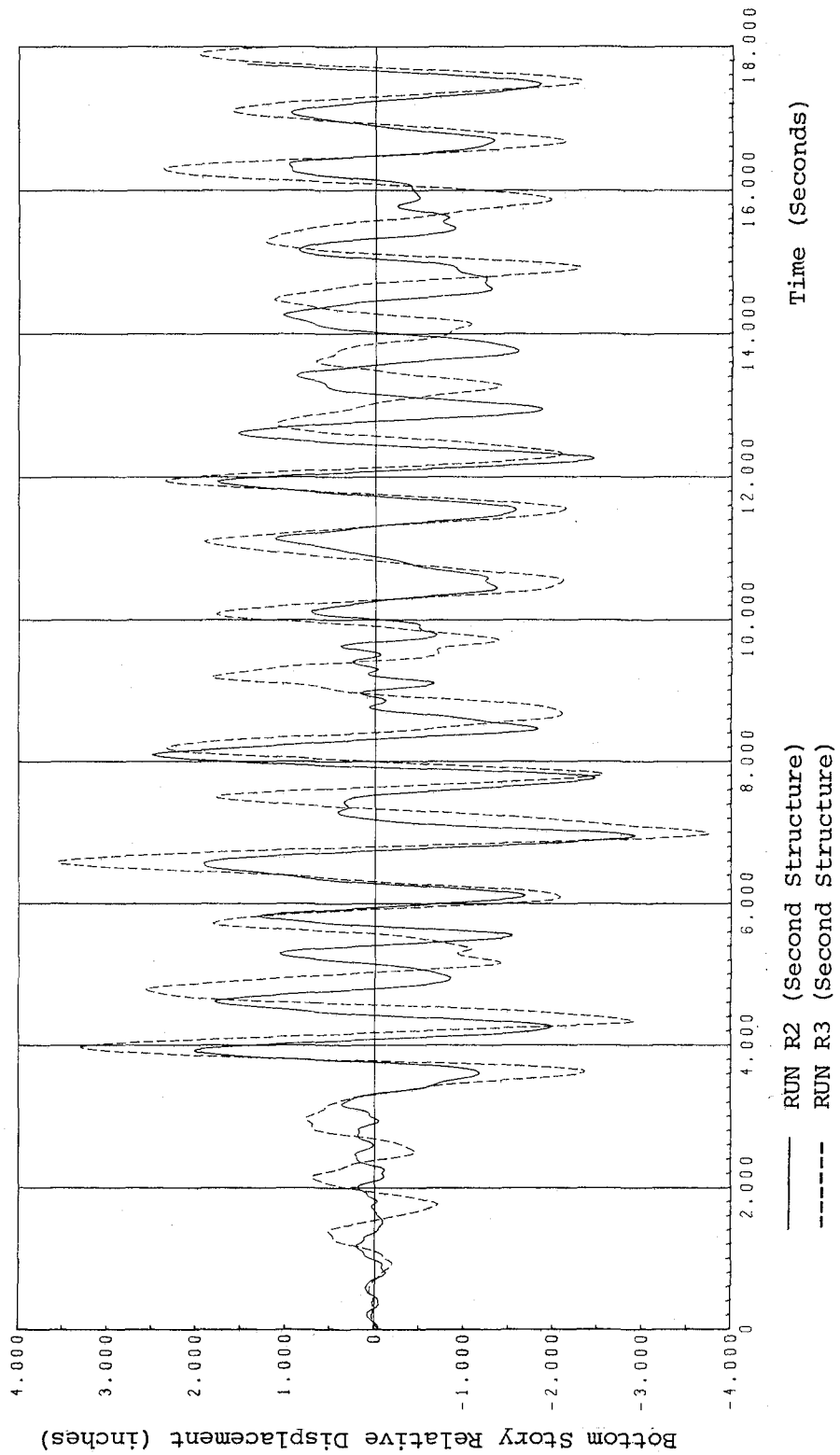


Fig. 4.16 (a) BOTTOM STORY RELATIVE DISPLACEMENT.  
RUNS R2 AND R3 OF SECOND STRUCTURE.

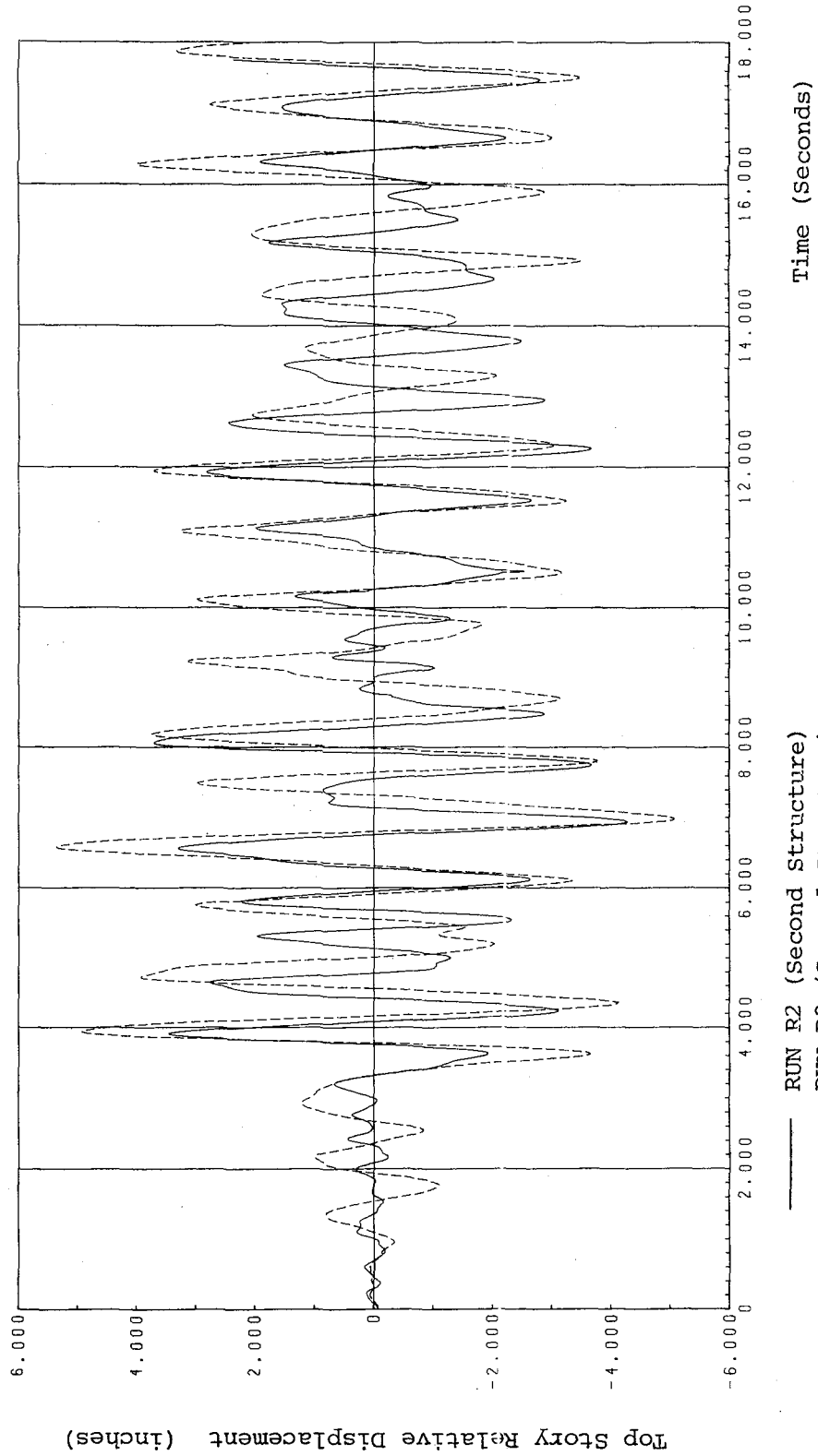


Fig. 4.16 (b) TOP STORY RELATIVE DISPLACEMENT.  
 RUNS R2 AND R3 OF SECOND STRUCTURE.

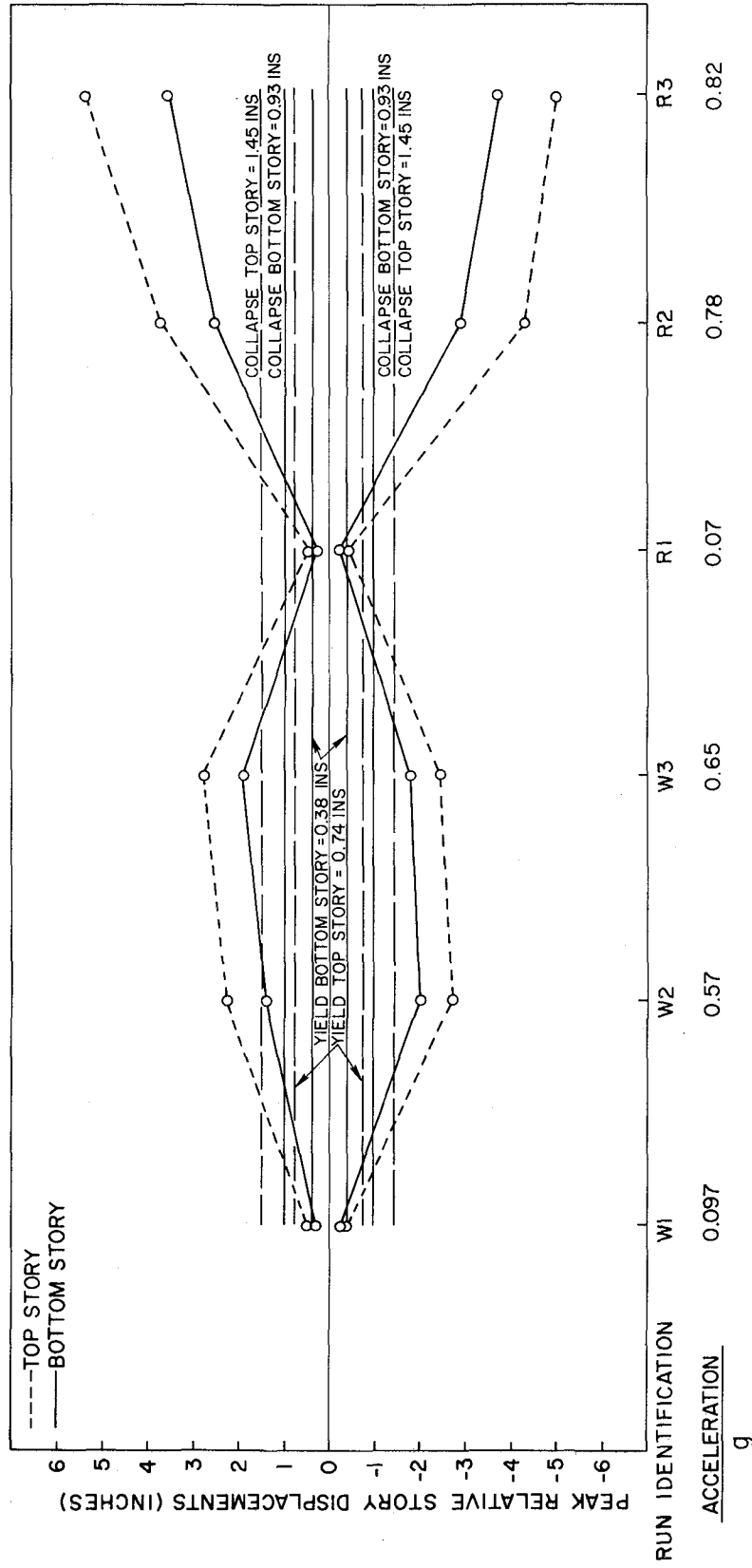


Fig. 4.17 PEAK VALUES OF RELATIVE STORY DISPLACEMENTS ATTAINED THROUGHOUT TEST HISTORY. YIELD AND COLLAPSE VALUES OBTAINED BY ELASTO-PLASTIC ANALYSIS.

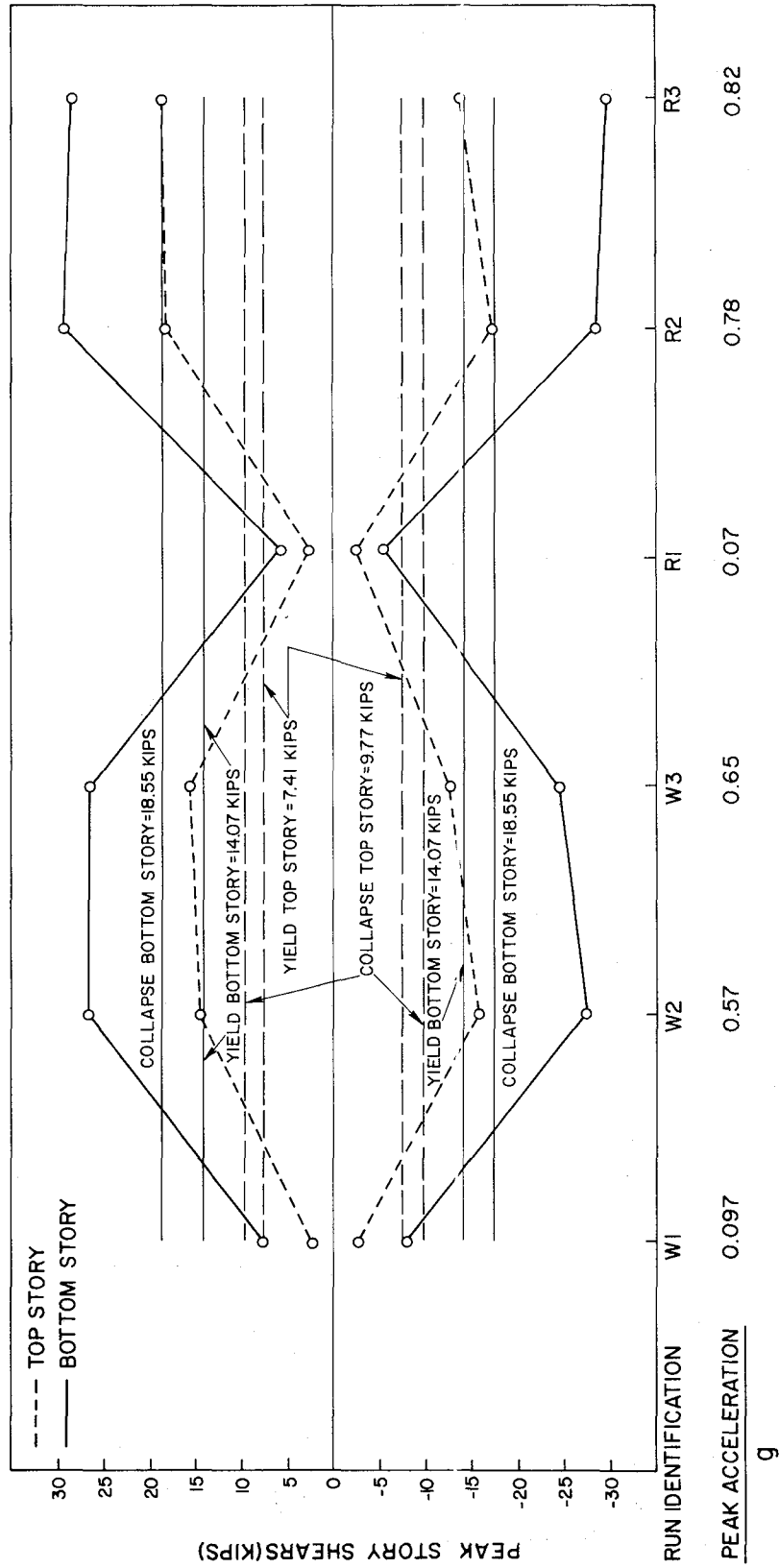


Fig. 4.18 PEAK STORY SHEARS ATTAINED THROUGHOUT TEST HISTORY.  
YIELD AND COLLAPSE VALUES OBTAINED USING ELASTO-PLASTIC ANALYSIS.

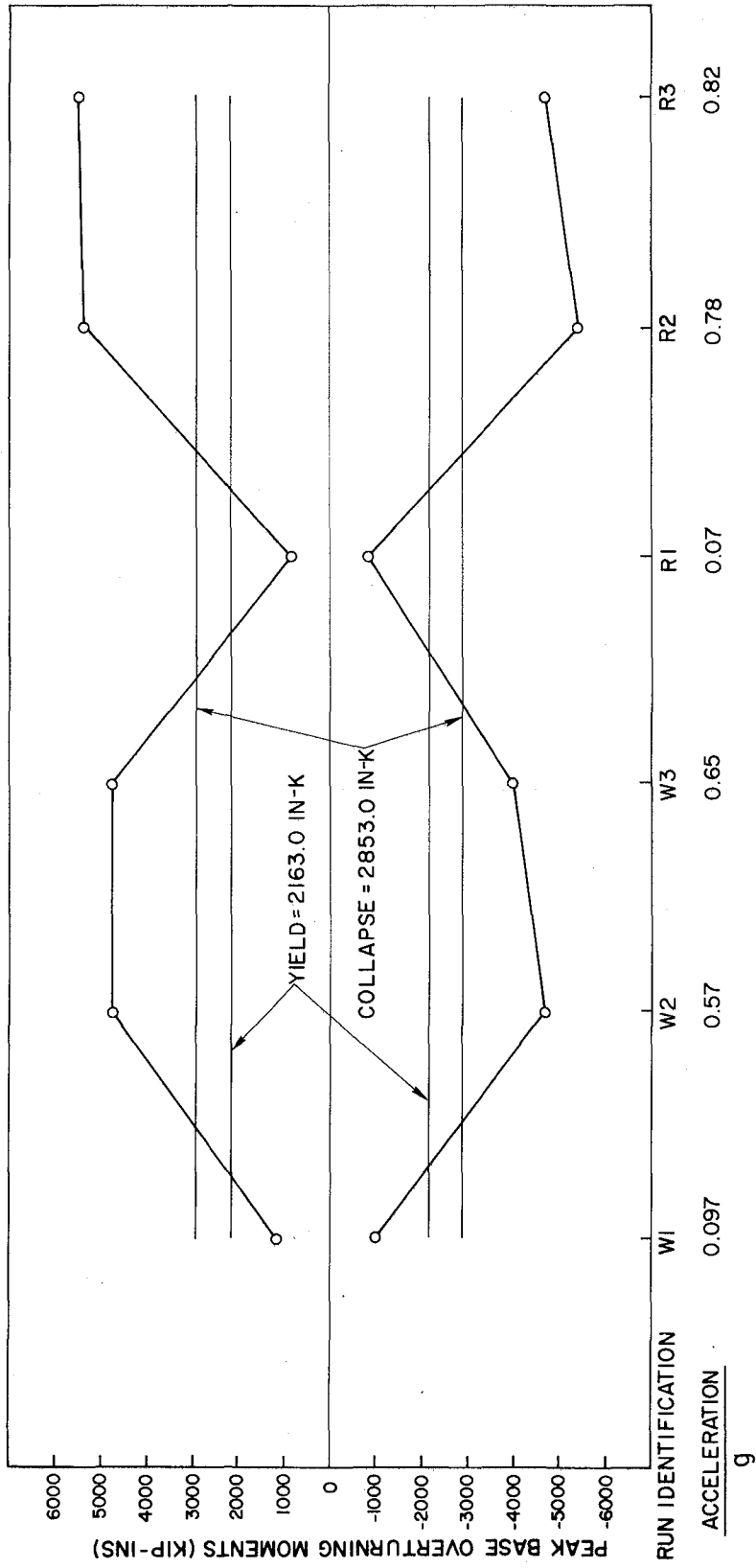


Fig. 4.19 PEAK BASE OVERTURNING MOMENTS ATTAINED THROUGHOUT TEST HISTORY. YIELD AND COLLAPSE LEVELS OBTAINED BY AN ELASTO-PLASTIC ANALYSIS

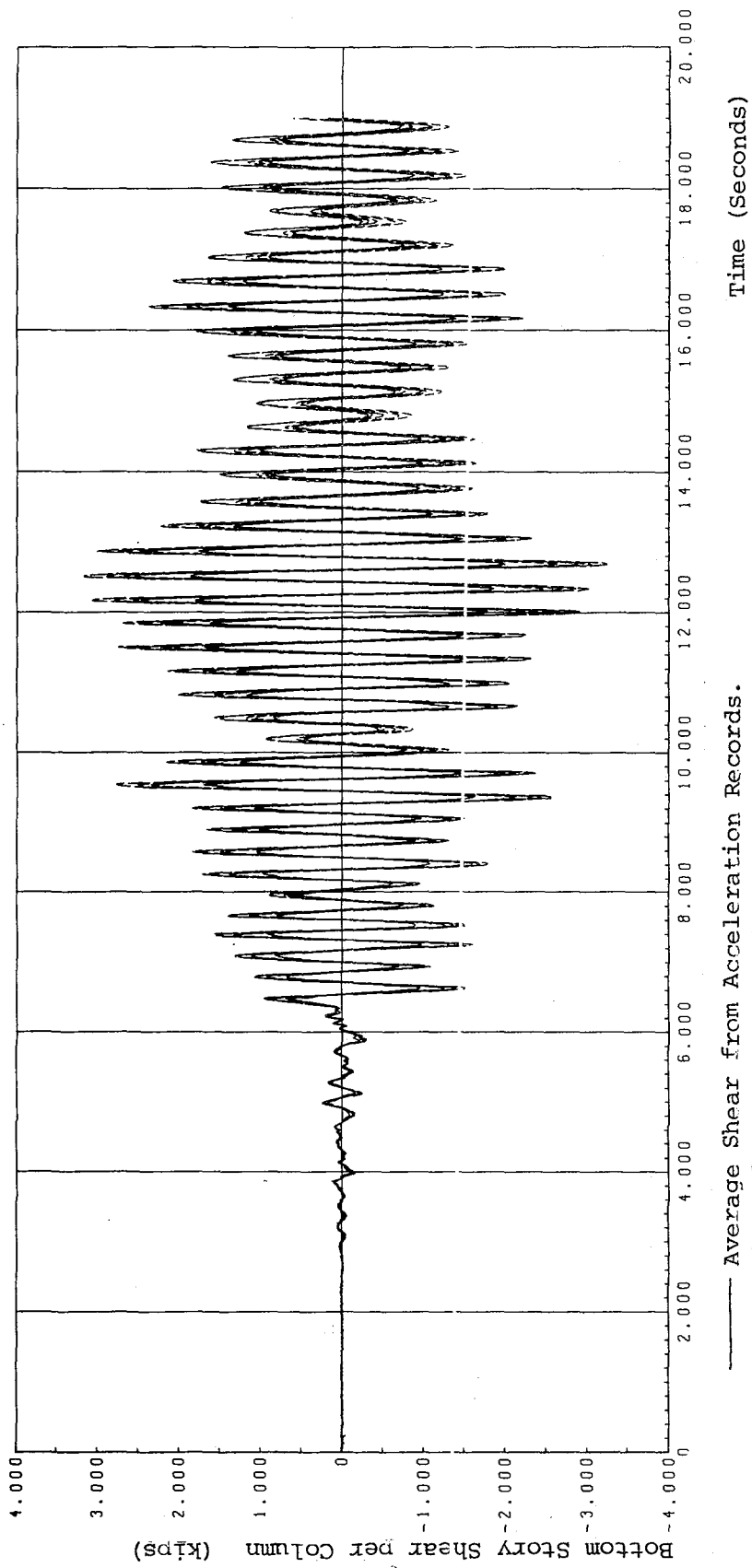


Fig. 4.20 AVERAGE BOTTOM STORY SHEAR PER COLUMN. RUN W1.  
ACCELERATION RECORDS VS. FORCE TRANSDUCERS.

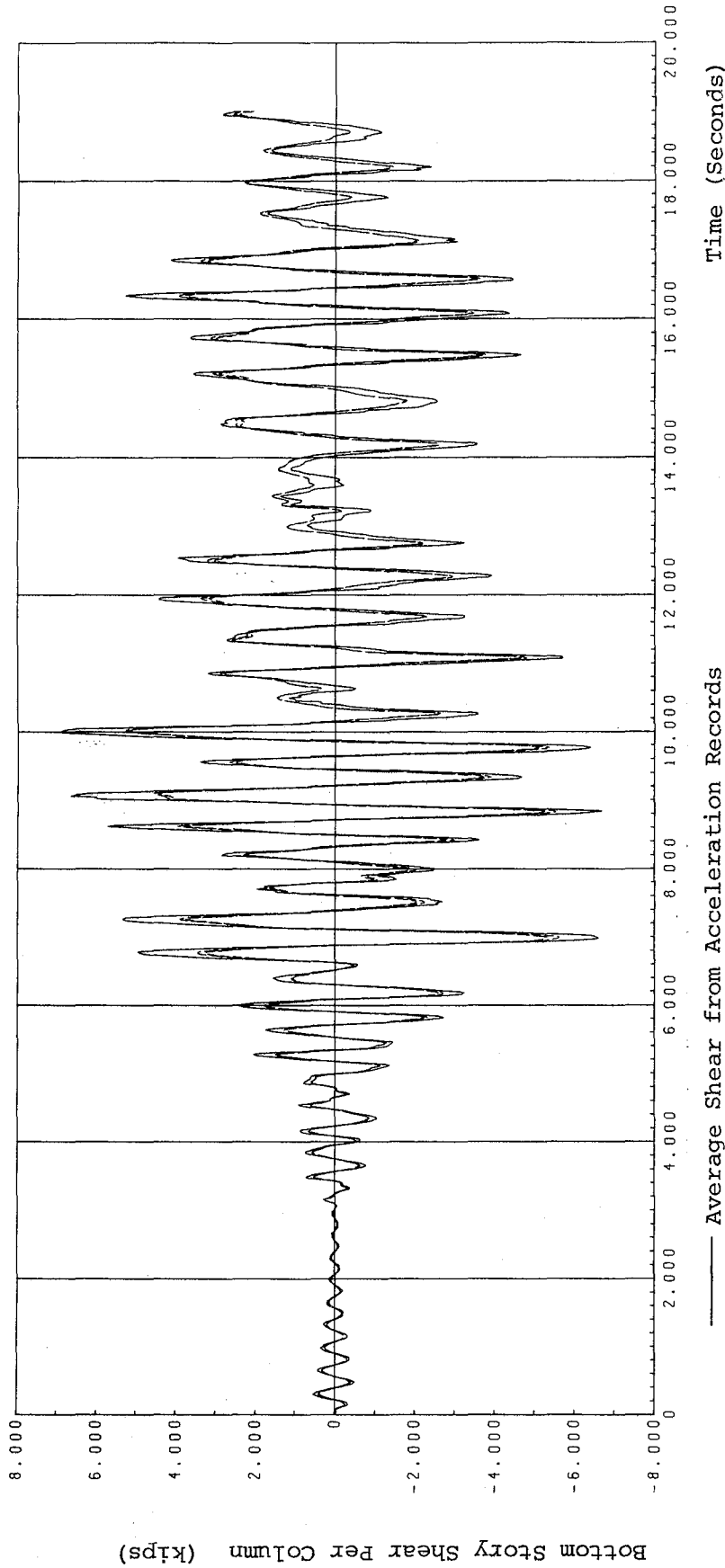


Fig. 4.21 (a) AVERAGE BOTTOM STORY SHEAR PER COLUMN. RUN W2.  
 ACCELERATION RECORDS VS. FORCE TRANSDUCERS.  
 NORTH SIDE COLUMNS.

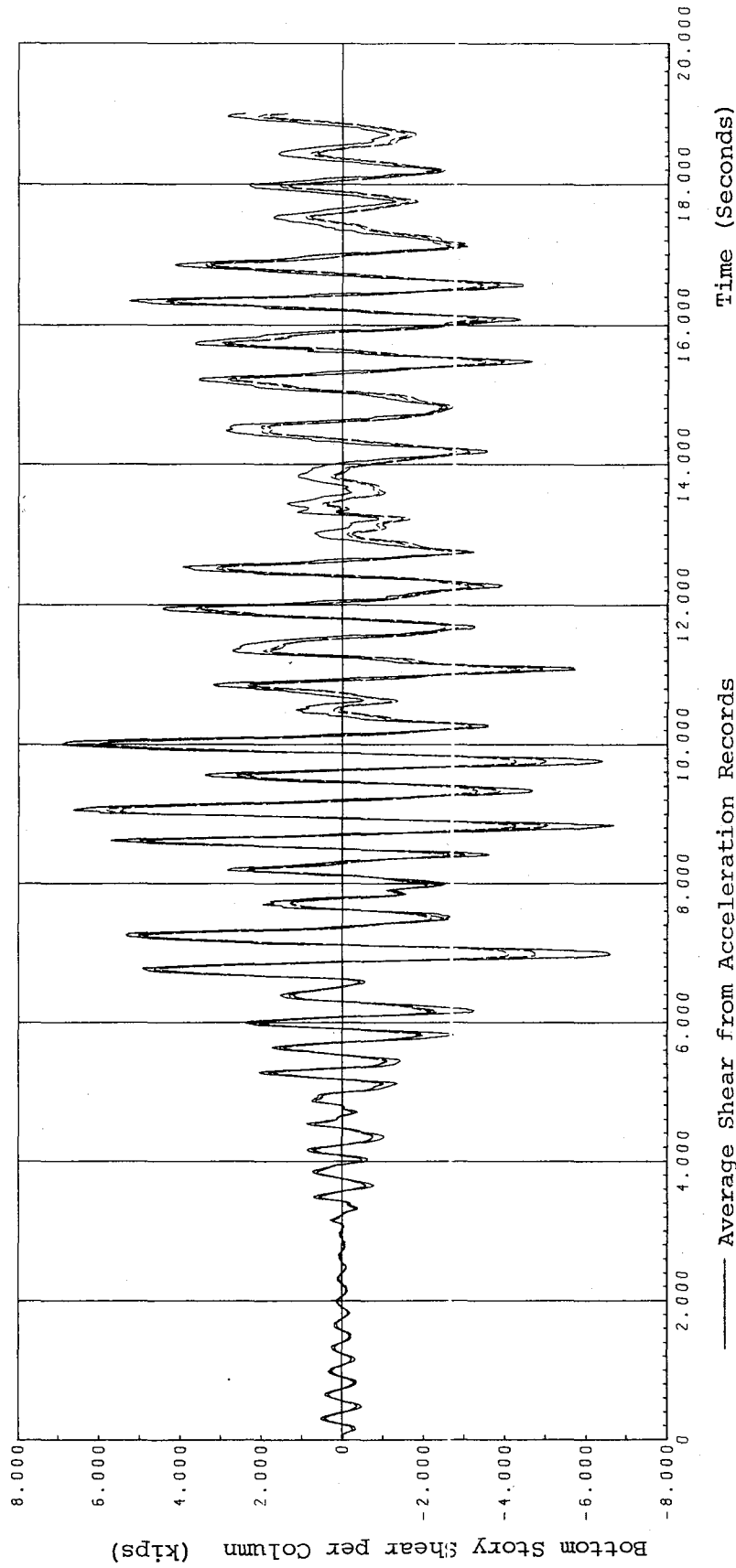


Fig. 4.21 (b) AVERAGE BOTTOM STORY SHEAR PER COLUMN. RUN W2.  
ACCELERATION RECORDS VS FORCE TRANSDUCERS.  
SOUTH SIDE COLUMNS.

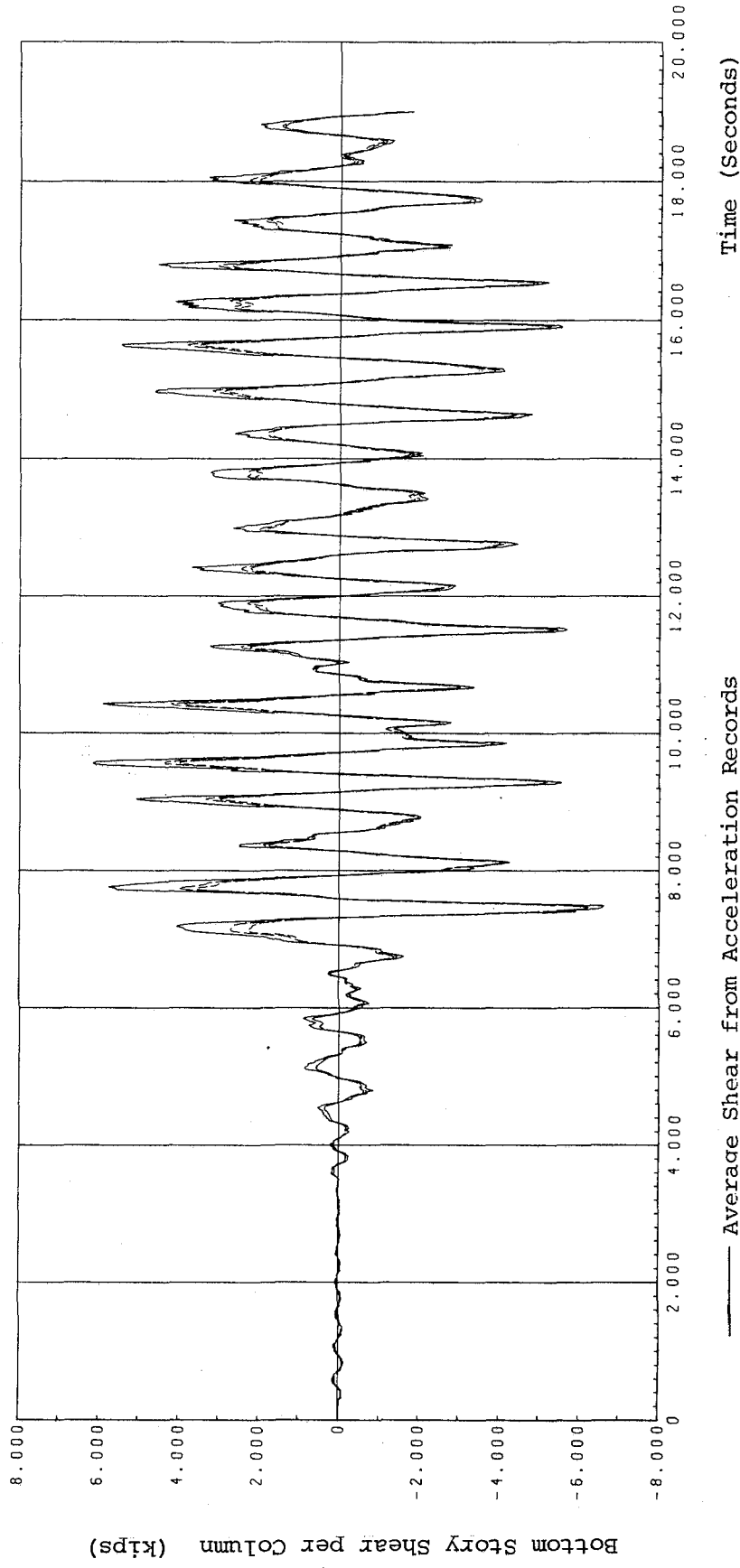


Fig. 4.22 (a) AVERAGE BOTTOM STORY SHEAR PER COLUMN. RUN W3.  
ACCELERATION RECORDS VS. FORCE TRANSDUCERS.  
NORTH SIDE COLUMNS.

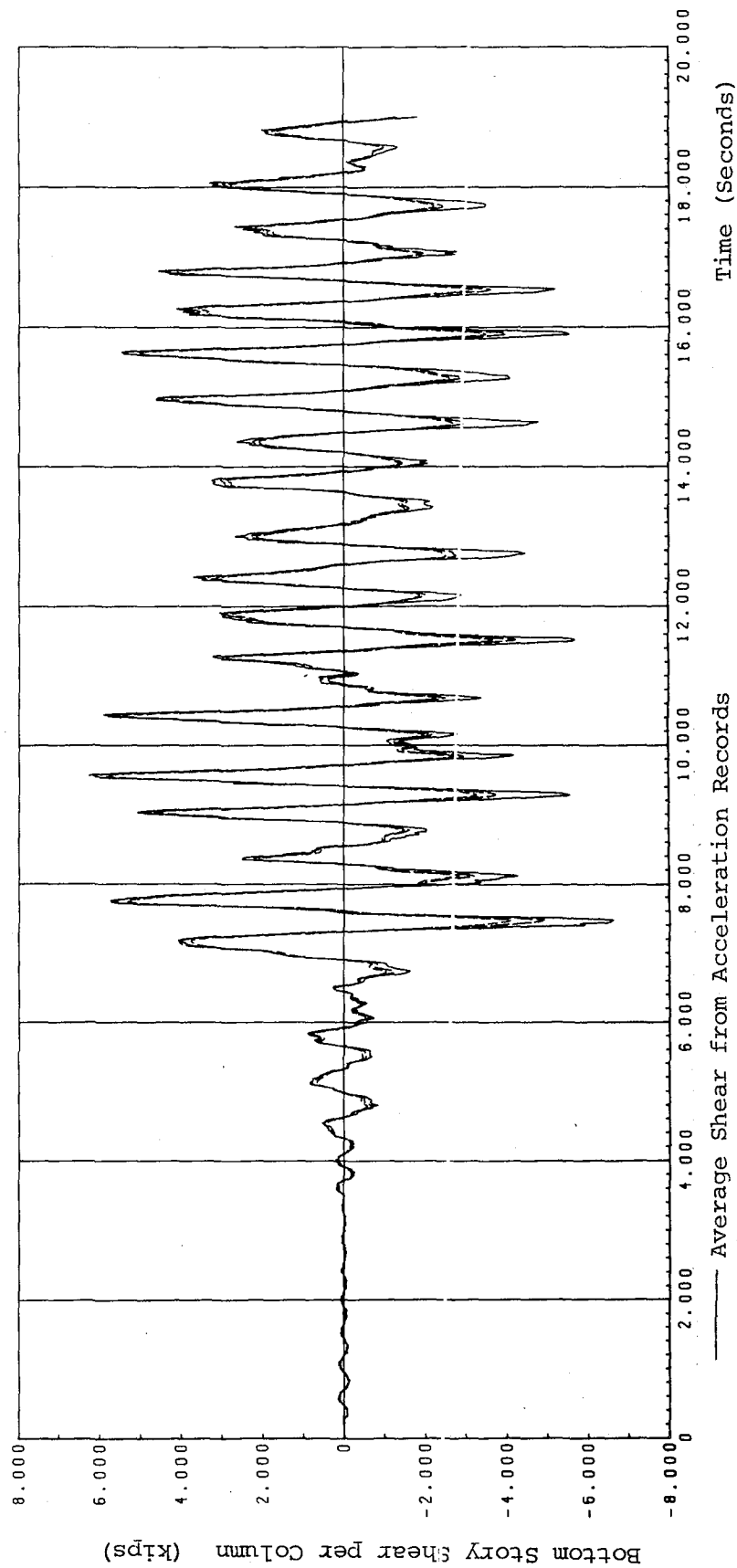


Fig. 4.22 (b) AVERAGE BOTTOM STORY SHEAR PER COLUMN. RUN W3.  
ACCELERATION RECORDS VS. FORCE TRANSDUCERS.  
SOUTH SIDE COLUMNS.

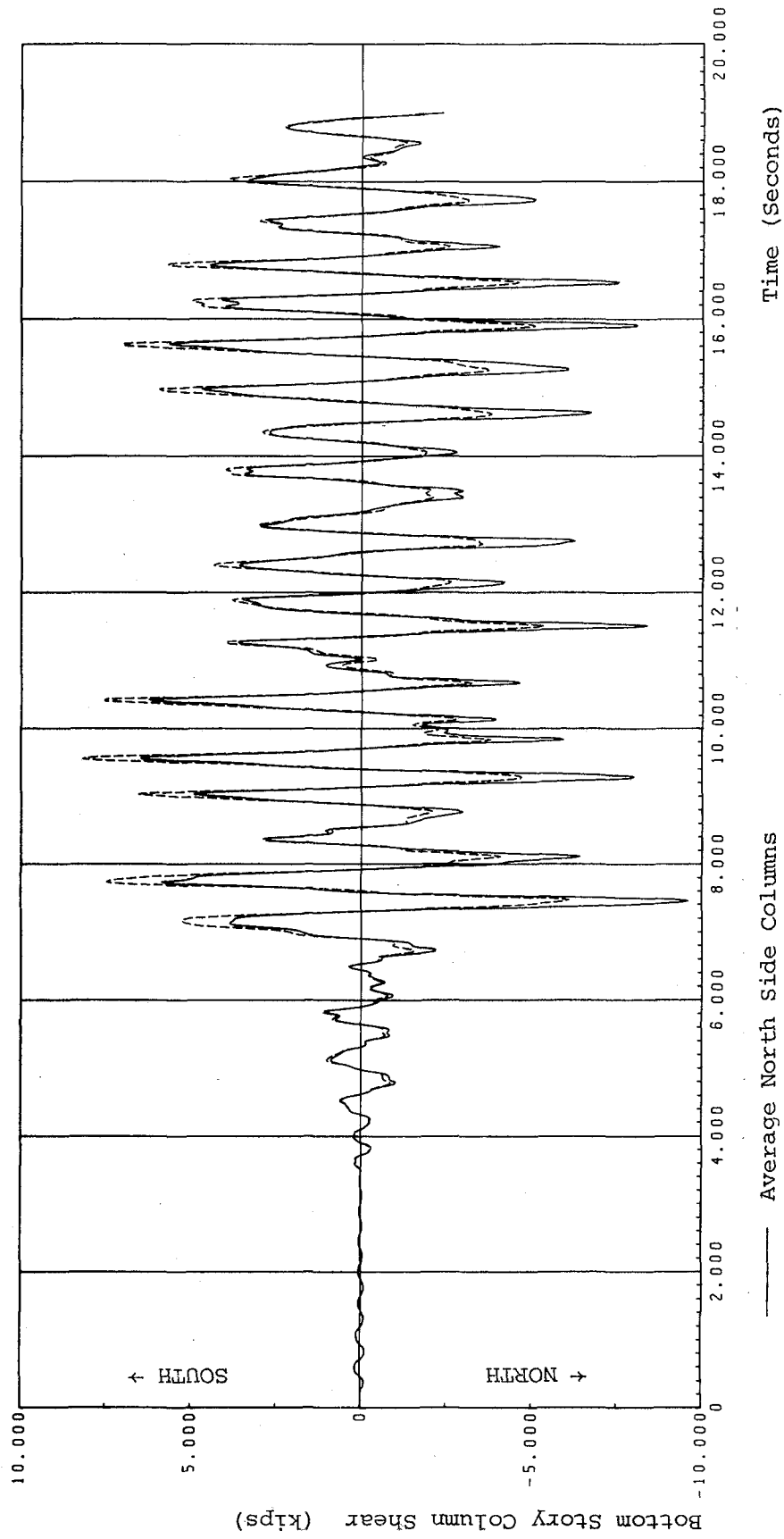


Fig. 4.23 BOTTOM STORY AVERAGE SHEAR PER COLUMN.  
RUN W3. NORTH SIDE VS SOUTH SIDE.

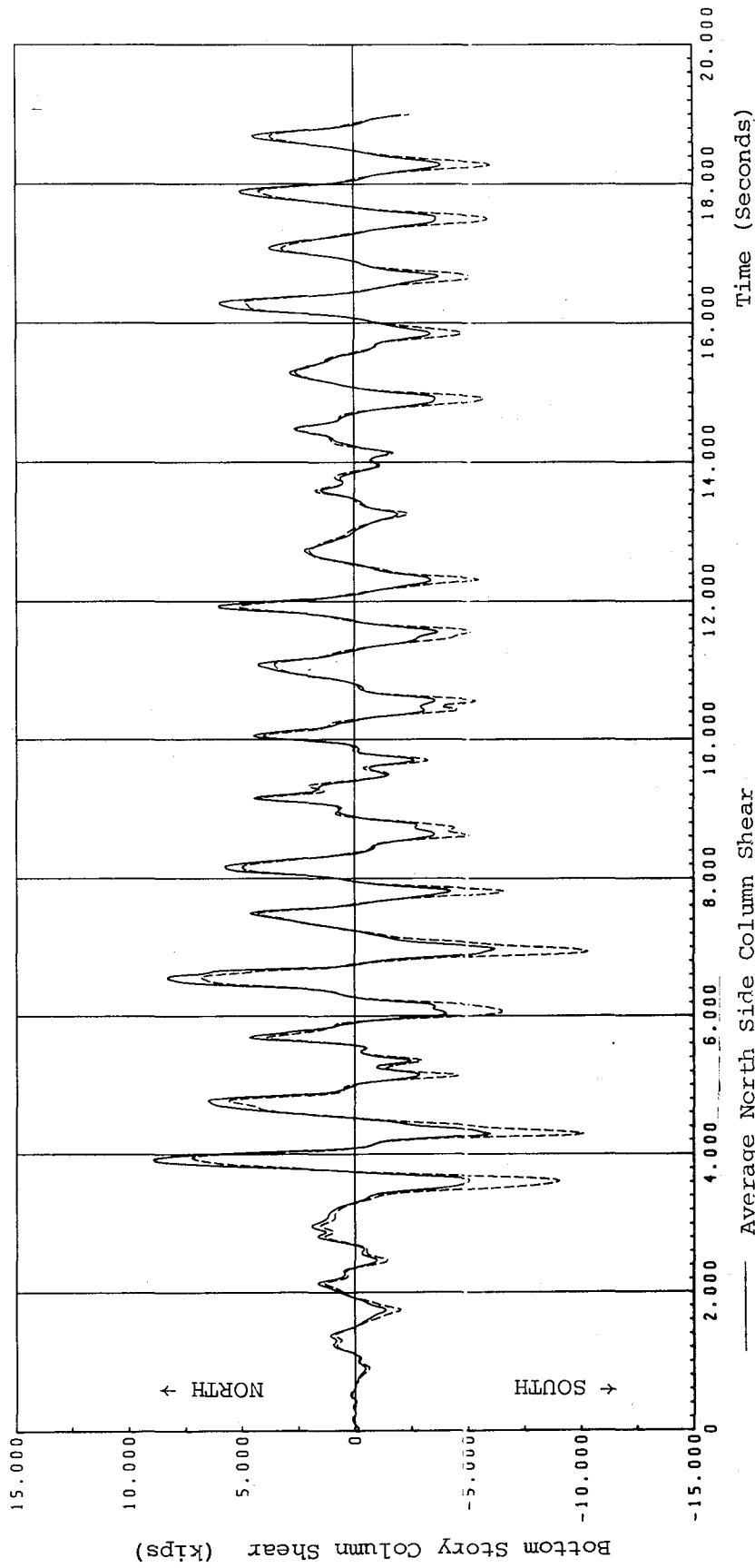


Fig. 4.24 AVERAGE BOTTOM STORY SHEAR PER COLUMN.  
RUN R3 - NORTH SIDE VS SOUTH SIDE.

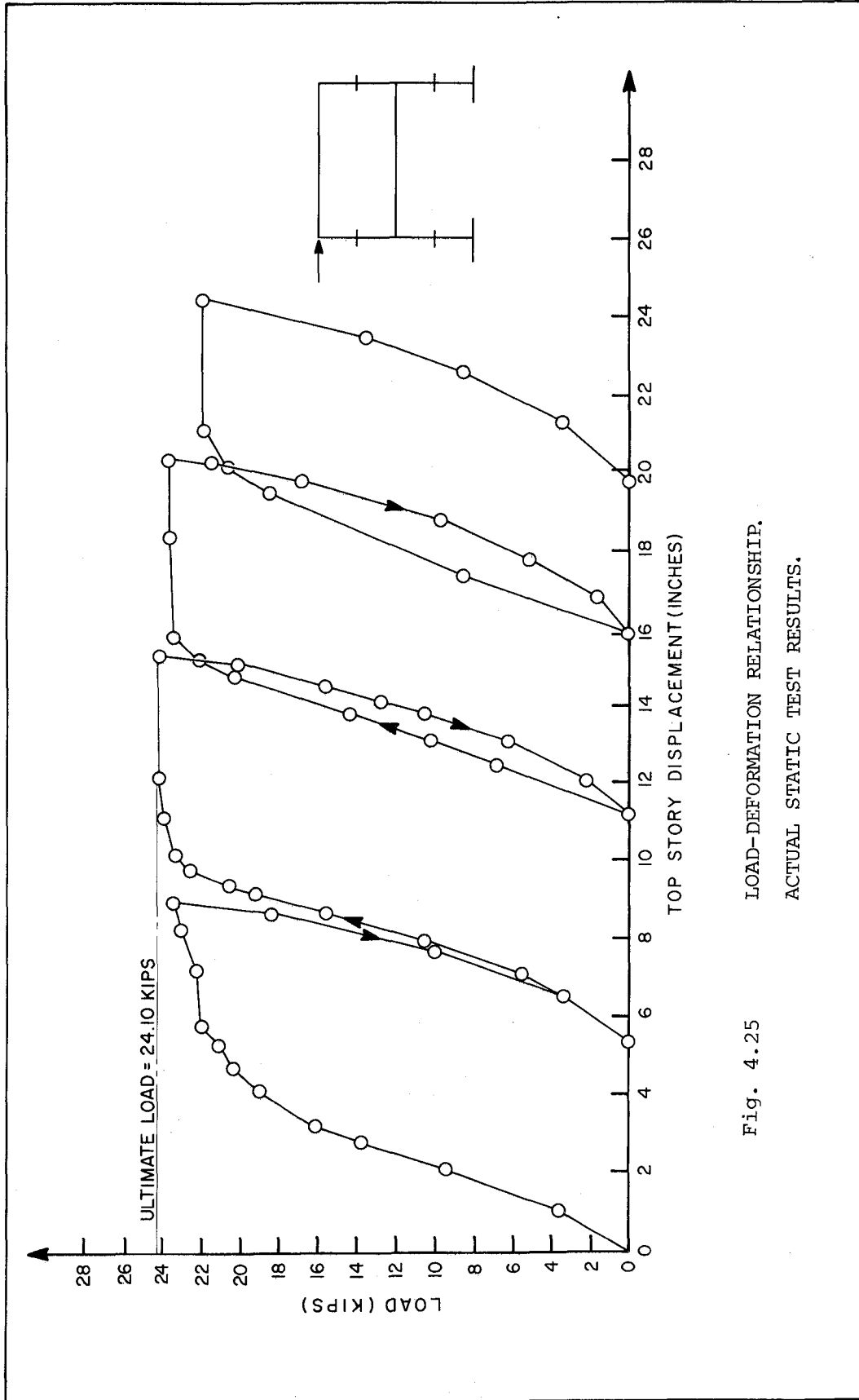


Fig. 4.25 LOAD-DEFORMATION RELATIONSHIP.  
ACTUAL STATIC TEST RESULTS.

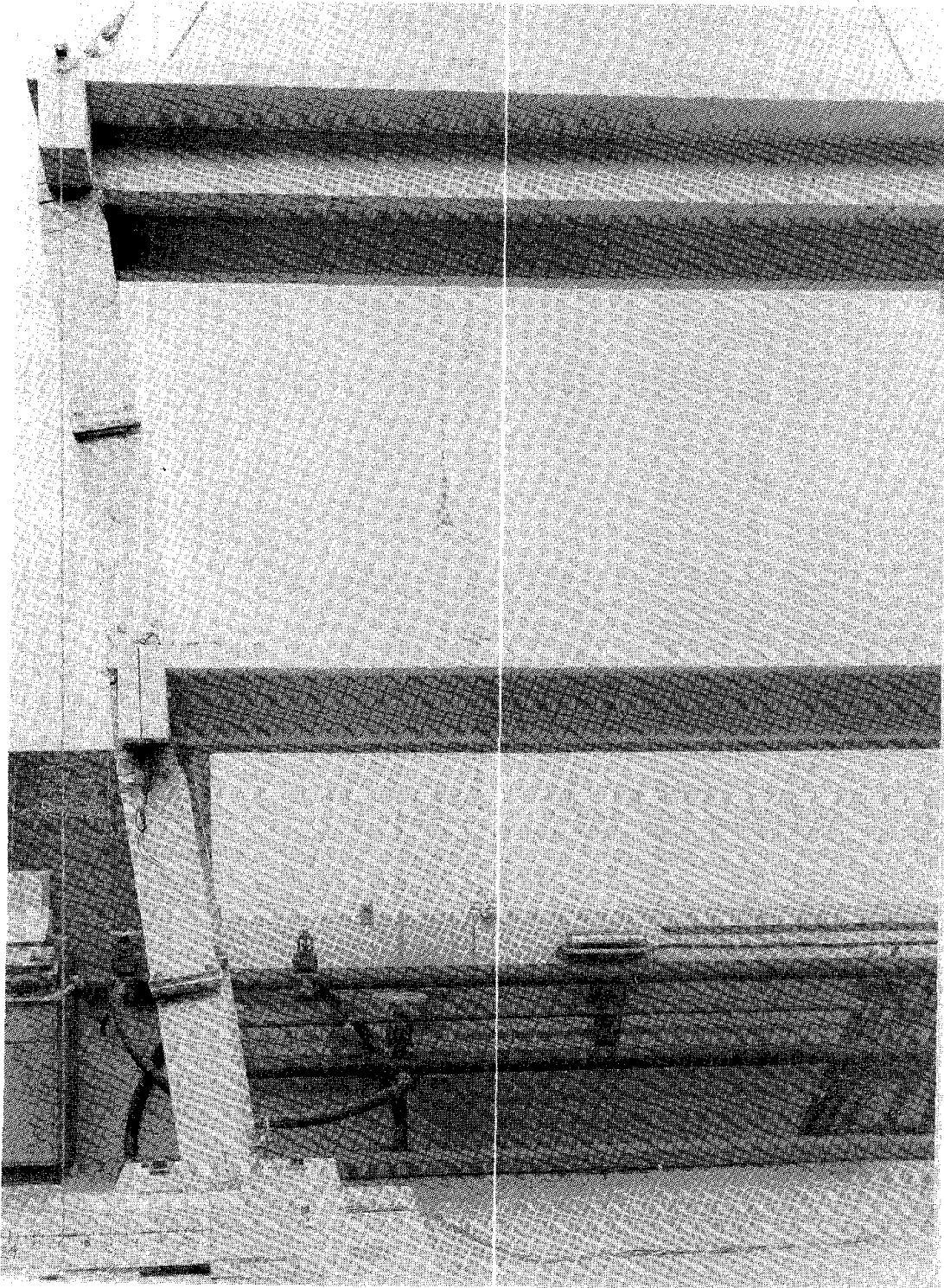


Fig. 4.26 DEFORMATION OF STRUCTURE MIDWAY THROUGH THE STATIC TEST.

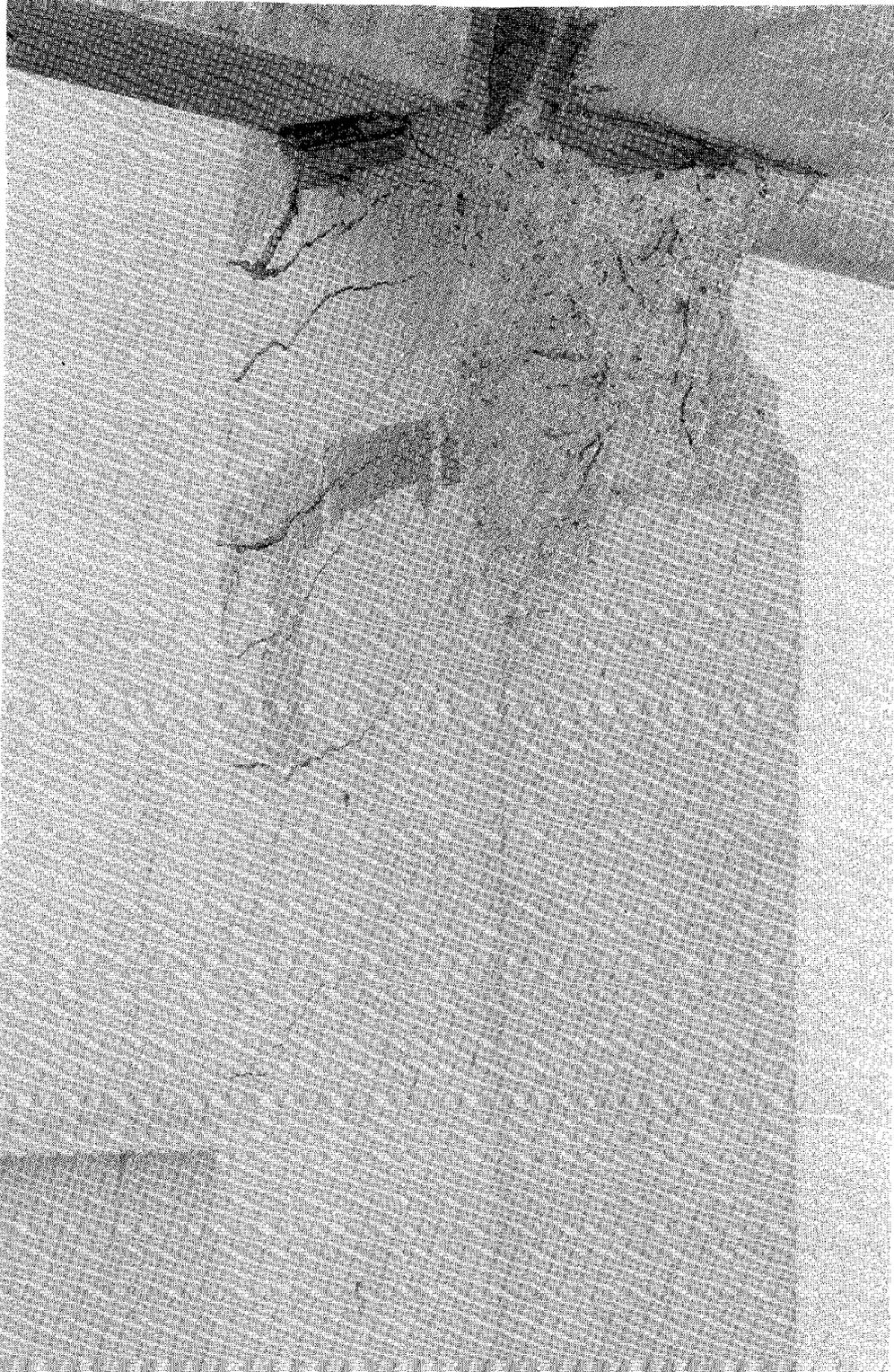


Fig. 4.27      DAMAGE PATTERN AT BOTTOM  
STORY GIRDER-COLUMN JOINT.

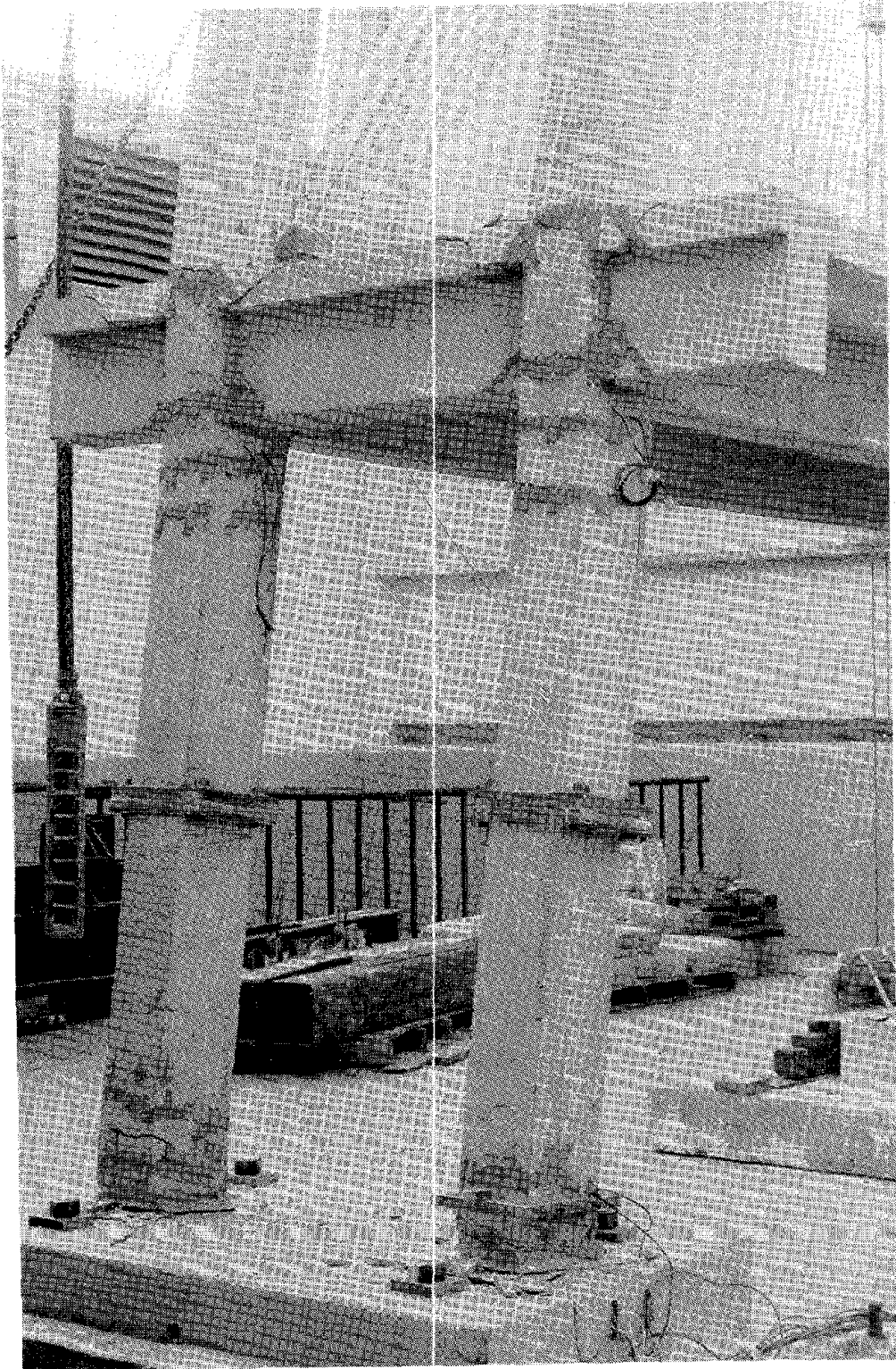


Fig. 4.28      TRANSVERSE VIEW OF FRAME SHOWING  
PATTERN AND EXTENT OF CRACKING OF  
COLUMNS.

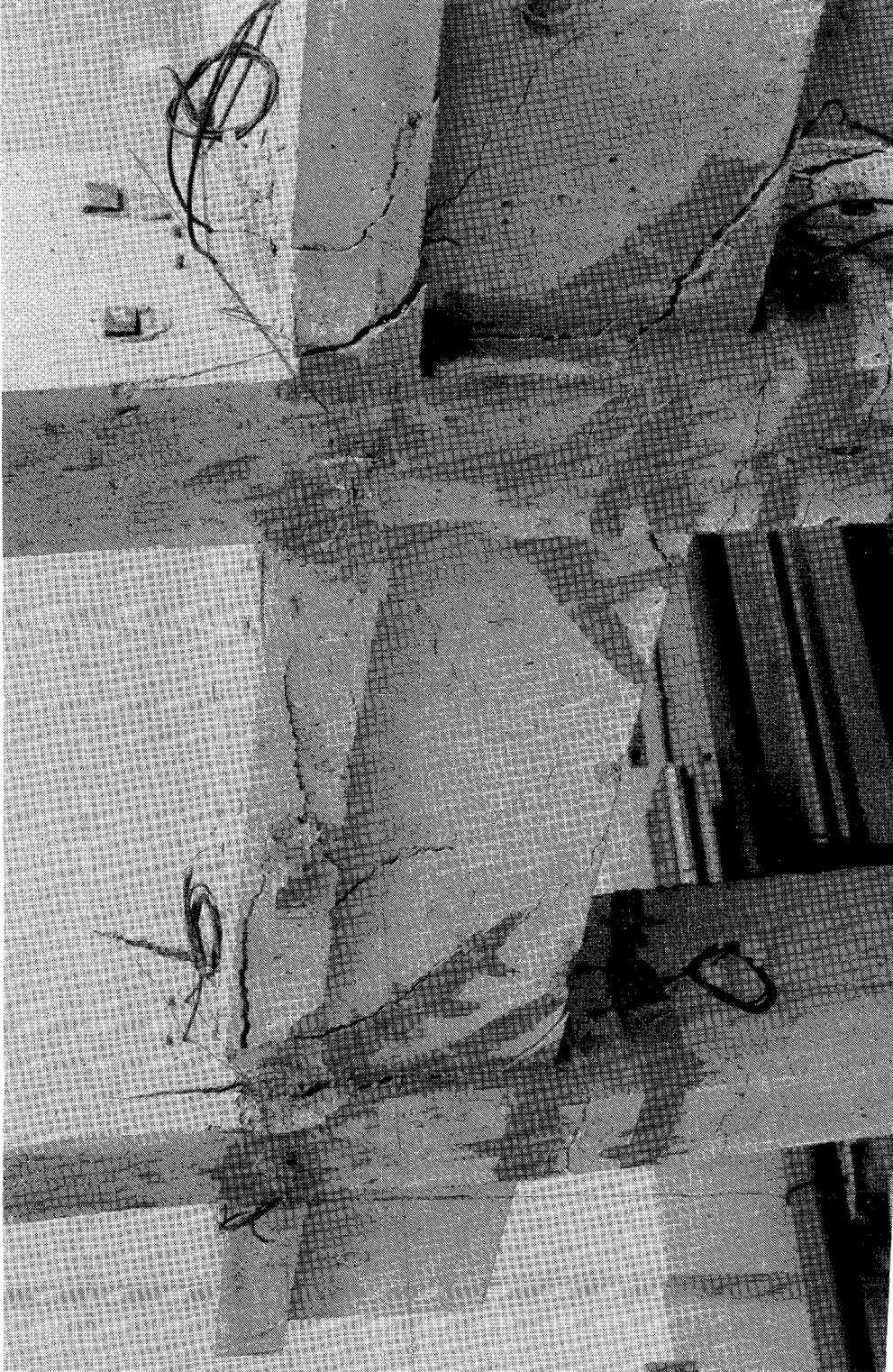


Fig. 4.29 EXTENSION AND WIDENING OF THE VERTICAL CRACK WHICH DEVELOPED IN THE COLUMN DURING DYNAMIC TESTING, SHOWN MIDWAY THROUGH THE STATIC TEST.

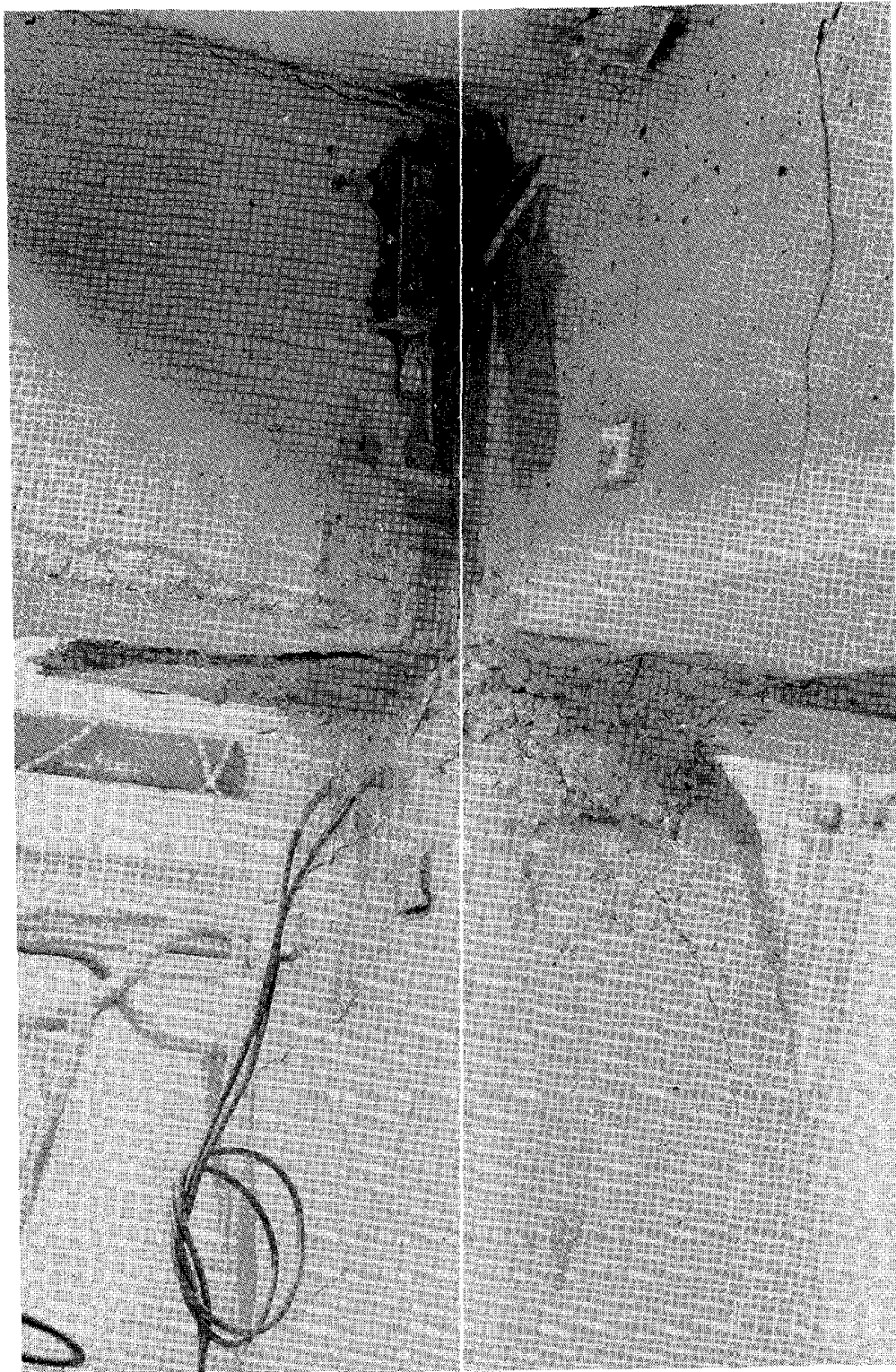


Fig. 4.30

GIRDER-COLUMN JOINT.  
EXTENT OF DAMAGE.

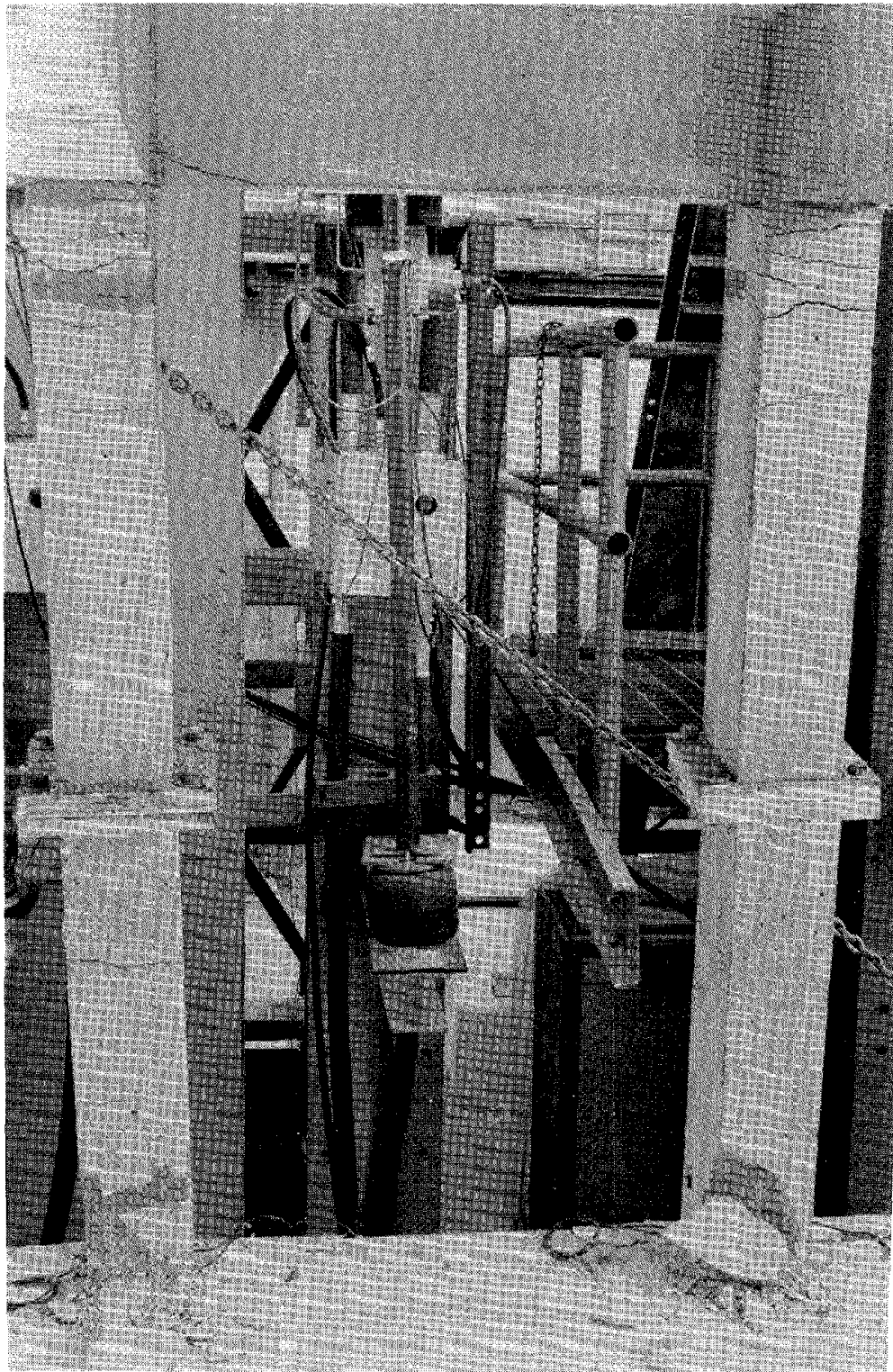


Fig. 4.31      DAMAGE OF COLUMNS TOWARDS LOADING ACTUATOR,  
AFTER "FUNCTIONAL" FAILURE .



Fig. 4.32 DAMAGE OF SLAB ABOVE TRANSVERSE GIRDER (AWAY FROM LOADING ACTUATOR)  
IN WHICH FRACTURE OF STEEL OCCURRED.



Fig. 4.33 TRANSVERSE GIRDER WHICH "FAILED" DUE TO FRACTURE OF REINFORCEMENT.

## 5. ANALYTICAL PREDICTION OF STRUCTURAL RESPONSE

### 5.1 GENERAL COMMENTS

In this chapter are described the analytical methods used to calculate the dynamic response of Frame 2, and the correlation of the analytical results with the observed structural behavior. The methods of analysis employed here are essentially the same as those described in the report on the testing of Frame 1<sup>(1)</sup>; however, in this case the physical parameters used in the analysis were adjusted to give the best possible fit with the new test data. For the purpose of these correlation studies, the story displacements were considered to be the most significant measure of structural response. Only the tests performed before repair of the structure are discussed. The first test, W1, was only a light intensity earthquake, not strong enough to cause any yielding of the reinforcing steel. However, the large reduction of frequency which occurred during that test provided a difficult problem in analytical correlation which is discussed briefly. The tests of greatest interest were W2 and W3, the two runs of nonlinear intensity performed before repair. The structure was essentially undamaged (although slightly cracked) at the start of test W2, so this test demonstrated the performance of a building in good condition when subjected to a ground motion severe enough to cause significant concrete cracking and yielding of the column steel. Test W3 showed how a damaged structure might perform when subjected to a strong aftershock--the initial damaged condition having an important effect on the response behavior.

Specific topics dealt with in this chapter include evaluation of

the linear elastic stiffness properties of the frame, and the use of four different mathematical models in attempting to correlate analytical results with the performance observed during the three tests. In all cases, the basic model was a plane frame with bilinear hysteretic joints at each end of each member. The four versions of this model were Model B, the basic system; Model D, which included a stiffness degradation mechanism; and Models E and F which combined two different deterioration mechanisms with the degradation mechanism. All of these models were originally devised by Dr. Pedro Hidalgo<sup>(1)</sup>, and his designations are used here for consistency.

## 5.2 EVALUATION OF LINEAR STIFFNESS PROPERTIES

As was noted in the report on Frame 1<sup>(1)</sup>, calculation of even the simple linear elastic stiffness of a concrete frame before any testing is not an easy task because the effective member section properties depend on the extent to which microcracking has taken place. Table 5.1 lists the periods of vibration of Frame 2 computed on the basis of three assumptions often used in evaluating member moment-of-inertia (and assuming  $E_c = 2640$  ksi, as measured in laboratory tests); also shown are the measured periods of vibration. Clearly none of the standard assumptions gives excellent agreement with the observed behavior.

In order that the mathematical model might reproduce the dynamic response of the frame, it was necessary to determine member properties which would provide the observed free vibration period. For this purpose, the cracked section moment of inertia values were adjusted following a two step procedure. First, two adjustment factors were derived: one for the top story columns and girder, the other for the

bottom story members. These two factors were determined such that the two story flexibility coefficients,  $F_{TT}$  and  $F_{BB}$ , of the mathematical model were identical to the measured values. The adjusted moments of inertia obtained in this way were as follows:

	TOP STORY	BOTTOM STORY
GIRDER	1456 in <sup>4</sup>	617 in <sup>4</sup>
COLUMN	519 in <sup>4</sup>	168 in <sup>4</sup>

Assuming that  $E_c = 2640$  ksi, the structure flexibility matrix provided by these section properties is

$$\underline{F} = \begin{bmatrix} 0.0228 & 0.0278 \\ 0.0278 & 0.0485 \end{bmatrix} \text{ in/kip}$$

in which the coefficient ratios are

$$F_{TT}/F_{BB} = 2.127, \quad F_{BT}/F_{BB} = 1.219.$$

These are very close to the ratios maintained during the test series.

Having an appropriate set of flexibility coefficients, it was then possible to obtain any desired fundamental frequency of vibration merely by adjusting the modulus of elasticity. For example, the fundamental frequency given by the above flexibility matrix is 3.02 Hz, using the measured value of  $E_c = 2640$  ksi. Thus to obtain the 3.13 Hz frequency observed just before test W2, it was necessary merely to use a modulus of

$$E = 2640 \left( \frac{3.13}{3.02} \right)^2 = 2836 \text{ ksi}$$

During subsequent stages of testing, as the frequency of vibration diminished because of structural damage, the flexibility was adjusted by making similar modifications to the modulus of elasticity.

### 5.3 "LINEAR" RESPONSE CORRELATION - MODEL B

The bilinear hinge mechanism which is assumed at the ends of each column and girder is depicted in Fig. 5.1. Thus each member remains fully elastic until the end moment exceeds the yield moment defined for that member, which depends on the axial force as well as the member section properties. For a test like W1, which induced no moments approaching the yield level, the Model B computer program behaves as a simple linear elastic response program.

The response of the frame to the table accelerations recorded during test W1 was calculated by this Model B program, using a first mode damping ratio of 2 per cent and adjusting the modulus of elasticity to provide the fundamental frequency observed before run W1 (3.80 Hz). The computed response history is shown together with the observed results in Fig. 5.2, where it can be seen that the correlation is good at first. However, the period of the observed response then begins to lengthen, as cracking of the sections causes loss of stiffness, and this change of period induces a nearly resonant condition with the earthquake input. The consequent resonant amplification of the observed response is not contained in the analytical solution.

As a second test of the linear program capability, the modulus of elasticity was adjusted to provide the frequency observed at the end of run W1 (3.13 Hz) and the analysis was repeated, with results shown in Fig. 5.3. In general, this is a much better correlation than was found in Fig. 5.2, but it is clear that a significant loss of stiffness occurred during the test and the unchanging mathematical model cannot simulate this effect adequately. On the other hand, no yielding of steel occurred and the stiffness degradation mechanism of Model D is not applicable to this situation.

Accordingly, it was decided to modify Model B to account for stiffness loss with less than yield moment deformations. Two different deterioration mechanisms were tried, both controlled by the amplitude of the first mode response,  $Y_1(t)$ . This quantity, which was used by Hidalgo in defining the stiffness degradation mechanism of Model D<sup>(1)</sup>, is given by

$$Y_1(t) = \underline{A} \underline{v}(t)$$

where  $\underline{A}$  is the top row of the inverse mode shape matrix,

$$\text{i.e. } \underline{\Phi}^{-1} \equiv \begin{bmatrix} A \\ \dots \\ B \end{bmatrix}$$

and  $\underline{v}(t)$  is the story displacement vector evaluated at time  $t$ . It should be noted that the mode shape matrix was assumed to remain constant during the response, even though yielding was taking place.

The first type of deterioration mechanism was assumed to come into operation each time  $Y_1$  reached 35 per cent of its yield value (the first mode deflection at which yield would occur). For each such displacement swing (either positive or negative), the modulus of elasticity was reduced by 1 per cent (0.01). Results obtained with this deterioration mechanism are shown in Fig. 5.4. As can be seen from this figure, the correlation is fairly good for the first 15 seconds of response. However, during the latter part of the time history the stiffness deterioration rate of the actual test structure decreases, a phenomenon not accounted for by the model which assumes a constant rate of deterioration. The result is that the mathematical model becomes excessively flexible.

The second type of deterioration mechanism was similar to the first except that it operated only if  $Y_1$  exceeded its previous maximum value as well as 30 per cent of the yield value. Thus deterioration only occurs during increasing amplitude phases of the response.

Results provided by this modified deterioration mechanism are shown in Fig. 5.5. This modification of the deterioration mechanism appears to have led to improvement of the correlation in the final stage of the response, but is not as good as the first version (Fig. 5.4) during the phase after first reaching the peak response. Hence it is not a reliable improvement.

#### 5.4 DEGRADING STIFFNESS ANALYSES - MODEL D

Because significant yield occurred in the frame during tests W2 and W3, it was clear that the resulting damage should be represented directly in the mathematical model and the stiffness degradation mechanism of Model D was considered appropriate for this purpose. As described by Hidalgo<sup>(1)</sup>, this stiffness degradation operates in the first mode component of the dynamic response, and is based on the Clough concept<sup>(4)</sup>. The basic mechanism is depicted in Fig. 5.6, in which the yield value of  $Y_1$  is that value which existed when the first yield hinge developed in the frame. It should be noted that the basic bilinear hinge mechanism continues to function in the frame analysis, in addition to this stiffness degradation which is superimposed on a global basis.

Response of the frame to test W2 was carried out using Model D, assuming a stiffness degradation parameter (second slope)  $\eta = 0.05$ , adjusting the modulus of elasticity to provide the frequency measured before test W2 (3.13 Hz) and introducing a damping ratio of 4 per cent. Results of the analysis, shown in Fig. 5.7, are seen to be in good agreement with the actual behavior for about 10 seconds, but then they begin to drift.

The correlation obtained in the analysis of test W3 is shown in

Fig. 5.8. In this calculation, the strain hardening parameter was set at  $\eta=0.05$ ; the damping ratio was increased to 5 per cent because it was assumed that the damaged condition of the frame would cause a greater energy loss. Also, the modulus of elasticity was adjusted to provide the frequency observed just before this test (2.03 Hz). The predicted response given by this mechanism is reasonably good for Test W3 as compared to run W2; in particular, no drift is observed in the analytical results. However during the latter phases, the effect of higher modes begins to cause significant variation between the predicted and measured responses.

#### 5.5 DEGRADING AND DETERIORATING STIFFNESS - MODELS E & F

The degrading stiffness model described above is effective in reducing stiffness of the structure during the stage of response when displacement amplitudes are increasing. This is consistent with the concept that damage and loss of stiffness should correlate with increased deformations. However, when the displacements no longer increase, the average stiffness (average of loading and unloading swings) remains constant, and this does not agree with the observed fact that the concrete continues to deteriorate as long as significant deformations are taking place. For this reason, Hidalgo developed the two stiffness deteriorating models (E and F) mentioned earlier. These stiffness deterioration mechanisms were similar in concept to those described above in connection with the linear response analysis; the essential feature is that the stiffness is reduced by a fixed percentage each time the first mode displacement amplitude exceeds a specified value. Fig. 5.9 describes the deterioration mechanisms used with Models E and F; it should be noted that the reference value of the first mode displacement which is

mentioned refers to its value when first yield occurs.

The two parameters controlling the response behavior during the stiffness degrading and deteriorating analyses are the strain hardening factor  $\eta$  (second slope) of the degradation mechanism and the deterioration ratio (DTR) representing the loss of stiffness during each cycle of deterioration. An analysis of the response during test W2, using Model E with  $\eta = 0.50$  and  $DTR = 0.01$  is shown in Fig. 5.10. Other parameters in the analysis were the same as for the case plotted in Fig. 5.7 ( $\xi = 4\%$ ,  $f_1 = 3.13$  Hz), so a comparison of Figs. 5.7 and 5.10 shows the influence of stiffness deterioration on the response. It is clear that the deterioration has further increased the drift which starts after the first 10 seconds; it has not achieved any improvement in correlation. Figure 5.11 shows the result of another analysis, using increased strain hardening ( $\eta = 0.80$ ) and a reduced deterioration rate ( $DTR = 0.005$ ). Again the drift behavior is changed, this time with drift in the opposite direction, but without any real improvement. Finally, the strain hardening ratio was reduced to  $\eta = 0.60$  and the damping ratio was reduced to  $\xi = 2\%$ , with results as shown in Fig. 5.12. This time the computed result shows reasonably good correlation with the observed response, with slightly less drift than was seen in Fig. 5.7 which did not include deterioration.

After this experience with Model E in correlation of the response during test W2, Model E was applied to test W3 to see if this test would function as well with a structure already damaged when the test began. Parameters used in the first attempt were  $\eta = 0.80$  and  $DTR = 0.01$  together with  $\xi = 4\%$  and  $f_1 = 2.03$  Hz. A slight drift resulted toward the end of the calculated response, as shown in Fig. 5.13; accordingly the deterioration rate was reduced to  $DTR = 0.005$  and the analysis was

repeated with results as shown in Fig. 5.14. This is probably the best correlation achieved in any of the nonlinear analyses to date.

With Model E deterioration, the stiffness reductions are applied only to the loading branch of the first mode hysteresis loop (Fig. 5.10). Model F differs in that the reduction applies to both loading and unloading branches of the loop. Figure 5.15 shows the response of test W2 calculated with Model F using parameters  $\eta = 0.50$ ,  $DTR = 0.01$ ,  $\xi = 4\%$  and  $f_1 = 3.13$ . These are the same as were used with Model E in Fig. 5.11, hence a comparison of Figs. 5.11 and 5.15 shows the relative behavior of Models E and F. It is evident that the response prediction of Model F is much better than that of Model E. However, in this case, instead of the drift being towards the end of the response time history, there is a slight sag during the middle portion of the earthquake. The reasons for this drift and subsequent recovery are not presently understood.

The computed response during test W3 using Model F is plotted in Fig. 5.16. Analysis parameters used in this case were the same as were used with Model E in Fig. 5.14, (except that the deterioration rate,  $DTR = 0.01$ ), and comparison of these two figures demonstrates the superiority of Model E in this analysis even though the Model F results are quite good.

One aspect of the analyses described above, which should be emphasized, is that in all cases the initial period of vibration of the mathematical model was adjusted to correspond with that measured before the start of the test. Because the period of vibration has a dominant influence on the dynamic response behavior, it is apparent that this empirical adjustment was a big step toward obtaining satisfactory correlation. In practice, however, such experimental data would not be

available and an analysis intended to test the adequacy of a given design would have to be based on an estimated value of the structure frequency.

The difficulties involved in estimating the stiffness of a reinforced concrete structure for purposes of dynamic response analysis were discussed earlier in this chapter. It was pointed out that both the distribution as well as the actual magnitude of the stiffness changed during a severe earthquake test, because of variable cracking of the concrete members. Accordingly in the foregoing analyses, the cracked section moments of inertia of the members were adjusted to provide computed frame stiffness coefficients equal to the measured values. Subsequent stiffness adjustments to duplicate the vibration frequency observed at any stage of testing were then made by merely modifying the modulus of elasticity of the concrete.

One approach to simplifying the estimation of the frame vibration properties, which seemed worthy of exploration as part of the present study, is to assume that all member moments of inertia are given directly by the standard cracked section hypothesis. Then the changes of stiffness which occur during the damage process can be accounted for entirely by changes in the modulus of elasticity of the concrete. This approach differed from that employed in the preceding analyses only in two respects:

- (1) No adjustment is made in the cracked section properties to improve the distribution of stiffness.
- (2) The damage condition of the structure is represented by a modulus adjustment factor, expressing the ratio of the current effective modulus to the basic measured value ( $E_c = 2640$  ksi in this case).

Example values of this modulus adjustment factor which would provide

the measured fundamental frequency at various stages of the test program are as follows:

<u>Before Test</u>	<u>Frequency</u>	<u>Adjustment Factor</u>
W-1	3.80 Hz	2.065
W-2	3.13 Hz	1.401
W-3	2.03 Hz	0.589

Note the factors greater than one which demonstrate that the condition of the frame had not yet achieved the theoretical cracked section state at the start of tests W-1 and W-2.

In order to test the effectiveness of this technique for approximating the structure vibration properties, several response analyses were made in which the frame stiffness was defined by the cracked section properties and a specified modulus adjustment factor. Results of one such analysis are shown in Fig. 5.17. In this case Model F was used to calculate the response during test W3. The adjustment factor was set at 0.57, giving  $f = 1.99$  Hz which is close to the starting frequency during the test. Other specified analytical parameters were  $\eta = 0.80$ ,  $DTL = 0.60$ ,  $DTR = 0.01$ , and damping ratio  $\xi = 4\%$ . The correlation shown in Fig. 5.17 demonstrates significant phase shifts between the analytical and observed results; after the first few seconds the frequency of the real structure has diminished considerably below that of the mathematical model. Accordingly a second analysis was made, reducing the modulus adjustment factor to 0.41 (giving  $f = 1.68$  Hz) to represent a greater degree of damage. Other analytical parameters were as before, except  $DTR = 0.005$ . Results of this analysis are shown in Fig. 5.18; the correlation is excellent, showing that the chosen adjustment factor is suitable for the structure condition during this test.

To study the generality of this modeling concept, the same type of analysis was performed for test W-5 of Frame 1--which had exhibited

about the same damage state as did Frame 2 in test W-3. Analysis parameters used in this study were the same as those employed in the response analysis of Fig. 5.18. Correlation of the calculated response with the behavior observed during test W-6 (first structure) is shown in Fig. 5.19. The correlation in this case also is quite good, although slight tendencies toward phase shifts are evident; apparently the adjustment factor of about 0.4 provides a good model of a rather severely damaged frame.

To examine the performance of this modeling technique for a structure which is essentially undamaged before the earthquake, it was also applied to test W-2 of Frame 2. The modulus adjustment factor in this case was set at 0.81, giving a frequency of 2.37 Hz, which is representative of the damage state at some stage during test W-2. Other analysis parameters were taken to be the same as those used in Figs. 5.18 and 5.19, except that the damping was arbitrarily set at  $\xi = 2\%$  to correspond with the initially undamaged condition of the frame. Results of this analysis, shown in Fig. 5.20, are quite good during the first part of the run, but then a spurious drift appears. To control the drift, the parameter  $\eta$  was reduced to 0.45 while all other parameters were left unchanged. Results of this re-analysis, shown in Fig. 5.21, demonstrate that most of the drift has been eliminated and that reasonable correlation has been achieved, although not as good as was obtained from test W-3.

Although these investigations have been too limited to enable any firm conclusions to be drawn, they do demonstrate that a relatively simple approach to estimating the frame stiffness can lead to adequate response analysis. Using frame analysis Model F, and defining the frame stiffness by the cracked section properties and an adjusted modulus of elasticity, produced good response calculations for two structures which were in heavily damaged conditions at the start of the test, and

a fair correlation for a structure which was essentially undamaged at the start of the test. Modulus adjustment factors of about 0.4 and 0.8 seem to describe adequately the damage state in the two situations, respectively.

TABLE 5.1 COMPARISON OF NATURAL FREQUENCIES  
AS GIVEN BY ANALYSES AND TESTS  
 (Structure Without Concrete Blocks)

	ANALYTICAL VALUES FOR DIFFERENT STIFFNESS FORMULATIONS			FREE VIBRATION TEST RESULTS (Before Dynamic Tests)
	GROSS SECTION	TRANSFORMED AREA SECTION	CRACKED SECTION	
FIRST MODE (Hz)	6.66	7.42	4.63	6.58
SECOND MODE (Hz)	18.28	20.36	13.09	20.58

# MODEL B

BI-LINEAR

CONSTANT PARAMETERS  $EI, \lambda, \xi$

$\lambda$  = STRAIN HARDENING RATIO  
AT SECTION LEVEL

$\xi$  = % CRITICAL DAMPING

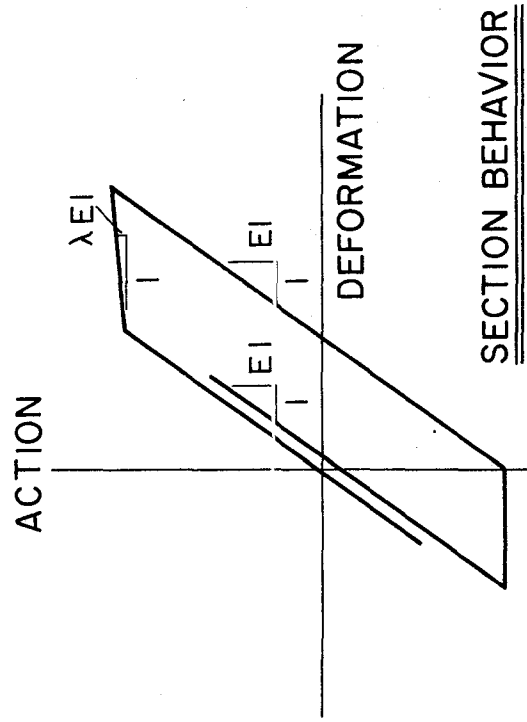


Fig. 5.1 BILINEAR MODEL (MODEL B)

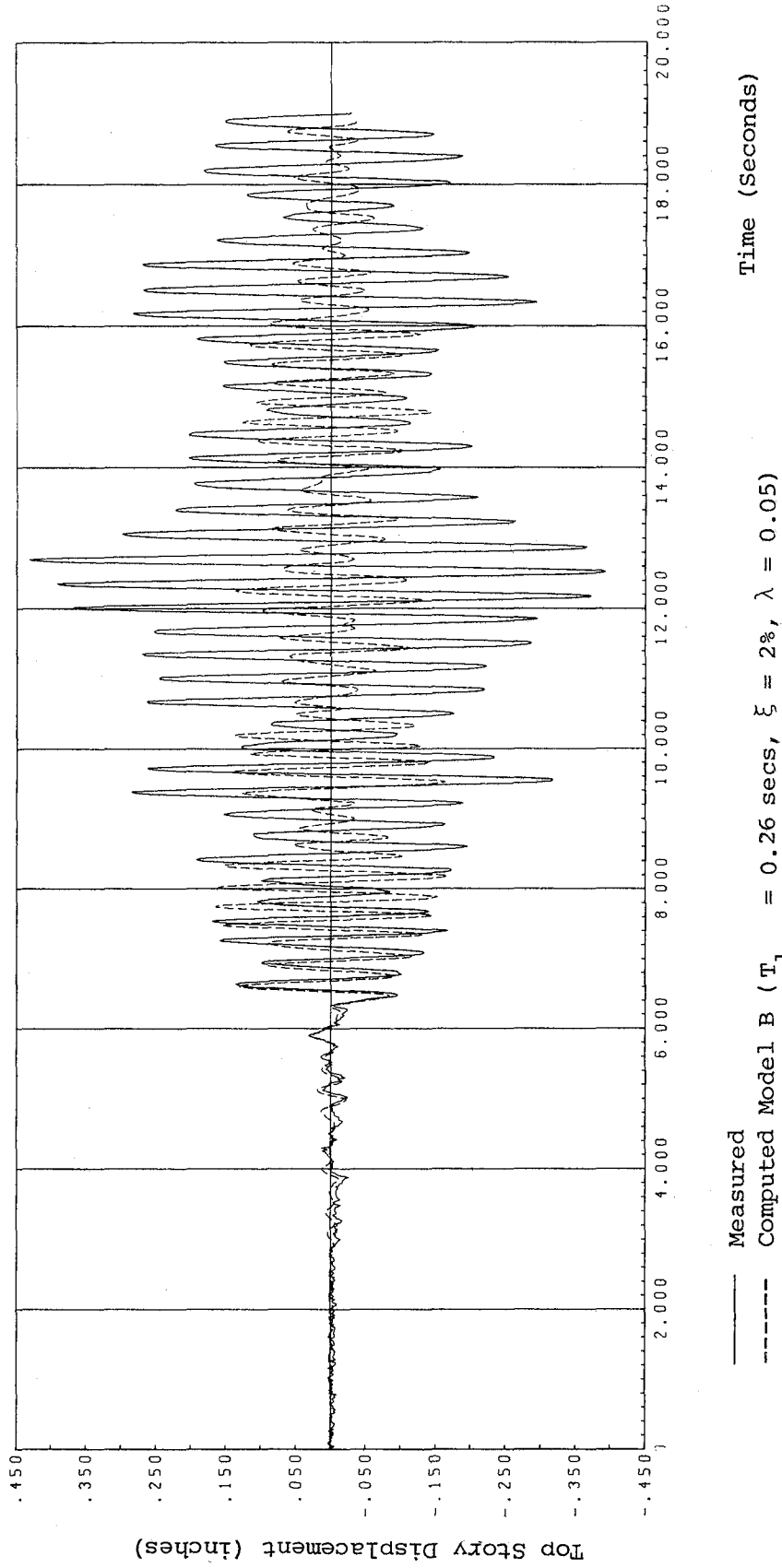


Fig. 5.2 CORRELATION FOR RUN W1. TOP STORY DISPLACEMENT. MODEL B.

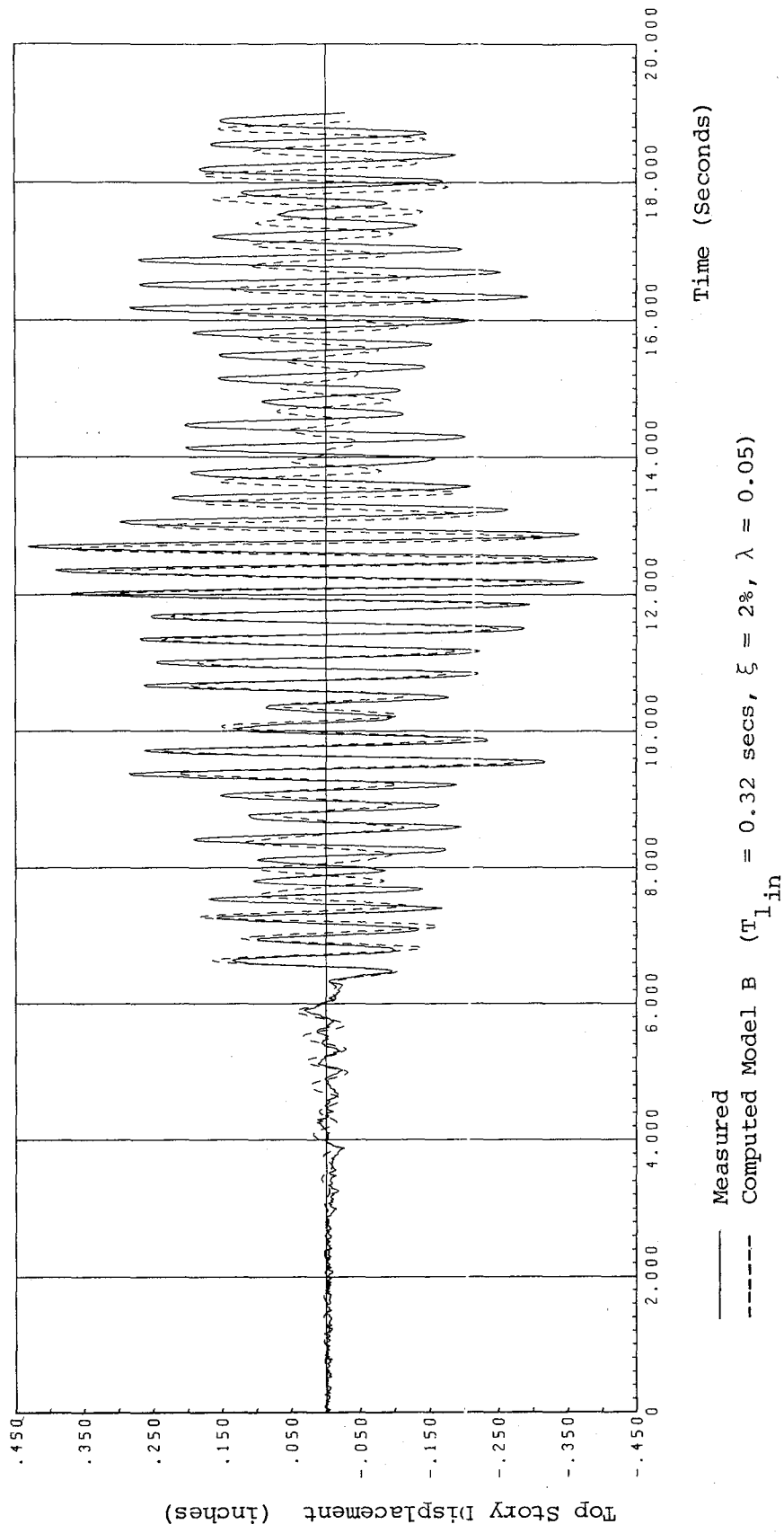


Fig. 5.3 CORRELATION FOR RUN W1. TOP STORY DISPLACEMENT. MODEL B.

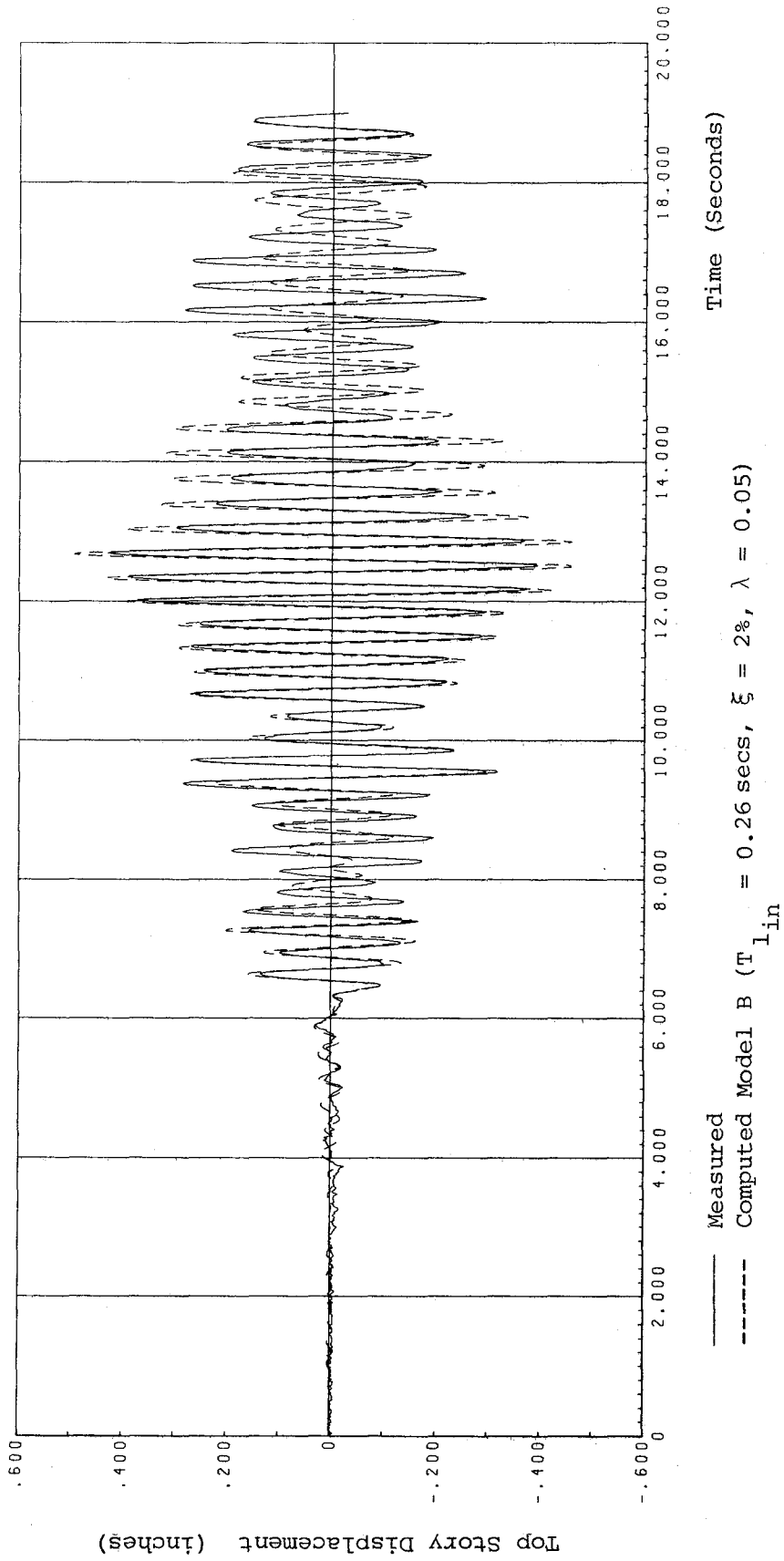


Fig. 5.4 CORRELATION FOR RUN W1. TOP STORY DISPLACEMENT.  
 MODEL B INCLUDING STIFFNESS DETERIORATION MECHANISM.

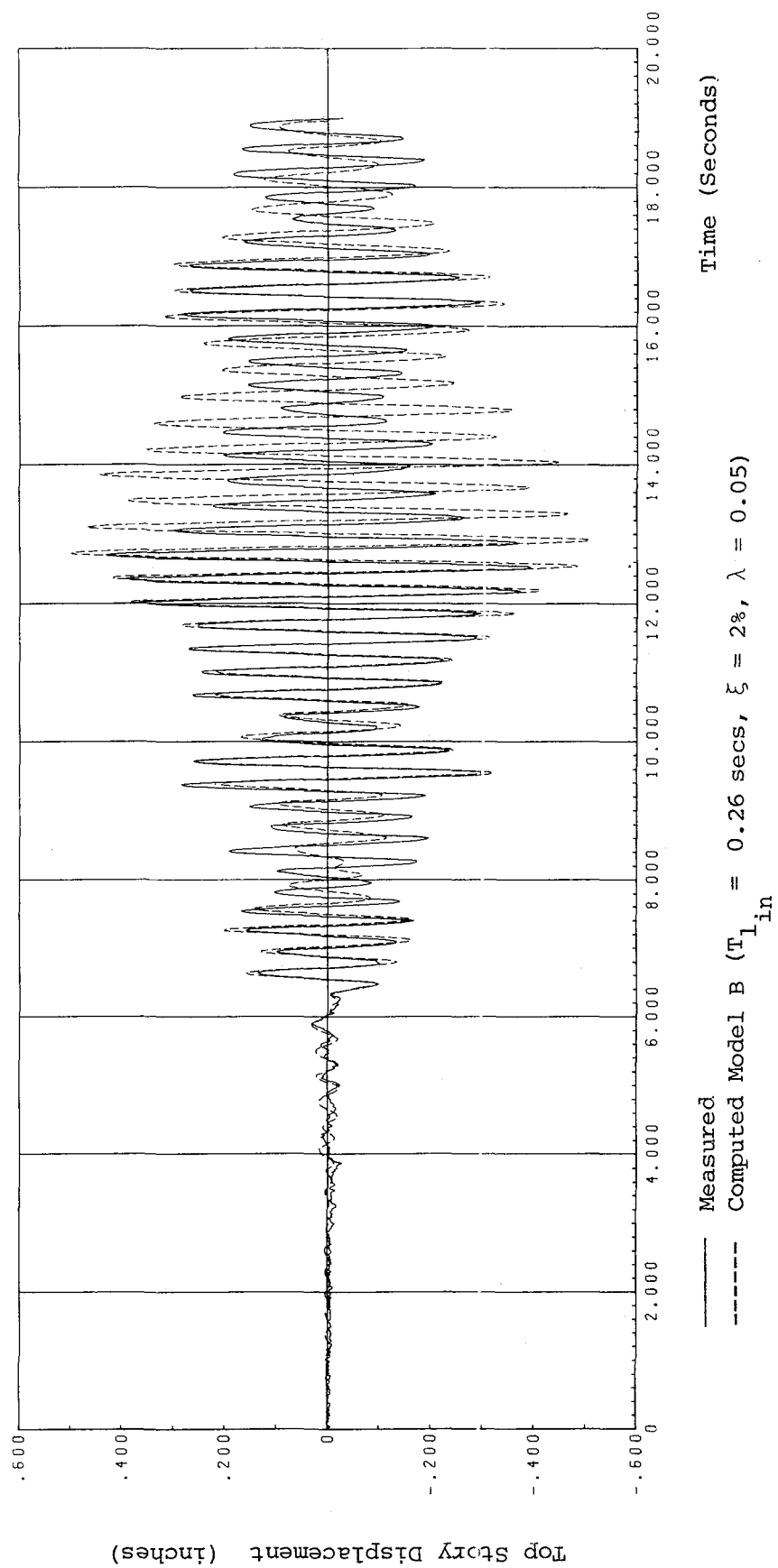


Fig. 5.5 CORRELATION FOR RUN W1. TOP STORY DISPLACEMENT.  
MODEL B INCLUDING STIFFNESS DETERIORATION MECHANISM.

## MODEL D

BI-LINEAR

CONSTANT  $\lambda, \eta, \xi$

STIFFNESS DEGRADATION  
ACCORDING TO CLOUGH'S  
MODEL, APPLIED TO  
COMPLETE STRUCTURE  
RESPONSE REPRESENTED  
BY FIRST MODE GENERALIZED  
COORDINATE  $Y(1)$

$$\{Y\} = [\phi^{-1}]\{v\}$$

$\lambda$  = STRAIN HARDENING RATIO  
AT SECTION BEHAVIOR

$\eta$  = STRAIN HARDENING RATIO  
AT STRUCTURE BEHAVIOR

$\xi$  = % CRITICAL DAMPING

$\{v\}$  = STORY DISPLACEMENTS

$[\phi]$  = MODE SHAPES MATRIX  
FOR INITIAL STIFFNESS

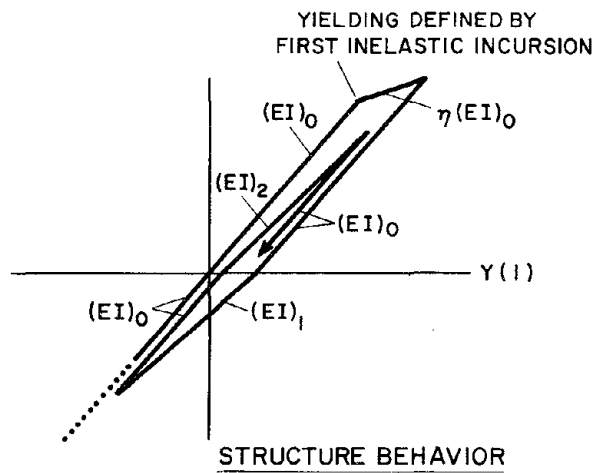
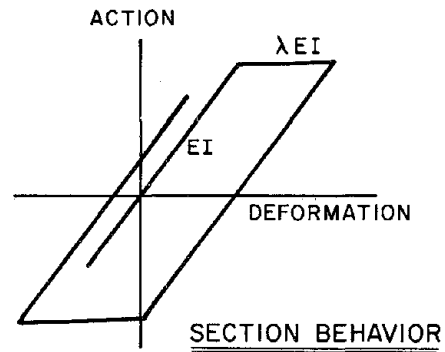


Fig. 5.6 BILINEAR STIFFNESS DEGRADING MODEL  
(MODEL D)

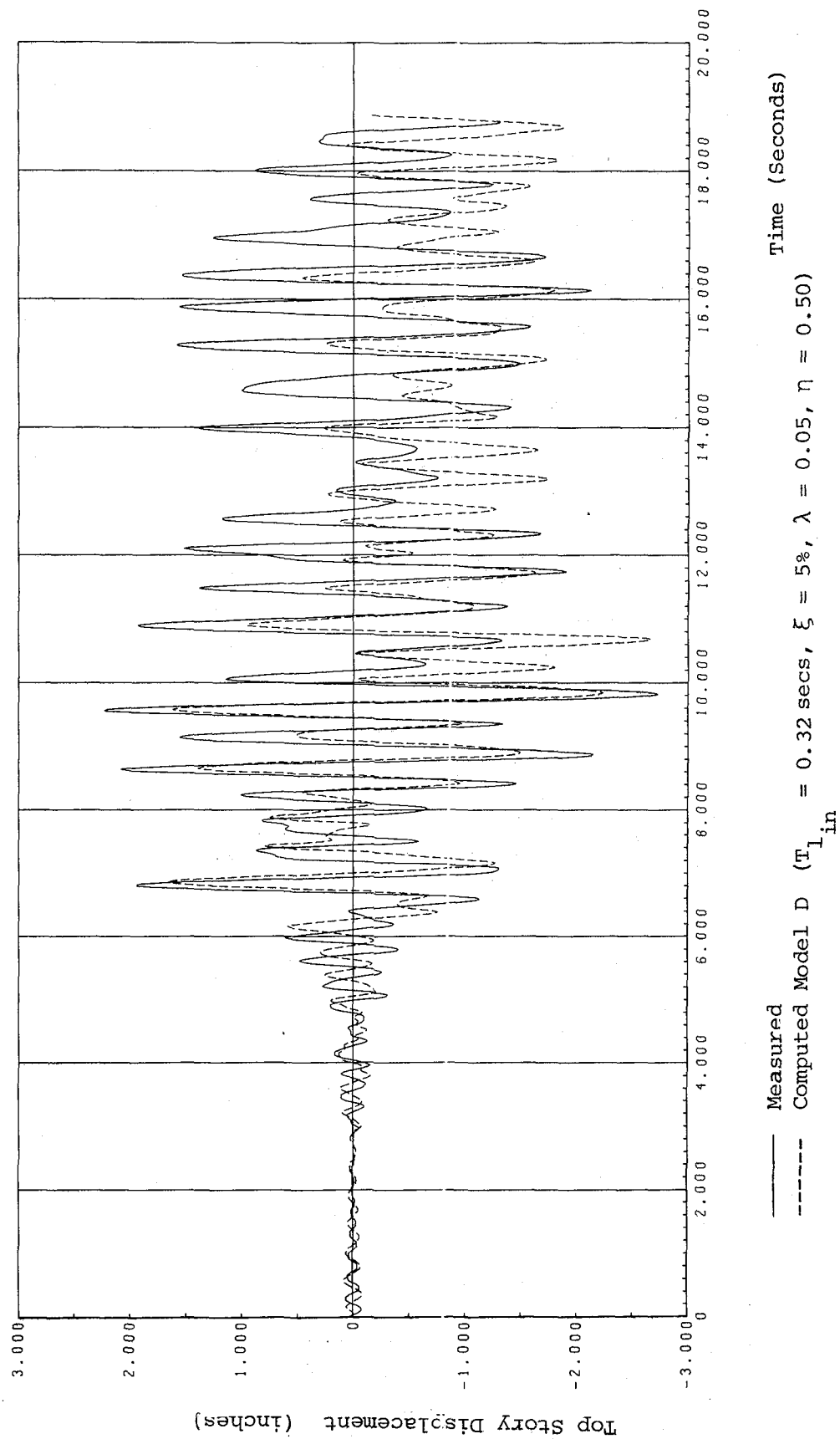


Fig. 5.7 CORRELATION FOR RUN W2. TOP STORY DISPLACEMENT. MODEL D.

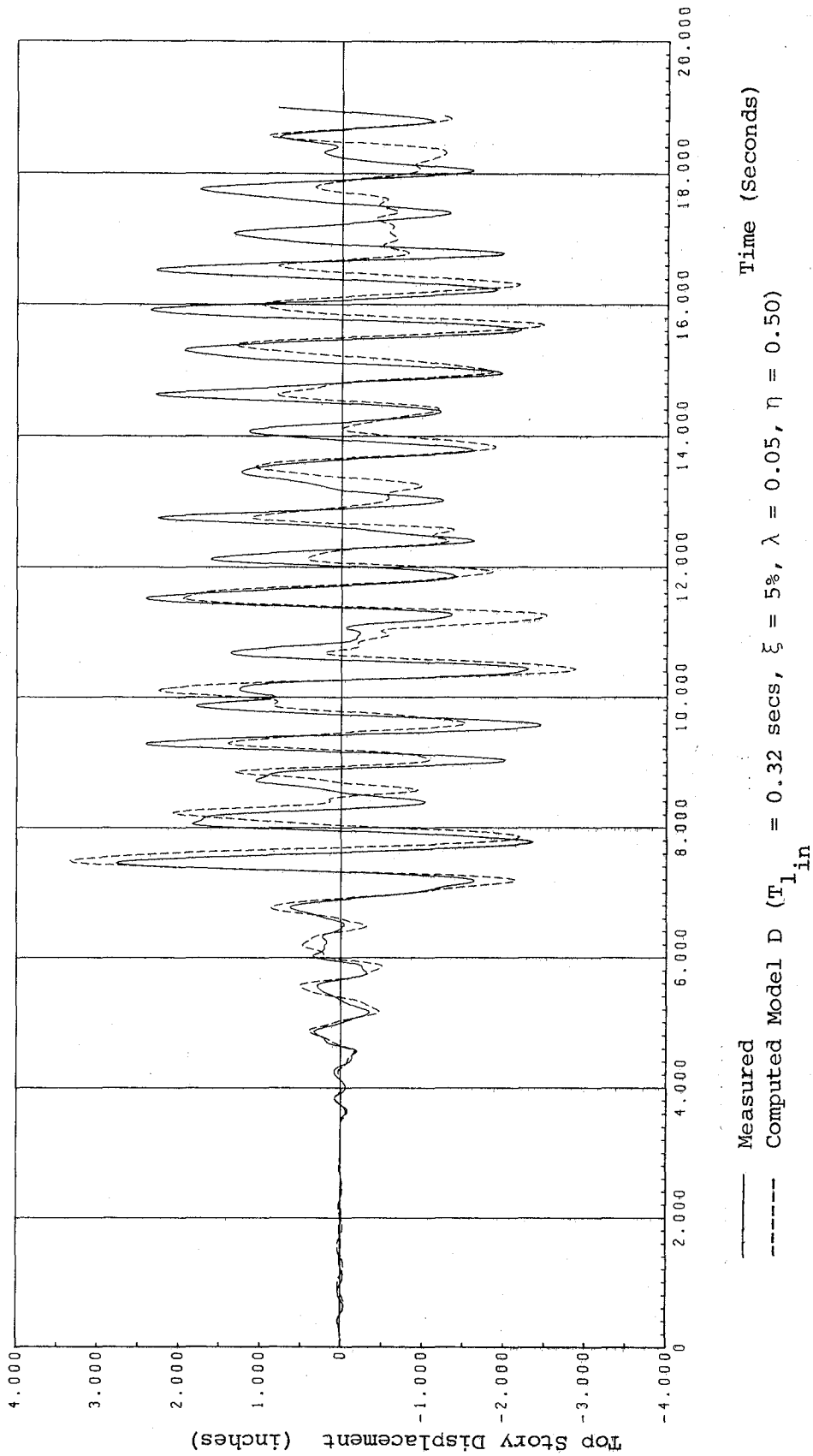
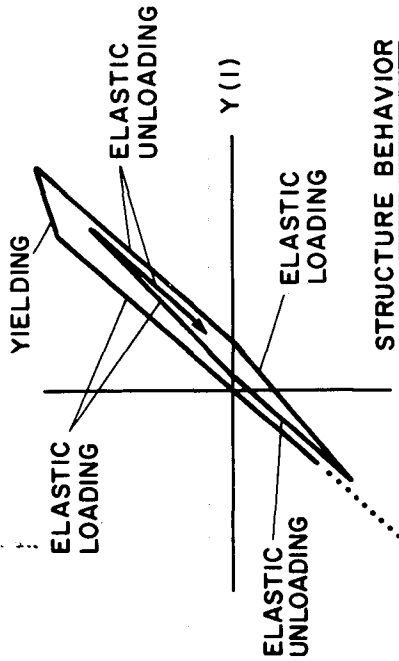


Fig. 5.8 CORRELATION FOR RUN W3. TOP STORY DISPLACEMENT. MODEL D.

MODELS E AND F (Same as model D with the addition of a stiffness deterioration mechanism)



STRUCTURE BEHAVIOR

MODEL E

Every time  $|v(i)| \geq DTL \times |v(i)_{YIELD}|$   
the stiffness of the structure is  
permanently reduced for the elastic  
loading branch only

MODEL F

Every time  $|v(i)| \geq DTL \times |v(i)_{YIELD}|$   
the stiffness of the structure is permanently  
reduced for both the elastic loading and elastic  
unloading branches (yielding branch remains un-  
changed)

$$(EI)^1 = (1.0 - n \times DTR)(EI)$$

$(EI)^1$  = Deteriorated Stiffness

$(EI)$  = Stiffness without deterioration

n = Number of times deterioration  
mechanism has Operated

$DTL < 1$  Deterioration Level

$DTR < 1$  Deterioration Rate

Fig. 5.9 BILLINEAR, STIFFNESS DEGRADING AND DETERIORATING MODELS  
(MODELS E AND F)

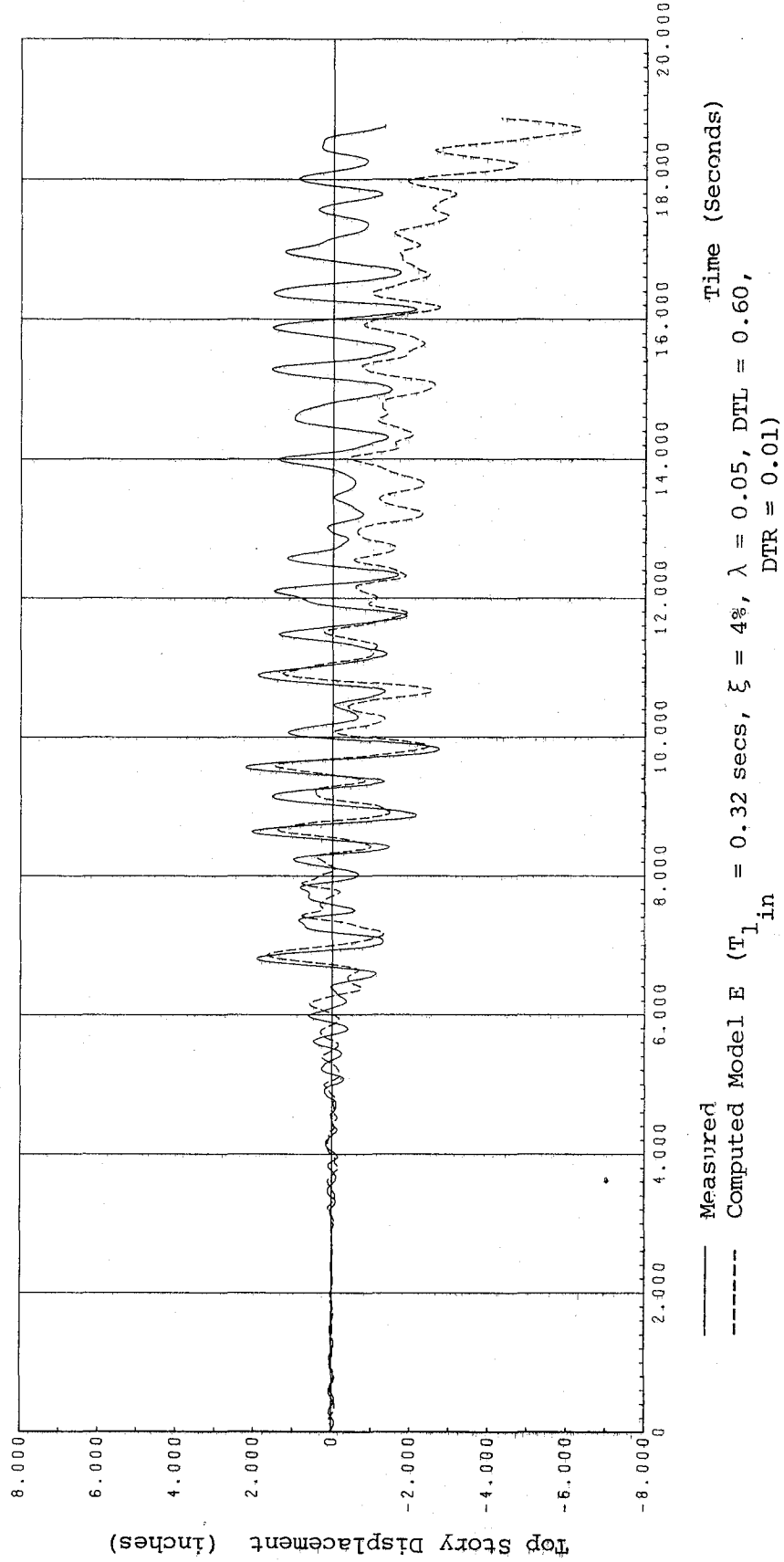


Fig. 5.10 CORRELATION FOR RUN W2. TOP STORY DISPLACEMENT. MODEL E.

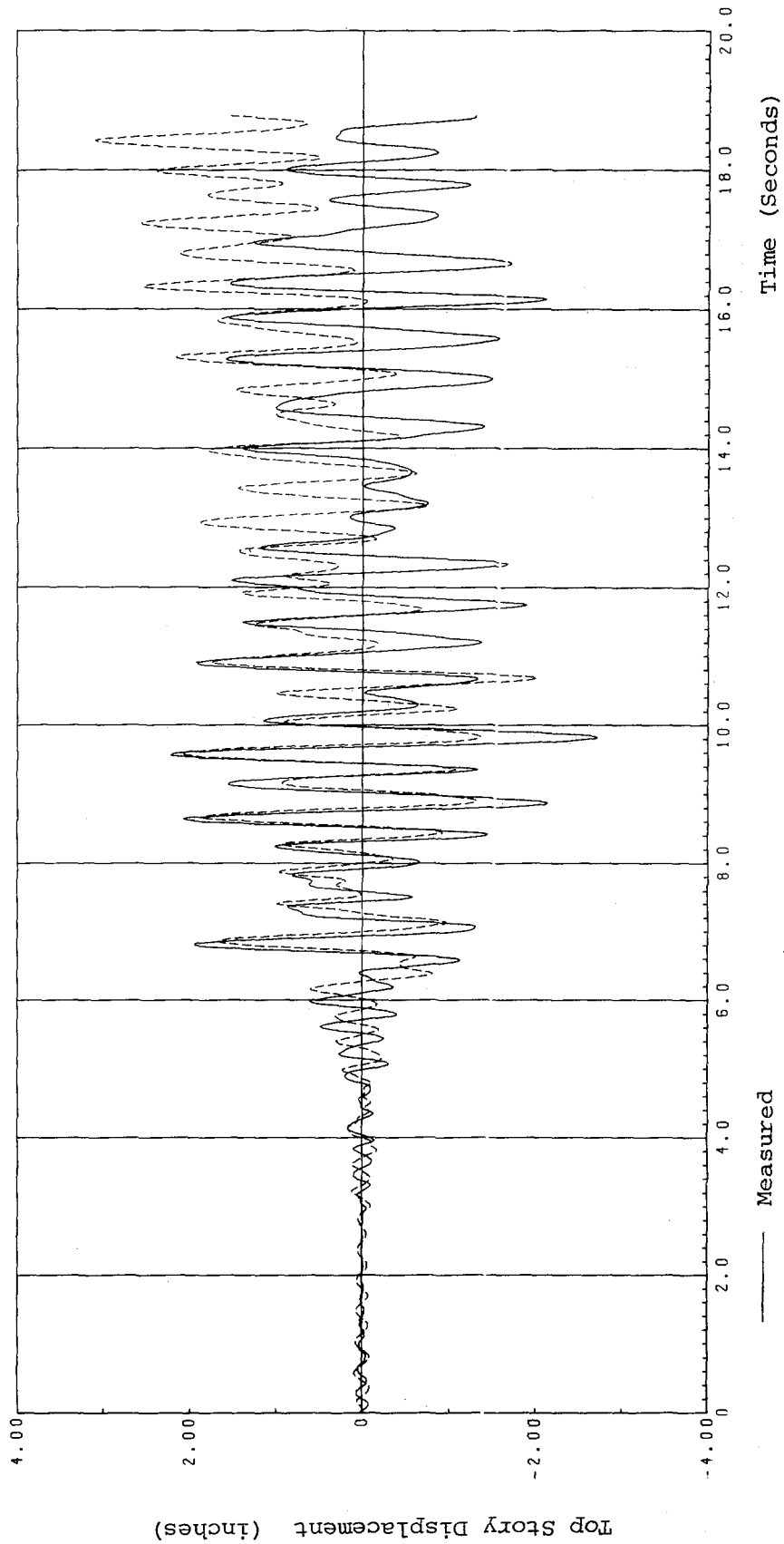


Fig. 5.11 CORRELATION FOR RUN W2. TOP STORY DISPLACEMENT. MODEL E.

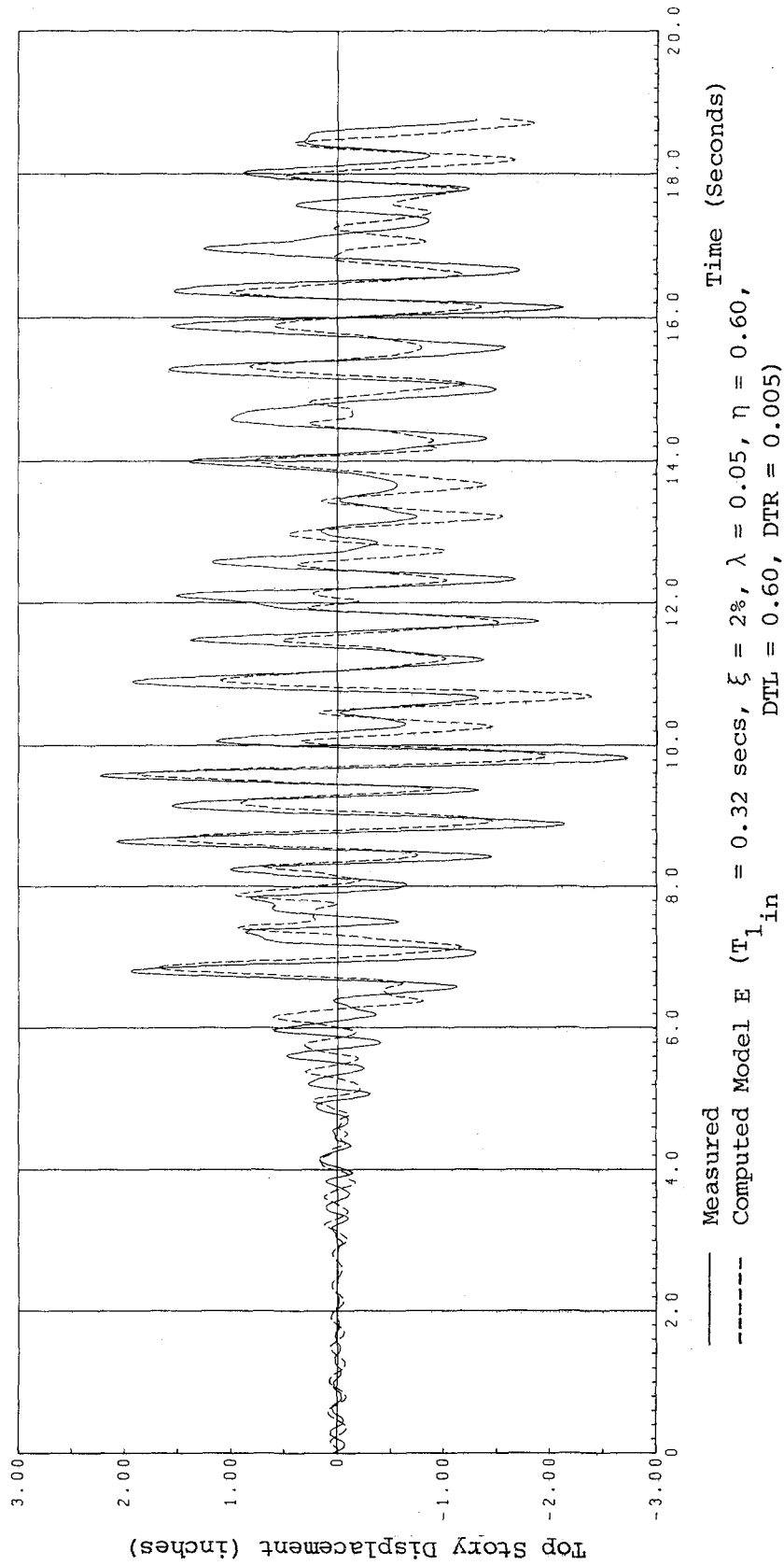


Fig. 5.12 CORRELATION FOR RUN W2. TOP STORY DISPLACEMENT. MODEL E.

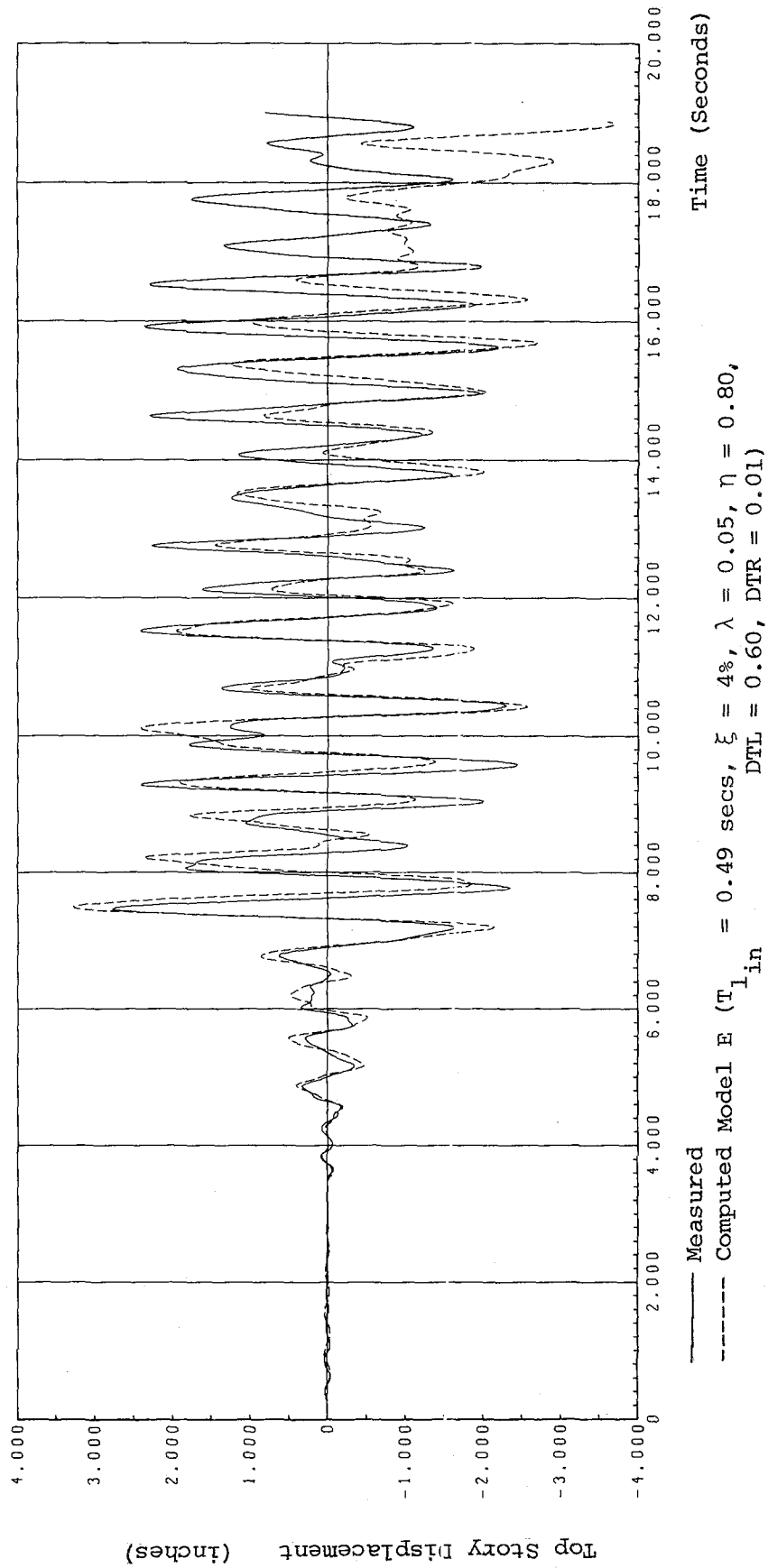


Fig. 5.13 CORRELATION FOR RUN W3. TOP STORY DISPLACEMENT. MODEL E.

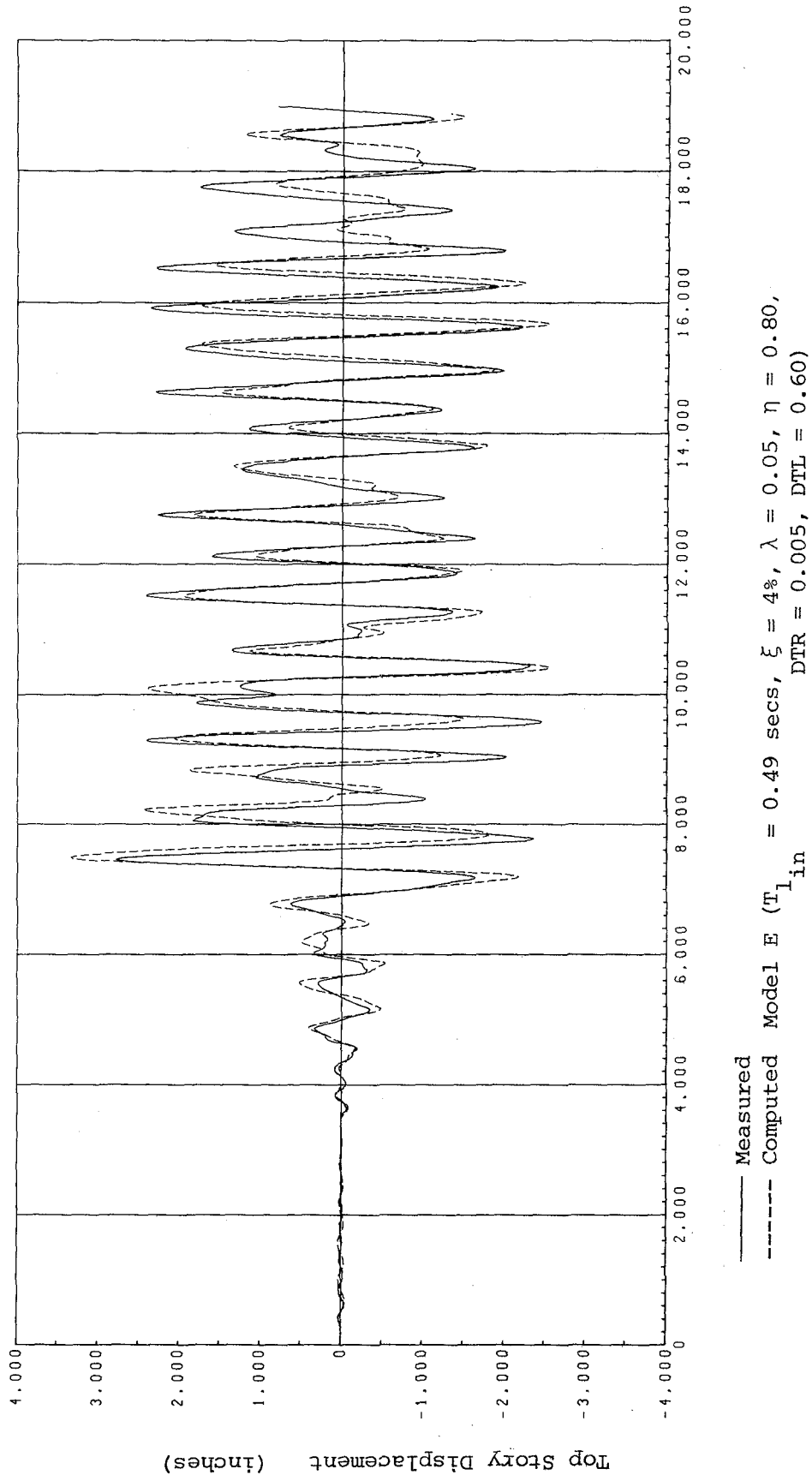


Fig. 5.14 CORRELATION FOR RUN W3. TOP STORY DISPLACEMENT. MODEL E.

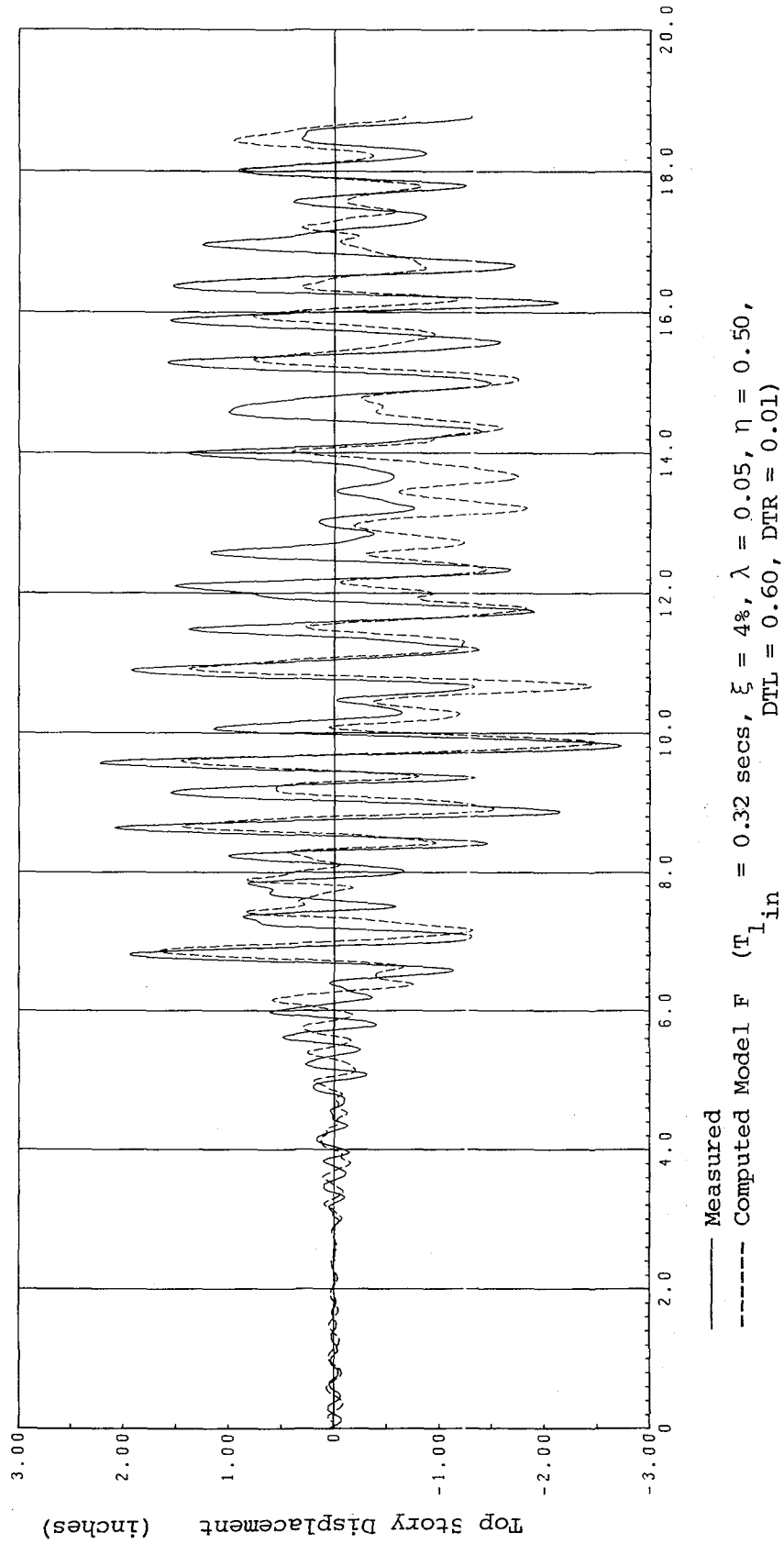


Fig. 5.15 CORRELATION FOR RUN W2. TOP STORY DISPLACEMENT. MODEL F.

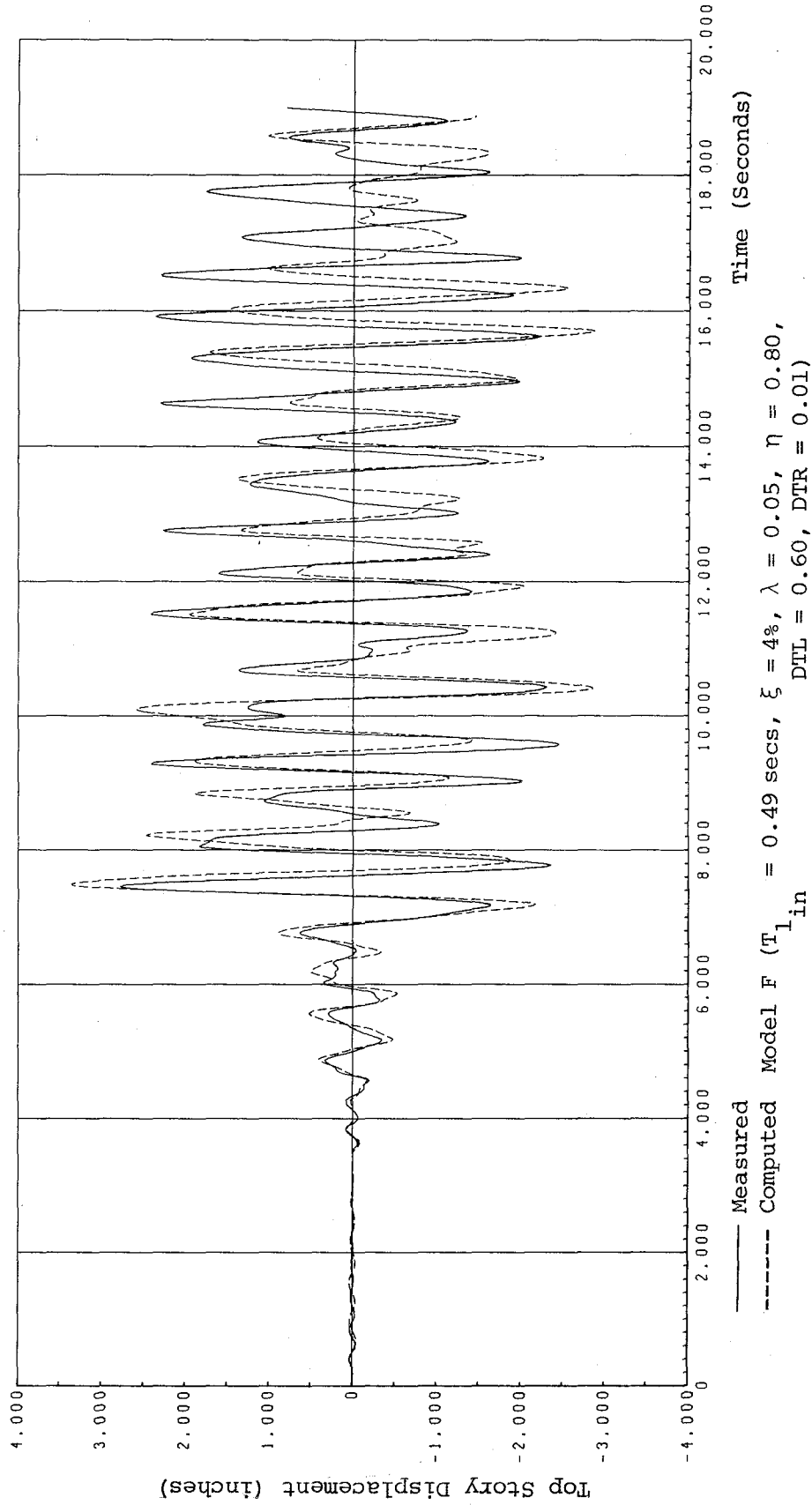


Fig. 5.16 CORRELATION FOR RUN W3. TOP STORY DISPLACEMENT. MODEL F.

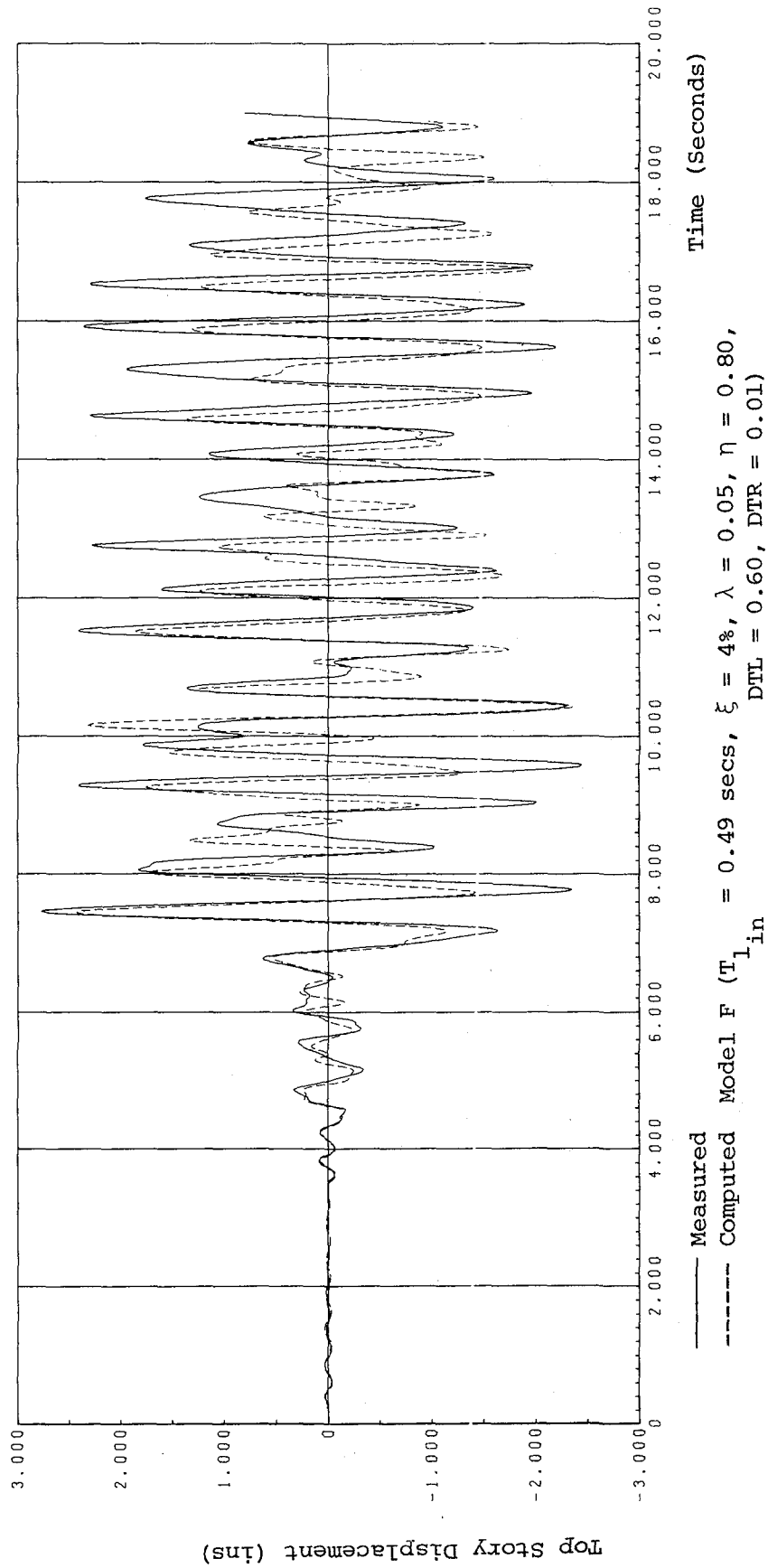


Fig. 5.17 CORRELATION FOR RUN W3. CRACKED SECTION PROPERTIES.  
TOP STORY DISPLACEMENT. MODEL F.

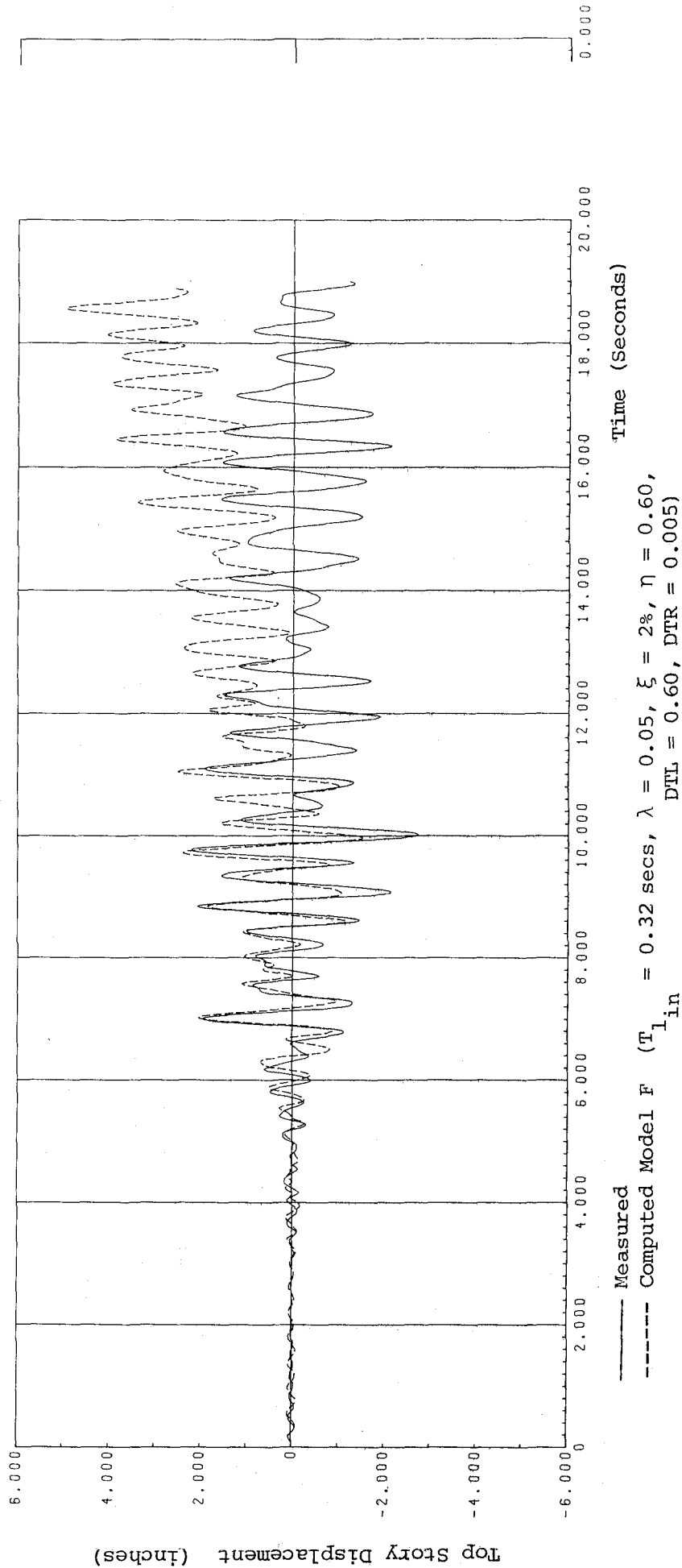


Fig. 5.20 CORRELATION FOR RUN W2. TOP STORY DISPLACEMENT.  
CRACKED SECTION PROPERTIES. MODEL F.

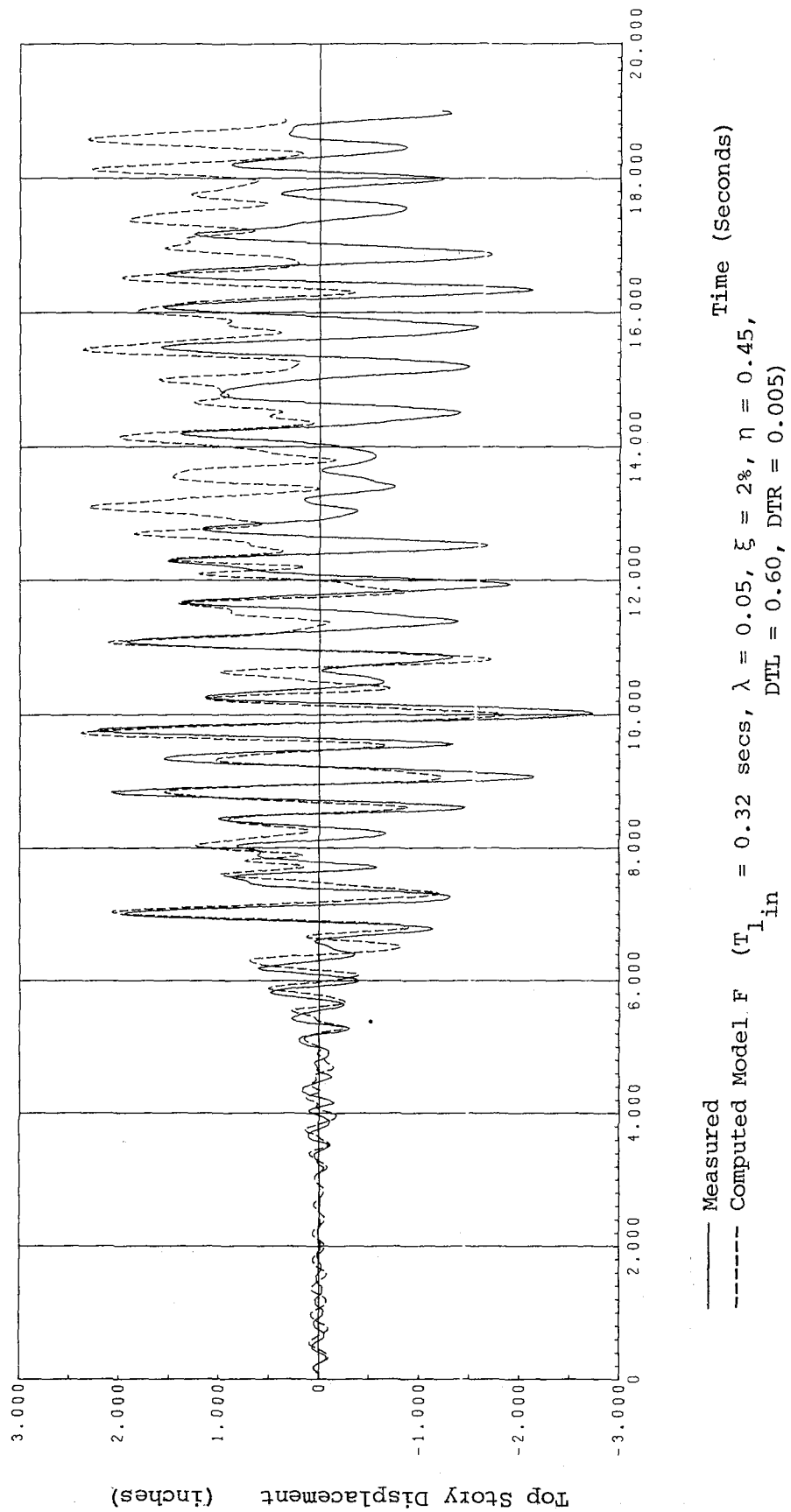


Fig. 5.21 CORRELATION FOR RUN W2. CRACKED SECTION PROPERTIES.  
 TOP STORY DISPLACEMENT. MODEL F.



## 6. CONCLUDING REMARKS

Although the testing of a single structure, as described in this report, is too limited a basis on which to draw general conclusions concerning the seismic behavior of reinforced concrete frames, the combined experience obtained with this frame and its predecessor does begin to lend credence to certain major observations. These are presented below in two categories, concerning the seismic resistance of the structure and regarding the correlation between its analytical and observed performance.

### 6.1 STRUCTURAL PERFORMANCE

(1) This frame, like its predecessor, was designed carefully according to ACI and Uniform Building Code requirements to achieve a highly ductile structure. It demonstrated excellent seismic resistance even when subjected to a succession of very severe earthquakes, with the damage being limited to cracking of concrete in the most highly stressed sections of the columns and girders. No permanent sidesway deformations could be observed, and the frame's ultimate strength capacity was not reduced by this cracking; but the sidesway stiffness was considerably diminished, of course.

(2) In contrast with Frame 1, which suffered a major crack near one end of the first floor slab due to erroneous termination of the slab mesh at that line, Frame 2 developed no major failure during testing. This fact demonstrates the value of close inspection during construction to ensure that the finished structure corresponds to the design.

(3) After repair by epoxy injection, the frame again demonstrated excellent seismic resistance. The repair did not restore the lateral

stiffness to its initial value, but the repaired frame was no more sensitive to damage than was the original structure.

(4) It is noteworthy that the dynamic forces developed in the frame during severe tests greatly exceeded the "ultimate load" capacity indicated by a simple elasto-plastic analysis procedure. This fact demonstrates the limitations of such simplified analyses in predicting earthquake performance; a more refined mathematical model is essential if realistic strength estimates are to be obtained.

(5) Comparisons of damage observed in Frames 1 and 2 indicate that earthquake damage to concrete frames tends to represent the cumulative effect of all strain cycles produced by the total seismic history. Amplitude and number of response cycles are significant factors, but the sequence in which they are developed apparently is not. Thus subjecting a virgin structure to intense loading before a sequence of smaller quakes seems to be no more destructive than if the process were reversed.

## 6.2 ANALYTICAL CORRELATIONS

(1) The most critical factor in achieving good analytical correlation with the experimental results is the initial frequency of the mathematical model. The two frames exhibited nearly identical responses when their natural frequencies before a test were similar and they were subjected to the same intensity. Similarly, a mathematical model provided quite good correlation if its initial stiffness were chosen to approximate the actual structure's starting frequency.

(2) Both mathematical Models E and F were found to give good correlations with the observed results for tests in which significant yielding occurred. Both consist of standard nonlinear frame analysis

programs based on bilinear joint regions, with a first mode stiffness degradation mechanism superposed. Loss of stiffness, expressed by a changed of the modulus of elasticity, depends both on the peak yield amplitude achieved and also on the number of cycles of significant deformation. At present the parameters which controlled this degradation and deterioration mechanism can only be selected empirically, and further experience is needed to define them better. A major problem at present is a spurious drift which results when inappropriate values are assigned to these parameters.

(3) The initial stiffness property of the frame was selected empirically in these studies to provide agreement with the observed initial frequency. In practice, however, the designer would have to define his analytical prediction model on the basis of design properties, and an effort was made here to simplify this "a priori" selection. Results obtained using the cracked section moment of inertia and a reduced modulus of elasticity for the concrete generally were satisfactory, so it appears that the designer need merely select the modulus reduction factor in accordance with the degree of cracking to which the structure has been subjected. Appropriate factors for the present tests ranged from over two for the original laboratory model to about 0.4 for a damaged structure subjected to aftershocks. Further experience is needed to select a factor suitable for a given building after several years of normal use.

### 6.3 EARTHQUAKE SIMULATOR TESTING

Although experience with the earthquake simulator is still quite limited, it is apparent that tests of this type represent an indispensable part of earthquake engineering research. Controlled amplitude

force or displacement testing provides an efficient means of studying the seismic capacity of structural components and assemblages, and for formulating mathematical models to represent their performance. However, the adequacy of such models, and of the computer programs in which they are utilized, can be verified only by testing complete structural systems subjected to simulated earthquake motions. Only then will the history of deformation to which each component is subjected represent the true earthquake behavior, in which the response mechanism influences the deformation history. On this basis it is clear that the earthquake simulator and the controlled displacement testing techniques are complementary, and that the ultimate verification depends on the earthquake simulator.

## REFERENCES

1. Hidalgo, P. and Clough, R., "Earthquake Simulator Study of a Reinforced Concrete Frame," Earthquake Engineering Research Center Report No. 74-13, December 1974.
2. Hognestad, E., "Study of a Combined Bending and Axial Load in Reinforced Concrete Members," Engineering Experiment Station Bulletin Series No. 399, University of Illinois, Urbana, Illinois, Nov. 1951.
3. Sudhakar, A., "Computer Program for Small Displacement Elasto-Plastic Analysis of Plane Steel and Reinforced Concrete Frames," Individual Study Student Report No. 561, SESM Division, Department of Civil Engineering, University of California, Berkeley, California, Fall Quarter 1972.
4. Clough, R., "Effects of Stiffness Degradation on Earthquake Ductility Requirements," Structures and Materials Research Report No. 66-16, Department of Civil Engineering, University of California, Berkeley, California, October 1966.



## APPENDIX A

### A.1 GENERAL

Section properties were evaluated for the purposes of analyses using the material properties of Figs. 2.4, 2.5 and 2.6 and Table 2.1 with the actual reinforcement layout of Fig. 2.7. The results of such calculations are shown below.

### A.2 TRANSFORMED AREA SECTION

$$E_s = 29000 \text{ ksi} \quad E_c = 2640 \text{ ksi}$$

$$n = \frac{E_s}{E_c} = 10.98$$

#### Column Section

$$A_{TR} = 5.75 \times 8.50 + 2 \times 9.98 \times 0.62 = 61.25 \text{ in}^2$$

$$I_{TR} = \frac{5.75 \times (8.50)^3}{12} + 2 \times 9.98 \times (2.33)^2 \times 0.62 = 361.45 \text{ in}^4$$

#### Bottom Story Girder

Depth of neutral axis from top fibre

$$y^* = 3.38 \text{ ins.}$$

$$\begin{aligned} I_{TR} &= \frac{36 \times (2.875)^3}{12} + 36 \times 2.875 \times (3.38 - 1.44)^2 \\ &+ \frac{5.75 \times (8.50)^3}{12} + 5.75 \times 8.50 \times (7.13 - 3.38)^2 \\ &+ 0.351 \times 9.98 \times (3.38 - 0.61)^2 + 0.66 \times 9.98 \times (3.38 - 1.03)^2 \\ &+ 0.351 \times 9.98 \times (3.38 - 2.11)^2 + 0.62 \times 9.98 \times (9.58 - 3.38)^2 \end{aligned}$$

$$I_{TR} = 1749.0 \text{ in}^4$$

**Preceding page blank**

Top Story Girder

Depth of neutral axis from top fibre

$$y^* = 3.28 \text{ ins.}$$

$$I_{TR} = 1650.0 \text{ in}^4$$

A.3 GROSS SECTIONColumn Section

$$A_g = 5.75 \times 8.50 = 48.88 \text{ in}^2$$

$$I_g = \frac{5.75 \times (8.50)^3}{12} = 294.3 \text{ in}^4$$

Bottom and Top Story Girders

Depth of neutral axis from top fibre

$$y^* = 3.26 \text{ ins}$$

$$I_g = \frac{36 \times (2.875)^3}{12} + 36 \times 2.875 \times (3.26 - 1.44)^2$$

$$+ \frac{5.75 \times (8.50)^3}{12} + 5.75 \times 8.50 \times (7.13 - 3.26)^2$$

$$I_g = 1440.0 \text{ in}^4$$

A.4 YIELD SURFACES

While computing the yield properties, compression reinforcement is included in the computation. Material properties of Figs. 2.4, 2.5 and 2.6 and Table 2.1 were used.

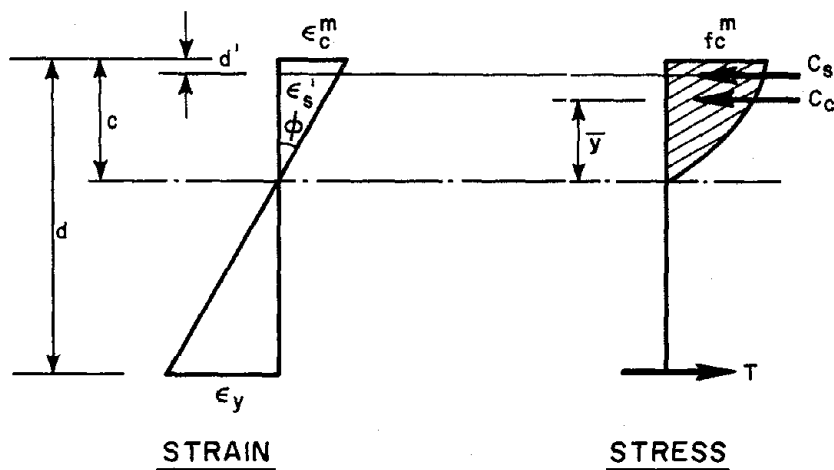
A.4.1 Column Section

$$A_s = A'_s = 0.62 \text{ in}^2, \quad E_s = E'_s = 29000 \text{ ksi}$$

$$d = 6.75 \text{ ins}, \quad d' = 1.75 \text{ ins}, \quad b = 5.75 \text{ ins}$$

$$f'_c = 4.395 \text{ ksi}, \quad E_c = 2640 \text{ ksi}, \quad \epsilon_{co} = 0.00335, \quad \epsilon_{CULT} = 0.005$$

## a) Yield Values (P = 0)



$\epsilon_y$ (in/in)	0.0014
$f_y$ (ksi)	41.5
T (kips)	25.7
c (ins)	2.80
$\epsilon_c^m$ (in/in)	0.0009924
$\epsilon_s'$ (in/in)	0.0003721
$C_s$ (kips)	6.90
$C_c$ (kips)	18.90
$\bar{y}$ (ins)	1.84
$M_o$ (in-kip)	148.8
$\phi_y = \frac{\epsilon_c^m}{c}$ (1/in)	0.000354
$I_{CR} = \frac{M_o}{E_c \phi_y}$ (in <sup>4</sup> )	159.0

b) Compression Yield Force ( $M = 0$ )

$$P_O = f'_c (A_g - A_s - A'_s) + (A_s + A'_s) f_y$$

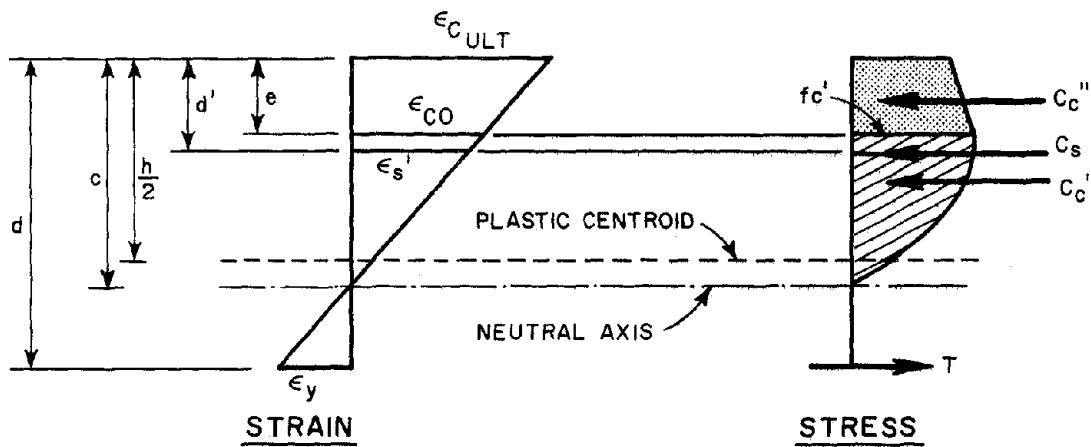
$$P_O \text{ (kips)} \quad 260.9$$

c) Tension Yield Force ( $M = 0$ )

$$P_T = (A_s + A'_s) f_y$$

$$P_T \text{ (kips)} \quad 51.5$$

d) Balanced Point



$\epsilon_y$ (in/in)	0.0014
$T$ (kips)	25.7
$c$ (ins)	5.27
$e$ (ins)	1.74
$C_s = T$ (kips)	25.7
$C_c'$ (kips)	57.7
$C_c''$ (kips)	40.7
$P_B$ (kips)	98.4

$M_B$ (in-kip)	352.1
$\phi_B$ (1/in)	0.000949
$I_B$ (in <sup>4</sup> )	140.5

A.4.2 Girder Sections. Tension at Bottom Fibre. Wire Mesh Reinforcement Included in Computations.

	Bottom Story	Top Story
T (kips)	25.73	22.44
c (ins)	1.66	1.38
$C_s$ (kips)	3.21	0.899
$C_c$ (kips)	22.30	21.38
C (kips)	25.51	22.28
$M_Y^+$ (in-kip)	232.1	205.5
$\phi_Y^+$ (1/in)	0.000177	0.000246
$I_{CR}^+$ (in <sup>4</sup> )	497.0	317.0

A.4.3 Girder Sections. Tension at Top Fibre. Wire Mesh Reinforcement Included in Computations.

In this case we see that the yield moment is not defined as before i.e. yielding of main reinforcement, since we have three layers of tension reinforcement. Hence the moment curvature relationship is plotted for various conditions defined in the Fig. A.1 and the yield moment is the moment defined in the same figure.

The notation for the forces in the tension reinforcement is as follows

$T_0$ : Force in the main tension reinforcement

$T_1$ : Force in the tension reinforcement closer to the top of slab

$T_2$ : Force in the tension reinforcement closer to the bottom of slab.

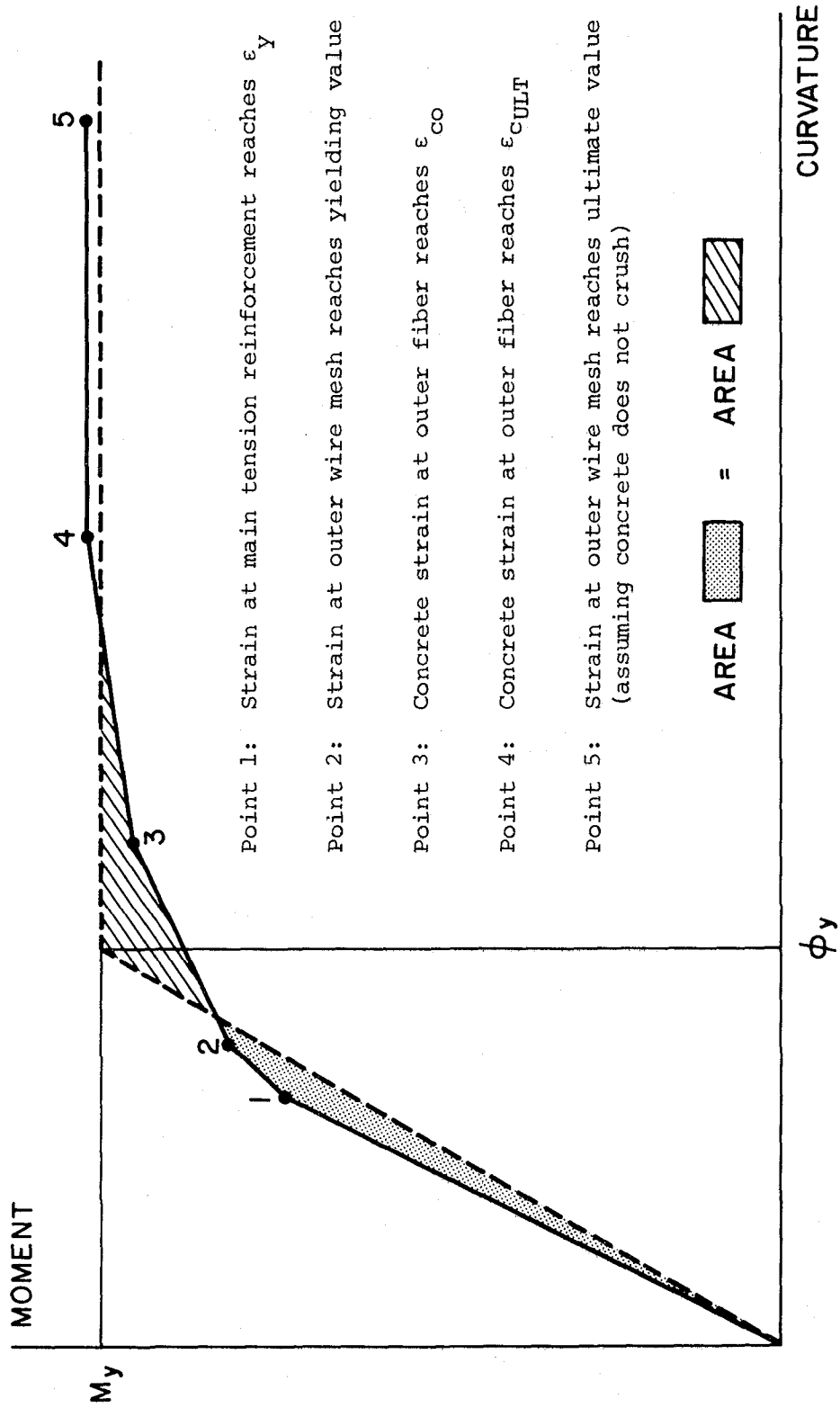


Fig. A.1 MOMENT-CURVATURE RELATIONSHIP FOR GIRDER SECTIONS.

IDEALIZED CURVE USED FOR ANALYSIS IS SHOWN BY DOTTED LINE.

Bottom Story Girder

	Point 1	Point 2	Point 3	Point 4	Point 5
c (ins)	4.90	4.82	3.45	3.26	3.30
C <sub>s</sub> (kips)	19.23	20.60	25.73	25.73	25.73
C <sub>c</sub> (kips)	50.86	53.31	58.12	61.98	63.19
C (kips)	70.09	73.91	83.85	87.71	88.92
T <sub>0</sub> (kips)	34.32	34.32	34.32	34.32	34.32
T <sub>1</sub> (kips)	20.34	22.71	25.19	27.13	27.40
T <sub>2</sub> (kips)	15.14	16.98	24.45	26.26	27.10
T (kips)	69.80	74.01	83.96	87.71	88.80
M (in-kips)	594.5	629.0	731.0	761.0	764.0
φ (in/in)	0.000336	0.000369	0.000971	0.00153	0.00201

Therefore  $\bar{M}_y = 720.0 \text{ in-kip}$

$\bar{\phi}_y = 0.0004 \text{ 1/in}$

$\bar{I}_{CR} = \frac{\bar{M}_y}{E_c \bar{\phi}_y} = 670.0 \text{ in}^4.$

Top Story Girder

	Point 1	Point 2	Point 3	Point 4	Point 5
c (ins)	4.77	4.72	3.33	2.94	3.07
C <sub>s</sub> (kips)	10.72	11.85	16.90	21.14	22.44
C <sub>c</sub> (kips)	47.25	50.94	56.10	55.86	56.09
C (kips)	57.97	62.79	73.00	77.00	78.53
T <sub>0</sub> (kips)	22.88	22.88	22.88	22.88	22.88
T <sub>1</sub> (kips)	20.03	22.71	25.36	27.25	28.04
T <sub>2</sub> (kips)	15.19	17.26	24.63	27.06	27.60
T (kips)	58.10	62.85	72.87	77.19	78.52
M (in-kips)	495.0	536.0	638.0	674.0	670.0
φ (1/in)	0.000326	0.000366	0.00101	0.00170	0.00282

Therefore  $\bar{M}_Y = 640.0$  in-kip

$\bar{\phi}_Y = 0.0004$  (1/in)

$\bar{I}_{CR} = 575.0$  in<sup>4</sup>.

EARTHQUAKE ENGINEERING RESEARCH CENTER REPORTS

- EERC 67-1 "Feasibility Study Large-Scale Earthquake Simulator Facility," by J. Penzien, J. G. Bouwkamp, R. W. Clough and D. Rea - 1967 (PB 187 905)
- EERC 68-1 Unassigned
- EERC 68-2 "Inelastic Behavior of Beam-to-Column Subassemblages Under Repeated Loading," by V. V. Bertero - 1968 (PB 184 888)
- EERC 68-3 "A Graphical Method for Solving the Wave Reflection-Refracton Problem," by H. D. McNiven and Y. Mengi 1968 (PB 187 943)
- EERC 68-4 "Dynamic Properties of McKinley School Buildings," by D. Rea, J. G. Bouwkamp and R. W. Clough - 1968 (PB 187 902)
- EERC 68-5 "Characteristics of Rock Motions During Earthquakes," by H. B. Seed, I. M. Idriss and F. W. Kiefer - 1968 (PB 188 338)
- EERC 69-1 "Earthquake Engineering Research at Berkeley," - 1969 (PB 187 906)
- EERC 69-2 "Nonlinear Seismic Response of Earth Structures," by M. Dibaj and J. Penzien - 1969 (PB 187 904)
- EERC 69-3 "Probabilistic Study of the Behavior of Structures During Earthquakes," by P. Ruiz and J. Penzien - 1969 (PB 187 886)
- EERC 69-4 "Numerical Solution of Boundary Value Problems in Structural Mechanics by Reduction to an Initial Value Formulation," by N. Distefano and J. Schujman - 1969 (PB 187 942)
- EERC 69-5 "Dynamic Programming and the Solution of the Biharmonic Equation," by N. Distefano - 1969 (PB 187 941)

---

Note: Numbers in parenthesis are Accession Numbers assigned by the National Technical Information Service. Copies of these reports may be ordered from the National Technical Information Service, 5285 Port Royal Road, Springfield, Virginia, 22161. Accession Numbers should be quoted on orders for the reports (PB --- ---) and remittance must accompany each order. (Foreign orders, add \$2.50 extra for mailing charges.) Those reports without this information listed are not yet available from NTIS. Upon request, EERC will mail inquirers this information when it becomes available to us.

- EERC 69-6 "Stochastic Analysis of Offshore Tower Structures," by A. K. Malhotra and J. Penzien - 1969 (PB 187 903)
- EERC 69-7 "Rock Motion Accelerograms for High Magnitude Earthquakes," by H. B. Seed and I. M. Idriss - 1969 (PB 187 940)
- EERC 69-8 "Structural Dynamics Testing Facilities at the University of California, Berkeley," by R. M. Stephen, J. G. Bouwkamp, R. W. Clough and J. Penzien - 1969 (PB 189 111)
- EERC 69-9 "Seismic Response of Soil Deposits Underlain by Sloping Rock Boundaries," by H. Dezfulian and H. B. Seed - 1969 (PB 189 114)
- EERC 69-10 "Dynamic Stress Analysis of Axisymmetric Structures under Arbitrary Loading," by S. Ghosh and E. L. Wilson - 1969 (PB 189 026)
- EERC 69-11 "Seismic Behavior of Multistory Frames Designed by Different Philosophies," by J. C. Anderson and V. V. Bertero - 1969 (PB 190 662)
- EERC 69-12 "Stiffness Degradation of Reinforcing Concrete Structures Subjected to Reversed Actions," by V. V. Bertero, B. Bresler and H. Ming Liao - 1969 (PB 202 942)
- EERC 69-13 "Response of Non-Uniform Soil Deposits to Travel Seismic Waves," by H. Dezfulian and H. B. Seed - 1969 (PB 191 023)
- EERC 69-14 "Damping Capacity of a Model Steel Structure," by D. Rea, R. W. Clough and J. G. Bouwkamp - 1969 (PB 190 663)
- EERC 69-15 "Influence of Local Soil Conditions on Building Damage Potential during Earthquakes," by H. B. Seed and I. M. Idriss - 1969 (PB 191 036)
- EERC 69-16 "The Behavior of Sands under Seismic Loading Conditions," by M. L. Silver and H. B. Seed - 1969 (AD 714 982)
- EERC 70-1 "Earthquake Response of Concrete Gravity Dams," by A. K. Chopra - 1970 (AD 709 640)
- EERC 70-2 "Relationships between Soil Conditions and Building Damage in the Caracas Earthquake of July 29, 1967," by H. B. Seed, I. M. Idriss and H. Dezfulian - 1970 (PB 195 762)

- EERC 70-3 "Cyclic Loading of Full Size Steel Connections," by E. P. Popov and R. M. Stephen - 1970 (PB 213 545)
- EERC 70-4 "Seismic Analysis of the Charaima Building, Caraballeda, Venezuela," by Subcommittee of the SEAONC Research Committee: V. V. Bertero, P. F. Fratessa, S. A. Mahin, J. H. Sexton, A. C. Scordelis, E. L. Wilson, L. A. Wyllie, H. B. Seed and J. Penzien, Chairman - 1970 (PB 201 455)
- EERC 70-5 "A Computer Program for Earthquake Analysis of Dams," by A. K. Chopra and P. Chakrabarti - 1970 (AD 723 994)
- EERC 70-6 "The Propagation of Love Waves across Non-Horizontally Layered Structures," by J. Lysmer and L. A. Drake - 1970 (PB 197 896)
- EERC 70-7 "Influence of Base Rock Characteristics on Ground Response," by J. Lysmer, H. B. Seed and P. B. Schnabel - 1970 (PB 197 897)
- EERC 70-8 "Applicability of Laboratory Test Procedures for Measuring Soil Liquefaction Characteristics under Cyclic Loading," by H. B. Seed and W. H. Peacock - 1970 (PB 198 016)
- EERC 70-9 "A Simplified Procedure for Evaluating Soil Liquefaction Potential," by H. B. Seed and I. M. Idriss - 1970 (PB 198 009)
- EERC 70-10 "Soil Moduli and Damping Factors for Dynamic Response Analysis," by H. B. Seed and I. M. Idriss - 1970 (PB 197 869)
- EERC 71-1 "Koyna Earthquake and the Performance of Koyna Dam," by A. K. Chopra and P. Chakrabarti - 1971 (AD 731 496)
- EERC 71-2 "Preliminary In-Situ Measurements of Anelastic Absorption in Soils Using a Prototype Earthquake Simulator," by R. D. Borcherdt and P. W. Rodgers - 1971 (PB 201 454)
- EERC 71-3 "Static and Dynamic Analysis of Inelastic Frame Structures," by F. L. Porter and G. H. Powell - 1971 (PB 210 135)
- EERC 71-4 "Research Needs in Limit Design of Reinforced Concrete Structures," by V. V. Bertero - 1971 (PB 202 943)
- EERC 71-5 "Dynamic Behavior of a High-Rise Diagonally Braced Steel Building," by D. Rea, A. A. Shah and J. G. Bouwkamp - 1971 (PB 203 584)

- EERC 71-6 "Dynamic Stress Analysis of Porous Elastic Solids Saturated with Compressible Fluids," by J. Ghaboussi and E. L. Wilson - 1971 (PB 211 396)
- EERC 71-7 "Inelastic Behavior of Steel Beam-to-Column Subassemblages," by H. Krawinkler, V. V. Bertero and E. P. Popov - 1971 (PB 211 335)
- EERC 71-8 "Modification of Seismograph Records for Effects of Local Soil Conditions," by P. Schnabel, H. B. Seed and J. Lysmer - 1971 (PB 214 450)
- EERC 72-1 "Static and Earthquake Analysis of Three Dimensional Frame and Shear Wall Buildings," by E. L. Wilson and H. H. Dovey - 1972 (PB 212 904)
- EERC 72-2 "Accelerations in Rock for Earthquakes in the Western United States," by P. B. Schnabel and H. B. Seed - 1972 (PB 213 100)
- EERC 72-3 "Elastic-Plastic Earthquake Response of Soil-Building Systems," by T. Minami - 1972 (PB 214 868)
- EERC 72-4 "Stochastic Inelastic Response of Offshore Towers to Strong Motion Earthquakes," by M. K. Kaul - 1972 (PB 215 713)
- EERC 72-5 "Cyclic Behavior of Three Reinforced Concrete Flexural Members with High Shear," by E. P. Popov, V. V. Bertero and H. Krawinkler - 1972 (PB 214 555)
- EERC 72-6 "Earthquake Response of Gravity Dams Including Reservoir Interaction Effects," by P. Chakrabarti and A. K. Chopra - 1972 (AD 762 330)
- EERC 72-7 "Dynamic Properties on Pine Flat Dam," by D. Rea, C. Y. Liaw and A. K. Chopra - 1972 (AD 763 928)
- EERC 72-8 "Three Dimensional Analysis of Building Systems," by E. L. Wilson and H. H. Dovey - 1972 (PB 222 438)
- EERC 72-9 "Rate of Loading Effects on Uncracked and Repaired Reinforced Concrete Members," by S. Mahin, V. V. Bertero, D. Rea and M. Atalay - 1972 (PB 224 520)
- EERC 72-10 "Computer Program for Static and Dynamic Analysis of Linear Structural Systems," by E. L. Wilson, K.-J. Bathe, J. E. Peterson and H. H. Dovey - 1972 (PB 220 437)

- EERC 72-11 "Literature Survey - Seismic Effects on Highway Bridges," by T. Iwasaki, C. Penzien and R. W. Clough - 1972 (PB 215 613)
- EERC 72-12 "SHAKE-A Computer Program for Earthquake Response Analysis of Horizontally Layered Sites," by P. B. Schnabel and J. Lysmer - 1972 (PB 220 207)
- EERC 73-1 "Optimal Seismic Design of Multistory Frames," by V. V. Bertero and H. Kamil - 1973
- EERC 73-2 "Analysis of the Slides in the San Fernando Dams during the Earthquake of February 9, 1971," by H. B. Seed, K. L. Lee, I. M. Idriss and F. Makdisi - 1973 (PB 223 402)
- EERC 73-3 "Computer Aided Ultimate Load Design of Unbraced Multistory Steel Frames," by M. B. El-Hafez and G. H. Powell - 1973
- EERC 73-4 "Experimental Investigation into the Seismic Behavior of Critical Regions of Reinforced Concrete Components as Influenced by Moment and Shear," by M. Celebi and J. Penzien - 1973 (PB 215 884)
- EERC 73-5 "Hysteretic Behavior of Epoxy-Repaired Reinforced Concrete Beams," by M. Celebi and J. Penzien - 1973
- EERC 73-6 "General Purpose Computer Program for Inelastic Dynamic Response of Plane Structures," by A. Kanaan and G. H. Powell - 1973 (PB 221 260)
- EERC 73-7 "A Computer Program for Earthquake Analysis of Gravity Dams Including Reservoir Interaction," by P. Chakrabarti and A. K. Chopra - 1973 (AD 766 271)
- EERC 73-8 "Behavior of Reinforced Concrete Deep Beam-Column Subassemblages under Cyclic Loads," by O. Kustu and J. G. Bouwkamp - 1973
- EERC 73-9 "Earthquake Analysis of Structure-Foundation Systems," by A. K. Vaish and A. K. Chopra - 1973 (AD 766 272)
- EERC 73-10 "Deconvolution of Seismic Response for Linear Systems," by R. B. Reimer - 1973 (PB 227 179)
- EERC 73-11 "SAP IV: A Structural Analysis Program for Static and Dynamic Response of Linear Systems," by K.-J. Bathe, E. L. Wilson and F. E. Peterson - 1973 (PB 221 967)
- EERC 73-12 "Analytical Investigations of the Seismic Response of Long, Multiple Span Highway Bridges," by W. S. Tseng and J. Penzien - 1973 (PB 227 816)

- EERC 73-13 "Earthquake Analysis of Multi-Story Buildings Including Foundation Interaction," by A. K. Chopra and J. A. Gutierrez - 1973 (PB 222 970)
- EERC 73-14 "ADAP: A Computer Program for Static and Dynamic Analysis of Arch Dams," by R. W. Clough, J. M. Raphael and S. Majtahedi - 1973 (PB 223 763)
- EERC 73-15 "Cyclic Plastic Analysis of Structural Steel Joints," by R. B. Pinkney and R. W. Clough - 1973 (PB 226 843)
- EERC 73-16 "QUAD-4: A Computer Program for Evaluating the Seismic Response of Soil Structures by Variable Damping Finite Element Procedures," by I. M. Idriss, J. Lysmer, R. Hwang and H. B. Seed - 1973 (PB 229 424)
- EERC 73-17 "Dynamic Behavior of a Multi-Story Pyramid Shaped Building," by R. M. Stephen and J. G. Bouwkamp - 1973
- EERC 73-18 "Effect of Different Types of Reinforcing on Seismic Behavior of Short Concrete Columns," by V. V. Bertero, J. Hollings, O. Kustu, R. M. Stephen and J. G. Bouwkamp - 1973
- EERC 73-19 "Olive View Medical Center Material Studies, Phase I," by B. Bresler and V. V. Bertero - 1973 (PB 235 986)
- EERC 73-20 "Linear and Nonlinear Seismic Analysis Computer Programs for Long Multiple-Span Highway Bridges," by W. S. Tseng and J. Penzien - 1973
- EERC 73-21 "Constitutive Models for Cyclic Plastic Deformation of Engineering Materials," by J. M. Kelly and P. P. Gillis - 1973 (PB 226 024)
- EERC 73-22 "DRAIN - 2D User's Guide," by G. H. Powell - 1973 (PB 227 016)
- EERC 73-23 "Earthquake Engineering at Berkeley - 1973" - 1973 (PB 226 033)
- EERC 73-24 Unassigned
- EERC 73-25 "Earthquake Response of Axisymmetric Tower Structures Surrounded by Water," by C. Y. Liaw and A. K. Chopra - 1973 (AD 773 052)
- EERC 73-26 "Investigation of the Failures of the Olive View Stairtowers during the San Fernando Earthquake and Their Implications in Seismic Design," by V. V. Bertero and R. G. Collins - 1973 (PB 235 106)

- EERC 73-27 "Further Studies on Seismic Behavior of Steel Beam-Column Subassemblages," by V. V. Bertero, H. Krawinkler and E. P. Popov - 1973 (PB 234 172)
- EERC 74-1 "Seismic Risk Analysis," by C. S. Oliveira - 1974 (PB 235 920)
- EERC 74-2 "Settlement and Liquefaction of Sands under Multi-Directional Shaking," by R. Pyke, C. K. Chan and H. B. Seed - 1974
- EERC 74-3 "Optimum Design of Earthquake Resistant Shear Buildings," by D. Ray, K. S. Pister and A. K. Chopra - 1974 (PB 231 172)
- EERC 74-4 "LUSH - A Computer Program for Complex Response Analysis of Soil-Structure Systems," by J. Lysmer, T. Udaka, H. B. Seed and R. Hwang - 1974 (PB 236 796)
- EERC 74-5 "Sensitivity Analysis for Hysteretic Dynamic Systems: Applications to Earthquake Engineering," by D. Ray - 1974 (PB 233 213)
- EERC 74-6 "Soil-Structure Interaction Analyses for Evaluating Seismic Response," by H. B. Seed, J. Lysmer and R. Hwang - 1974 (PB 236 519)
- EERC 74-7 Unassigned
- EERC 74-8 "Shaking Table Tests of a Steel Frame - A Progress Report," by R. W. Clough and D. Tang - 1974
- EERC 74-9 "Hysteretic Behavior of Reinforced Concrete Flexural Members with Special Web Reinforcement," by V. V. Bertero, E. P. Popov and T. Y. Wang - 1974 (PB 236 797)
- EERC 74-10 "Applications of Reliability-Based, Global Cost Optimization to Design of Earthquake Resistant Structures," by E. Vitiello and K. S. Pister - 1974 (PB 237 231)
- EERC 74-11 "Liquefaction of Gravelly Soils under Cyclic Loading Conditions," by R. T. Wong, H. B. Seed and C. K. Chan - 1974
- EERC 74-12 "Site-Dependent Spectra for Earthquake-Resistant Design," by H. B. Seed, C. Ugas and J. Lysmer - 1974

- EERC 74-13 "Earthquake Simulator Study of a Reinforced Concrete Frame," by P. Hidalgo and R. W. Clough - 1974 (PB 241 944)
- EERC 74-14 "Nonlinear Earthquake Response of Concrete Gravity Dams," by N. Pal - 1974 (AD/A006583)
- EERC 74-15 "Modeling and Identification in Nonlinear Structural Dynamics, I - One Degree of Freedom Models," by N. Distefano and A. Rath - 1974 (PB 241 548)
- EERC 75-1 "Determination of Seismic Design Criteria for the Dumbarton Bridge Replacement Structure, Vol. I: Description, Theory and Analytical Modeling of Bridge and Parameters," by F. Baron and S.-H. Pang - 1975
- EERC 75-2 "Determination of Seismic Design Criteria for the Dumbarton Bridge Replacement Structure, Vol. 2: Numerical Studies and Establishment of Seismic Design Criteria," by F. Baron and S.-H. Pang - 1975
- EERC 75-3 "Seismic Risk Analysis for a Site and a Metropolitan Area," by C. S. Oliveira - 1975
- EERC 75-4 "Analytical Investigations of Seismic Response of Short, Single or Multiple-Span Highway Bridges," by Ma-chi Chen and J. Penzien - 1975 (PB 241 454)
- EERC 75-5 "An Evaluation of Some Methods for Predicting Seismic Behavior of Reinforced Concrete Buildings," by Stephen A. Mahin and V. V. Bertero - 1975
- EERC 75-6 "Earthquake Simulator Study of a Steel Frame Structure, Vol. I: Experimental Results," by R. W. Clough and David T. Tang - 1975 (PB 243 981)
- EERC 75-7 "Dynamic Properties of San Bernardino Intake Tower," by Dixon Rea, C.-Y. Liaw, and Anil K. Chopra - 1975 (AD/A008406)
- EERC 75-8 "Seismic Studies of the Articulation for the Dumbarton Bridge Replacement Structure, Vol. I: Description, Theory and Analytical Modeling of Bridge Components," by F. Baron and R. E. Hamati - 1975
- EERC 75-9 "Seismic Studies of the Articulation for the Dumbarton Bridge Replacement Structure, Vol. 2: Numerical Studies of Steel and Concrete Girder Alternates," by F. Baron and R. E. Hamati - 1975

- EERC 75-10 "Static and Dynamic Analysis of Nonlinear Structures," by Digambar P. Mondkar and Graham H. Powell - 1975 (PB 242 434)
- EERC 75-11 "Hysteretic Behavior of Steel Columns," by E. P. Popov, V. V. Bertero and S. Chandramouli - 1975
- EERC 75-12 "Earthquake Engineering Research Center Library Printed Catalog" - 1975 (PB 243 711)
- EERC 75-13 "Three Dimensional Analysis of Building Systems," Extended Version, by E. L. Wilson, J. P. Hollings and H. H. Dovey - 1975 (PB 243 989)
- EERC 75-14 "Determination of Soil Liquefaction Characteristics by Large-Scale Laboratory Tests," by Pedro De Alba, Clarence K. Chan and H. Bolton Seed - 1975
- EERC 75-15 "A Literature Survey - Compressive, Tensile, Bond and Shear Strength of Masonry," by Ronald L. Mayes and Ray W. Clough - 1975
- EERC 75-16 "Hysteretic Behavior of Ductile Moment Resisting Reinforced Concrete Frame Components," by V. V. Bertero and E. P. Popov - 1975
- EERC 75-17 "Relationships Between Maximum Acceleration, Maximum Velocity, Distance from Source, Local Site Conditions for Moderately Strong Earthquakes," by H. Bolton Seed, Ramesh Murarka, John Lysmer and I. M. Idriss - 1975
- EERC 75-18 "The Effects of Method of Sample Preparation on the Cyclic Stress-Strain Behavior of Sands," by J. Paul Mulilis, Clarence K. Chan and H. Bolton Seed - 1975
- EERC 75-19 "The Seismic Behavior of Critical Regions of Reinforced Concrete Components as Influenced by Moment, Shear and Axial Force," by B. Atalay and J. Penzien - 1975
- EERC 75-20 "Dynamic Properties of an Eleven Story Masonry Building," by R. M. Stephen, J. P. Hollings, J. G. Bouwkamp and D. Jurukovski - 1975
- EERC 75-21 "State-of-the-Art in Seismic Shear Strength of Masonry - An Evaluation and Review," by Ronald L. Mayes and Ray W. Clough - 1975
- EERC 75-22 "Frequency Dependencies Stiffness Matrices for Viscoelastic Half-Plane Foundations," by Anil K. Chopra, P. Chakrabarti and Gautam Dasgupta - 1975
- EERC 75-23 "Hysteretic Behavior of Reinforced Concrete Framed Walls," by T. Y. Wong, V. V. Bertero and E. P. Popov - 1975

- EERC 75-24 "Testing Facility for Subassemblages of Frame-Wall Structural Systems," by V. V. Bertero, E. P. Popov and T. Endo - 1975
- EERC 75-25 "Influence of Seismic History on the Liquefaction Characteristics of Sands," by H. Bolton Seed, Kenji Mori and Clarence K. Chan - 1975
- EERC 75-26 "The Generation and Dissipation of Pore Water Pressures during Soil Liquefaction," by H. Bolton Seed, Phillippe P. Martin and John Lysmer - 1975
- EERC 75-27 "Identification of Research Needs for Improving a Seismic Design of Building Structures," by V. V. Bertero - 1975
- EERC 75-28 "Evaluation of Soil Liquefaction Potential during Earthquakes," by H. Bolton Seed, I. Arango and Clarence K. Chan 1975
- EERC 75-29 "Representation of Irregular Stress Time Histories by Equivalent Uniform Stress Series in Liquefaction Analyses," by H. Bolton Seed, I. M. Idriss, F. Makdisi and N. Banerjee 1975
- EERC 75-30 "FLUSH - A Computer Program for Approximate 3-D Analysis of Soil-Structure Interaction Problems," by J. Lysmer, T. Udaka, C.-F. Tsai and H. B. Seed - 1975
- EERC 75-31 "ALUSH - A Computer Program for Seismic Response Analysis of Axisymmetric Soil-Structure Systems," by E. Berger, J. Lysmer and H. B. Seed - 1975
- EERC 75-32 "TRIP and TRAVEL - Computer Programs for Soil-Structure Interaction Analysis with Horizontally Travelling Waves," by T. Udaka, J. Lysmer and H. B. Seed - 1975
- EERC 75-33 "Predicting the Performance of Structures in Regions of High Seismicity," by Joseph Penzien - 1975
- EERC 75-34 "Efficient Finite Element Analysis of Seismic Structure - Soil - Direction," by J. Lysmer, H. Bolton Seed, T. Udaka, R. N. Hwang and C.-F. Tsai - 1975
- EERC 75-35 "The Dynamic Behavior of a First Story Girder of a Three-Story Steel Frame Subjected to Earthquake Loading," by Ray W. Clough and Lap-Yan Li - 1975
- EERC 75-36 "Earthquake Simulator Study of a Steel Frame Structure, Volume II - Analytical Results," by David T. Tang - 1975
- EERC 75-37 "ANSR-I General Purpose Computer Program for Analysis of Non-Linear Structural Response," by Digambar P. Mondkar and Graham H. Powell - 1975

- EERC 75-38 "Nonlinear Response Spectra for Probabilistic Seismic Design and Damage Assessment of Reinforced Concrete Structures," by Masaya Murakami and Joseph Penzien - 1975
- EERC 75-39 "Study of a Method of Feasible Directions for Optimal Elastic Design of Framed Structures Subjected to Earthquake Loading," by N. D. Walker and K. S. Pister - 1975
- EERC 75-40 "An Alternative Representation of the Elastic-Viscoelastic Analogy," by Gautam Dasgupta and Jerome L. Sackman - 1975
- EERC 75-41 "Effect of Multi-Directional Shaking on Liquefaction of Sands," by H. Bolton Seed, Robert Pyke and Geoffrey R. Martin - 1975
- EERC 76-1 "Strength and Ductility Evaluation of Existing Low-Rise Reinforced Concrete Buildings - Screening Method," by Tsuneo Okada and Boris Fresler - 1976
- EERC 76-2 "Experimental and Analytical Studies on the Hysteretic Behavior of Reinforced Concrete Rectangular and T-Beams," by Shao-Yeh Marshall Ma, Egor P. Popov and Vitelmo V. Bertero - 1976
- EERC 76-3 "Dynamic Behavior of a Multistory Triangular-Shaped Building," by J. Petrovski, R. M. Stephen, E. Gartenbaum and J. G. Bouwkamp - 1976
- EERC 76-4 "Earthquake Induced Deformations of Earth Dams," by Norman Serff and H. Bolton Seed - 1976
- EERC 76-5 "Analysis and Design of Tube-Type Tall Building Structures," by H. de Clercq and G. H. Powell - 1976
- EERC 76-6 "Time and Frequency Domain Analysis of Three-Dimensional Ground Motions, San Fernando Earthquake," by Tetsuo Kubo and Joseph Penzien - 1976
- EERC 76-7 "Expected Performance of Uniform Building Code Design Masonry Structures," by R. L. Mayes, Y. Omote, S. W. Chen and R. W. Clough - 1976
- EERC 76-8 "Cyclic Shear Tests on Concrete Masonry Piers, Part I - Test Results," by R. L. Mayes, Y. Omote and R. W. Clough 1976
- EERC 76-9 "A Substructure Method for Earthquake Analysis of Structure-Soil Interaction," by Jorge Alberto Gutierrez and Anil K. Chopra - 1976
- EERC 76-10 "Stabilization of Potentially Liquefiable Sand Deposits Using Gravel Drain Systems," by H. Bolton Seed and John R. Booker - 1976

- EERC 76-11 "Influence of Design and Analysis Assumptions on Computed Inelastic Response of Moderately Tall Frames," by G. H. Powell and D. G. Row - 1976
- EERC 76-12 "Sensitivity Analysis for Hysteretic Dynamic Systems: Theory and Applications," by D. Ray, K. S. Pister and E. Polak - 1976
- EERC 76-13 "Coupled Lateral Torsional Response of Buildings to Ground Shaking," by Christopher L. Kan and Anil K. Chopra - 1976
- EERC 76-14 "Seismic Analysis of the Banco de America," by V. V. Bertero, S. A. Mahin and J. A. Hollings - 1976
- EERC 76-15 "Reinforced Concrete Frame 2: Seismic Testing and Analytical Correlation," by Ray W. Clough and Jawahar Gidwani 1976



